PARTICLE DEPOSITION IN INDUSTRIAL DUCT BENDS

by
Thomas Michael Peters

A dissertation submitted to the faculty of the University of North Carolina at Chapel Hill in partial fulfillment of the requirements for the degree of Doctor of Philosophy in the Department of Environmental Sciences and Engineering, School of Public Health.

Chapel Hill
2004

Approved by:


Dr. David Leith, Advisor

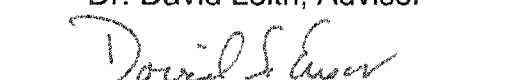
Dr. David Ensor, Reader

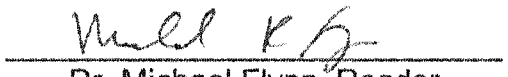
Dr. Michael Flynn, Reader


Prof. Richard Kamens, Reader


Dr. Alberto Scotti, Reader

INFORMATION TO USERS

The quality of this reproduction is dependent upon the quality of the copy submitted. Broken or indistinct print, colored or poor quality illustrations and photographs, print bleed-through, substandard margins, and improper alignment can adversely affect reproduction.

In the unlikely event that the author did not send a complete manuscript and there are missing pages, these will be noted. Also, if unauthorized copyright material had to be removed, a note will indicate the deletion.

ProQuest Information and Learning Company
300 North Zeeb Road
P.O. Box 1346
Ann Arbor, MI 48106-1346

ABSTRACT

THOMAS MICHAEL PETERS: Particle Deposition In Industrial Duct Bends

(Under the direction of David Leith, Sc.D.)

Workplace illnesses result from exposure to harmful contaminants. Local exhaust systems can reduce these exposures and prevent the onset of disabling illnesses. Although extensive procedures aid engineers when designing these systems, particles that deposit in ducts can reduce the effectiveness of local exhaust systems and place workers at undue risk.

This work seeks to develop a model to estimate particle deposition in bends of an exhaust system. To accomplish this goal, a new method was developed to measure particle deposition by size in exhaust ducts at conditions typical of industry. While previous methods are limited to relatively small particles, small diameter ducts, and low Reynolds numbers, the new method enables measurement of particle deposition by size in any part or assemblage of parts of an exhaust system. Moreover, this method is adaptable to laboratory or field settings.

Using this new method, a factorial experiment examined particle deposition in full-size, industrial, duct bends. These experiments identified that models previously published under-represent drag force and over-estimate deposition when particle motion is outside the Stokes regime. Further, small but significant differences in particle deposition occur with changes in bend orientation. Particle penetration was not a multiplicative function of bend angle as theory predicts, due to the developing nature of turbulent flow in bends.

A new model was developed using the experimental data above to describe particle deposition by size in 90° bends of industrial ducts. This new model accounts for non-Stokes particle motion and for variable deposition patterns as a function of particle Stokes number. Whereas previous models fit the data poorly, r^2 less than 30%, the new model explains 86% of the variability associated with the data.

The goal of this work was realized; the new model allows estimation of particle deposition by size in bends of industrial ducts. The methods developed here can be used to investigate other parts of a duct system, such as expansions and tees. Ultimately, these studies should enable engineers to avoid compromised exhaust systems due to deposits of particles.

To Susan, Benjamin, Olivia, and Elizabeth...
each wonderful in your own way; together, magnificent.

ACKNOWLEDGEMENTS

I cannot fully express my gratitude to the "Baity" experience. First and foremost, to my advisor, David Leith, for his guidance, encouragement, and friendship. To Maryanne Boundy, for her razor-sharp editorial skill, her unassuming advice, and her warmth, which included shelter for a family of four during the ice storm and midnight sitting when Lizzie was born. To all of my friends, for sharing in many wonderful adventures.

I wish to thank my committee members, who were especially helpful: David Ensor, for suggesting *in-situ* sampling; Mike Flynn, for provided many valuable insights; Alberto Scotti, for challenging my fluids knowledge; and Rich Kamens, for candidly sharing his views.

I am deeply grateful for the support that paid the mortgage, purchased diapers, and bought kids shoes. To Ford Motor Company and the United Auto Workers, who provided a gift to the university to support research in air engineering. To the Department of Education Fellowship for Interdisciplinary Training in Environmental Engineering. To National Institute of Occupational Safety and Health, for their fellowship from the Educational Resource Center. To Bob Gussman, a fine friend, for encouraging my return to school and for providing side work.

Of course, I would like to thank my family. To my Grandfathers, who gave me tools, not only to hammer and to saw with, but also to imagine and to dream with. To my father – a self-taught engineer and inventor – who instilled in me the value of hard work and showed me how to get things done. To my mother, who encouraged 'getting my hands dirty'. Thank you to my children, who fill me with great pride: Benny for helping me see the best in myself, Oli for letting me use her 'answer bear', and Lizzie for making me smile. Lastly, thank you to Susan, for being a wonderful mother, a true friend, and an unwavering supporter.

CONTENTS

LIST OF TABLES

LIST OF FIGURES

LIST OF ABBREVIATIONS AND SYMBOLS

a	duct radius
A_d	duct cross-sectional area
A_e	effective deposition area
a_m	constant used in the McFarland et al. (1997) model
b_m	constant used in the McFarland et al. (1997) model
C_{ae}	C_c associated with the aerodynamic diameter
C_c	Cunningham slip correction factor
C_D	coefficient of drag
c_m	constant used in the McFarland et al. (1997) model
CM	cumulative mass
C_{Stk}	C_c associated with the Stokes diameter
D	downstream sampling location
D_{16}	diameter associated with 16% of the cumulative mass
D_{50}	cutpoint diameter, diameter associated with 50% of the cumulative mass
D_{84}	diameter associated with 84% of the cumulative mass
D_{ae}	aerodynamic particle diameter
D_{duct}	duct diameter
d_m	constant used in the McFarland et al. (1997) model
D_p	geometric particle diameter
D_{Stk}	Stokes equivalent diameter
De	Dean number = $\frac{Re}{\sqrt{R_0}} = \frac{\sqrt{\rho_f^2 U_0^2 R_b}}{\mu_f}$
dM	differential mass
$dM_{i,down}$	differential mass for a given interval downstream of the bend
$dM_{i,up}$	differential mass for a given interval upstream of the bend
f	fraction of internal surface area where particles deposit
FCA_g	fraction of duct area closed by grid
g	gravitational constant, 9.81 m s^{-2}
G	particle mass generation rate

GSD	geometric standard deviation = $\sqrt{\frac{D_{84}}{D_{16}}}$
h	sedimentation pipette height
H-H	horizontal-to-horizontal orientation
H-V	horizontal-to-vertical orientation
i	particle size interval
L	arc length through which bend sweeps = $R_b\,\theta$
M	mass of dust
M_g	mass of dust collected on the grid
M_{down}	mass of dust downstream of the bend
M_{up}	mass of dust upstream of the bend
MMAD	mass median aerodynamic diameter
P	fraction of particles penetrating
$P_{\%}$	percent of particles penetrating
$P_{\%,45}$	percent of particles penetrating through a 45° bend
$P_{\%,90}$	percent of particles penetrating through a 90° bend
P_{grav}	fraction of particles penetrating considering gravity settling
P_x	fraction of particles penetrating determined experimentally
Q	airflow rate
R_0	curvature ratio = $\frac{R_b}{a}$
R_b	centerline radius or curvature of the bend
Re	flow Reynolds number = $\frac{D_{duct}U_0}{\nu}$
Re_p	Reynolds number = $\frac{D_pV}{\nu}$
$Re_{p\infty}$	free-stream particle Reynolds number = $\frac{D_pU_0}{\nu}$
Re_{pr}	radial particle Reynolds number = $\frac{D_pV_r}{\nu}$
U	upstream sampling position
U_0	mean axial velocity upstream of the bend
V	velocity of particle relative to the fluid velocity

V_r	velocity with which the particle moves radially toward the outer wall of the bend
V_{ts}	particle terminal settling velocity
SL_{GRID}	grid-measured surface loading
SL_{GEN}	generator-estimated grid surface loading
Stk	particle Stokes number based on duct radius = $\frac{\tau U_0}{a}$
Stk_T	transition Stokes number = $\frac{V_r t}{a} = \frac{V_r R_b \theta}{a U_0}$
t	time for air to pass through the bend
t_a	time required for a particle to settle during analysis
t_s	time of sampling
χ	shape factor
ϕ	poloidal angle, angle in a cross-sectional plane of the duct
η_{dep}	percent of incoming particles that deposit for a given size
$\eta_{dep,\,tot}$	percent of incoming particles that deposit for all sizes
$\eta_{dep,i}$	percent of incoming particles that deposit for a given size interval
μ_f	fluid dynamic viscosity
ν	fluid kinematic viscosity
θ	toroidal angle, angle through which the bend sweeps
ρ_0	particle unit density = 1000 kg m^{-3}
ρ_f	fluid density
ρ_p	particle density
τ	particle relaxation time = $\frac{C_c \rho_p D_p^2}{18\mu_f}$

I. OVERVIEW

A. Introduction

Each day approximately 165 Americans die from work-related illnesses; costs associated with occupational illnesses and injuries are estimated at $155 billion, or 3% of the US gross domestic product (Leigh et al., 2000). Workplace illnesses result from exposures to hazardous workplace contaminants, including harmful gases, dusts, and mists (NIOSH, 2002). Due to long latency periods between the initial exposure and ensuing symptoms, some illnesses go undetected until well after workers suffer irreversible damage (Cullen, 2002). These occupational-related disabilities and deaths continue despite clear associations between workplace contaminants and illness: e.g., asbestos exposure causes asbestosis; coal dust exposure causes pneumoconiosis; quartz exposure causes silicosis; and cotton dust exposure causes byssinosis (NIOSH, 2003).

For thousands of years, mechanical ventilation has been used to decrease workplace exposures to hazardous contaminants. Around 300 BC, Pliny the Elder described waving a linen cloth near a miner to reduce his exposure to dusts (Agricola, 1556). In the middle ages, Agricola documented various techniques to supply clean air into mineshafts, including wind diverters and horse-driven bellows (Agricola, 1556). During the industrial age, more complex mechanical ventilation systems were introduced to meet increasingly varied and widespread exposures of the working population to hazardous contaminants. In the first half of the twentieth century, mechanical ventilation first became required to protect workers' health.

Today, local exhaust systems are installed in virtually every industrial facility to capture harmful contaminants before they reach the worker. In such systems, hoods located throughout a facility capture contaminants that are entrained in workplace air. The contaminant-laden air is transported through connecting ducts to a central air-cleaning device where the contaminant is removed. Then the cleaned air is

either circulated back into the facility or exhausted outside (ACGIH, 1998). When these systems are designed correctly, installed properly, and receive regular maintenance checks, they reduce worker exposure.

A variety of manuals assist engineers in designing local exhaust systems (ACGIH, 1998; Alden and Kane, 1982; ASHRAE, 1998). These handbooks link proven capture and cleaning technology with specific industrial processes. Because exhaust systems usually represent a substantial financial investment in a workplace, design procedures aim to balance high capture efficiencies with low costs. When designing these systems, engineers select a hood and an air cleaner for a given process, calculate the airflow for adequate contaminant capture, determine the minimum transport velocity to move the contaminant to the air cleaner, and size the connecting ducts and fan (Burgess et al., 1989).

Even with these guidelines, particles that deposit in a duct sometimes clog or restrict airflow. When such airflow restrictions occur, hood capture fails, workplace contaminant levels rise, and excessive exposures occur. Deposited particles in exhaust ducts also represent fire hazards and collapse hazards (Gregory et al., 1991; May and Berard, 1987).

Problems attributed to particle deposits in ducts are not limited to factory exhaust systems. In restaurant kitchens, fires often are attributed to grease deposits in ducts (Gerstler, 2002). In homes and office buildings, sick building syndrome results when mold spores deposit in supply ducts (Muhic and Butala, 2004). Ducts laden with hazardous particles, which were released intentionally (i.e., bioterrorist attacks) or otherwise, can entail costly remediation.

This work seeks to develop models to estimate particle deposition in bends of industrial ducts. With such estimates, particle deposits can be reduced and/or accommodated through regularly scheduled duct maintenance. Then, the effectiveness of an exhaust system will no longer be susceptible to problems arising from particle deposits.

B. Background

1. Literature Review

Industrial hygienists use the criterion of minimum transport velocity, the minimum velocity required to move particles from a hood to the air cleaner (ACGIH, 1998). DallaValle (1932) first published two empirical formulas to associate values with this criterion. He arrived at these formulas by observing the behavior of four mineral dusts moving through typical exhaust ducts. Hatch (1940) advised restraint in selecting transport velocities. He found that although high velocities were advantageous in transporting particles, they reduced duct lifespan due to the scouring of interior walls and incurred greater operating costs because of their high pressure drop. Baliff et al. (1948) adjusted DallaValle's values downward after observing the behavior of many industrial dusts through a plate glass window mounted on a duct. Rajhans and Tompkins (1967) suggested even lower values were adequate for bouncy mineral dusts.

More precise methods allow determination of particle deposition by size in ducts. In the 'wash-off' method, deposited monodisperse particles are washed from a surface and quantified fluorometrically (Liu and Agarwal, 1974). This technique is limited to particles smaller than 30 μm due to difficulties in generating larger monodisperse aerosols. Other schemes use time-of-flight instruments to determine airborne particle size distribution upstream and downstream of exhaust system components (Leith et al., 1996); however, difficulties in aspirating large particles restrict use of these instruments to particles smaller than around 10 μm (Fan et al., 1992). These methods are difficult to adapt to industrial conditions, where duct diameters are large, airflow is highly turbulent, and particles are large.

Thus, relatively little is known about particle deposition in industrial ducts. Studies of deposition in straight ducts are most numerous. Experimental measurements of deposition by size are available for Re of up to 365,000 (Alexander and Coldren, 1951; Friedlander and Johnstone, 1957; Liu and Agarwal, 1974; Montgomery and Corn, 1970). Various models are available to estimate deposition in straight ducts due to turbulent inertial deposition, gravitational settling,

and diffusion (El-Shobokshy, 1983; Friedlander and Johnstone, 1957; Muyshondt et al., 1996). However, these models provide estimates of particle deposition that vary by orders of magnitude, and they have not been validated for conditions typical of exhaust ventilation. In straight, rectangular air conditioning ducts, Sippola and Nazaroff (2003) found that these models under-estimated particle deposition; they provided their own empirical equations for this situation.

Fewer studies are available for other parts of an exhaust system. Pui et al. (1987) and McFarland et al. (1997) provided models to estimate particle deposition in bends with moderately turbulent airflow ($Re < 19{,}000$). Hacker et al. (1953) and Crane and Evans (1977) numerically simulated particle deposition from bends with highly turbulent airflow ($236{,}000 \leq Re \leq 3{,}700{,}000$), but these studies are difficult to apply to a new set of conditions. Published studies are unavailable to estimate deposition in expansions and branch entries.

Efforts have been made to estimate particle deposition in complete duct systems. Good agreement between model estimates and experiments have been observed for small diameter aerosol sampling lines (McFarland et al., 1991; Yamano and Brockmann, 1989). Wallin and Malmström (Wallin, 1994; Wallin and Malmstrom, 1995) estimated particle deposition in heating and air conditioning ventilation (HVAC) ducts; however, their efforts were not validated with experiments. Sippola and Nazaroff (2003) estimated particle deposition in rectangular air conditioning ducts, but they used the correlation for small-diameter, round bends with moderate turbulence published by McFarland et al. (1997).

2. Shortcomings of Literature

The criterion of minimum transport velocity is inadequate to ensure proper long-term operation of exhaust systems. Even when established values for this criterion are followed, particles that deposit in ducts can compromise the effectiveness of an exhaust system. Moreover, the criterion of minimum transport velocity is not suited for liquid particles that adhere to duct walls upon impact. To resolve this situation, a better understanding of particle deposition by size in industrial ducts is needed.

Methods to obtain this information are unavailable. The crude, visual observations relied upon in past studies do not provide sufficiently detailed information. Newer methods are difficult to apply to conditions typical of industrial ducts.

Thus, particle deposition by size in industrial ducts remains unclear. Experimental data are sparse, and models to estimate deposition are unavailable or not validated for the ventilation engineer to estimate particle deposition in industrial exhaust ducts.

C. Objectives

The specific objectives of this work are the following:

- **To develop a new method to measure particle deposition.** A new method is needed to measure particle deposition by size in industrial ducts at conditions typical of industry.
- **To investigate particle deposition in duct bends.** Experimental data are needed to validate, adapt, and develop models for deposition of large particles in large-diameter, industrial duct bends with highly turbulent airflow. Specifically, this objective pertains to deposition of drops or solid particles where duct walls are sticky.
- **To provide a model to estimate particle deposition in duct bends.** A new model is required to explain the experimental results from the second objective. Again, this objective pertains to particles that adhere to duct walls upon impact.

D. Findings

Each of the remaining three chapters of this dissertation contains a manuscript devoted to one of the objectives listed above. These manuscripts are in various stages in the publication process.

Chapter II, in press in the *Journal of Aerosol Science*, presents a new method to measure particle deposition of large particles in industrial ducts. The new method enables measurement of particle deposition by size in a simple, spatially integrated,

and inexpensive manner. This method is applicable to ducts of any size and shape and for use in both laboratory and field studies.

Chapter III, accepted by the *Annals of Occupational Hygiene*, describes a factorial experiment that explores particle deposition in industrial duct bends. This study identifies inadequacies in models published previously for estimating deposition by size in bends of industrial exhaust systems. Because this experiment is the first of its kind, it should be useful for benchmarking computer simulations and building new models.

Chapter IV, submitted to *Aerosol Science and Technology*, presents a new model to estimate particle deposition in 90° bends. The new model corrects for particle motion outside of Stokes regime and for variable deposition patterns as a function of Stokes number. Whereas earlier models over-estimate deposition for large particles in industrial bends, the new model agrees better with the data presented in Chapter III.

E. Recommendations for Further Research

The research discussed in this dissertation should be extended to provide a more complete understanding of particle deposition in industrial ducts.

First, alternative particle sizing techniques may enhance the new method to measure particle deposition by size. Although the current analysis method, the Andreasen sedimentation pipette, provided a direct measure of particle mass by size, it was slow and cumbersome. Alternative instruments, such as the Coulter counter, allow rapid and automated analysis, and if compatible with the new method, may reduce the time required to measure particle deposition for a given set of conditions from approximately three days to several hours.

Second, further experiments are necessary to resolve some observations concerning bends. Additional experiments are required to determine if air leakage caused the substantially lower deposition observed in tests with the segmented bend. If so, future bend design might incorporate air leakage to reduce particle deposition. Tests are also needed to explain why deposition in a 45° bend is not a multiplicative function of bend angle.

Finally, other parts of a duct system and other conditions should be studied. Additional work is needed to define deposition by size in expansions, tees, and straight sections for drops or when bend walls are sticky. More work is required to understand deposition for particles of varying bounciness. The results of such studies will identify the inadequacies of the one-size-fits-all approach to minimum transport velocity, and ultimately, will enable engineers to ensure that exhaust systems protect workers for their entire lifetime.

II. MEASUREMENT OF PARTICLE DEPOSITION IN INDUSTRIAL DUCTS

A. Abstract

A new method was developed to measure particle deposition in industrial ducts. Greased wire grids were used to capture particles *in situ* by impaction upstream and downstream of a duct bend. Particles were recovered from the grid using a hexane extraction procedure. Cumulative mass distributions of the recovered particles were determined with a sedimentation pipette; these distributions were then used to compute particle deposition by size. As these procedures were compatible with solid particles only, the interior surface of the bend was coated with grease to eliminate solid particle bounce so that results obtained here could be compared to published models for droplet deposition in bends. In a 20.3-cm-diameter, 90° bend at an air velocity of 27.4 m s^{-1}, deposition increased from approximately 35% at 15 μm to nearly 100% at 100 μm. These data generally agreed with models developed for small sampling tubes.

B. Introduction

Ventilation systems transport particles through ducts (ASHRAE, 1998). To avoid particle deposition, air velocities in each duct must be maintained above a minimum transport velocity (ACGIH, 1998; Baliff et al., 1948; DallaValle, 1932). This velocity ranges from 10 m s^{-1} for welding fumes to 30 m s^{-1} for heavy or moist dusts (Alden and Kane, 1982). Optimal economy results when the velocity in each branch of a ductwork system approaches the minimum transport velocity (ACGIH, 1998; Curd et al., 2001; Hatch, 1940; Rajahns and Thompkins, 1967).

Even with these guidelines, particles that deposit in a duct can sometimes clog or restrict branch lines over time, resulting in insufficient contaminant capture at hoods, fire hazards, or ductwork collapse (Gregory et al., 1991; May and Berard, 1987). Engineers frequently avoid these problems through trial-and-error, often with mixed

results. Models to predict deposition as a function of particle, duct, and airflow characteristics would eliminate these *ad hoc* methods, allow evaluation of system performance over time, and integrate the ductwork into overall ventilation designs.

However, methods used to measure particle deposition are restricted to small diameter tubes, low Reynolds numbers, and small particle sizes (Muyshondt et al., 1996; Papavergos and Hedley, 1984). In the 'wash-off' method, deposited monodisperse particles are washed from a surface and quantified fluorometrically (Liu and Agarwal, 1974). This method is limited to laboratory investigations of particles smaller than 30 μm, is difficult to adapt to large ducts, and requires many tests to fully characterize deposition. Other schemes allow field portability and rapid analysis by extracting particles directly from a duct (Leith et al., 1996); however, difficulties in aspiration and transport restrict use of these techniques to particles smaller than about 10 μm (Fan et al., 1992; Gong et al., 1993; McFarland et al., 1991).

Without adequate measurement methods, data have been unavailable to develop a full set of particle deposition models for industrial ductwork. For bends, Table 2.1 compares the conditions typical of industrial ducts to the experimental conditions that have been used to develop published models. Both the McFarland et al. (1997) and the Pui et al. (1987) models are based on small diameter tubes and low Reynolds numbers when compared to industrial conditions. Moreover, these models are limited to liquid droplets and do not address issues of bounce and build-up unique to solid particles. Thus, data are needed to validate models for liquid droplets in ductwork bends. For solid particles in bends and for other ductwork geometries, such as contractions and junctions, models are nonexistent; in these situations, data are needed to develop new models.

Accordingly, the objectives of this paper are: (1) to present a new method to measure deposition by particle size in industrial ducts; (2) to measure deposition in a bend at conditions typical of industry; and (3) to compare these measurements with published models that were developed for other conditions.

Table 2.1: Conditions typical of industry compared to those used to develop models for particle deposition in bends.

	Typical Exhaust System	McFarland et al. (1997)[a]	Pui et al. (1987)
Flow Reynolds Number, Re	$10^4 < Re < 10^6$	$Re = 8x10^3, 2x10^4$	$Re = 10^4$
Airflow Velocity, U_0, m s^{-1}	$10 < U_0 < 30$	$U_0 = 8, 19$	$U_0 = 18, 31$
Particle Diameter, D_p, µm	$1 < D_p < 100$	$D_p = 10$	$2.5 < D_p < 10$
Stokes Number[b], Stk	$0.1 < Stk < 7$	$Stk = 0.1, 0.7$	$0.3 < Stk < 1.4$
Particle Reynolds Number, $Re_{p\infty}$	$1 < Re_{p\infty} < 500$	$0.05 < Re_{p\infty} < 1.5$	$1 < Re_{p\infty} < 13$
Duct Diameter, D_{duct}, cm	$10 < D_{duct} < 100$	$D_{duct} = 1.6$	$D_{duct} = 0.5, 0.85$
Bend Curvature Ratio, R_0	$2.5 < R_0 < 5$	$2 < R_0 < 10$	$R_0 = 5.7$
Bend Angle, θ, degrees	$45 < \theta < 135$	$45 < \theta < 180$	90
Aerosol Type	Liquid and/or Solid	Liquid	Liquid

[a] For McFarland et al. (1997), physical experiments only; not numerical analysis

[b] Based on the duct radius, $Stk = \frac{\tau U_0}{a}$

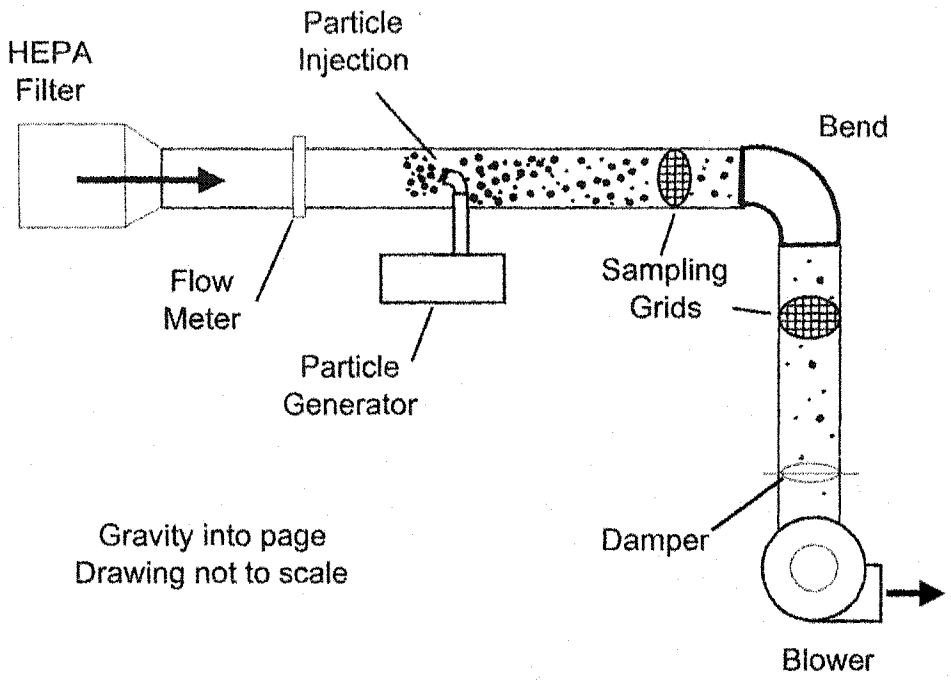

Figure 2.1: Experimental set-up.

C. Methods

1. Set-up and Procedures

Figure 2.1 shows the set-up used to measure particle deposition by size in an industrial duct bend. A blower (Buffalo Forge, Buffalo, NY, Type 25 MW) pulled room air through a HEPA filter into a duct with diameter D_{duct} = 20.3 cm. The air passed through a calibrated sharp-edged orifice meter, traveled $25D_{duct}$ through a straight duct, and then entered a horizontal, 90° bend. A damper was used to maintain an average velocity of 27.4 m s^{-1} entering the bend. Sampling grids were inserted alternately into the duct at two slots located $0.1D_{duct}$ upstream and $3D_{duct}$ downstream of the bend.

The interior of the bend was smooth except for two seams where the stamped halves were welded together. Bend curvature ratio, defined as the bend radius divided by the duct radius, was 3.0. The interior surface of the bend was coated with petroleum jelly (Vaseline®, Cheesbrough-Ponds USA Co., Greenwich, CT) to capture and retain solid particles that hit the wall.

An aerosol generator introduced polydisperse dust $17.5D_{duct}$ upstream of the bend at a rate of 2.3 ± 0.3 mg s^{-1}. The dust was composed of spherical glass particles with 10% by mass in the size range of 5 μm to 25 μm and 90% by mass greater than 25 μm (Plinke et al., 1995). A delivery system was adapted from a fluidized bed generator (Model 3400, TSI, Inc., St. Paul, MN) to feed the glass particles to a Venturi nozzle. The nozzle then injected the particles into the center of the duct, counter to the direction of airflow.

A summary of experimental procedures is provided below. Appendix A provides detailed step-by-step procedures.

a) Sampling

A circular sampling grid of diameter D_{duct} was cut from a sheet of welded-wire mesh (P/N 93322T41, McMaster-Carr, Atlanta, GA). The mesh was selected such that individual wires, 0.119 cm in diameter, would capture by impaction more than 95% of the particles larger than 5 μm at velocities higher than 15 m s^{-1} (Landahl and Herrmann, 1949). The grids were immersed into melted petroleum jelly to obtain a 0.5 mm grease coating that would prevent particle bounce and encourage particle retention (Pak et al., 1992). With the grease coating, the fraction of the duct cross-sectional area closed by the grid, FCA_g, was 0.209.

For a given sampling event, the coated sampling grid was positioned in the duct slot perpendicular to the airflow. For the air velocities and the particle sizes encountered in this work, the sampling grid was expected to capture all geometrically incident particles. Thus, the mass of dust, M, in the air stream during a sampling event was estimated as:

$$M = \frac{M_g}{FCA_g} \qquad (2.1)$$

where M_g is the mass of dust collected on the grid.

Several options were available to implement the grid sampling method. Samples could have been collected in the upstream and downstream simultaneously, eliminating any issues due to fluctuations in generator output; however, the presence of the upstream grid might have altered deposition in the bend and, hence, the material collected on the downstream grid. Although flow disruptions would have

been minimal because the pressure drop of the grid was small compared to the dynamic pressure of the air in the duct, this approach was rejected in favor of sampling alternately between the upstream and downstream positions.

b) Recovery

The grid was immersed in 100-mL hexane to dissolve the grease coating and to recover collected particles. The cleaned grid was removed after heating the hexane to a boil. The particles settled for two minutes, and then the hexane was aspirated. Settling and aspiration steps were repeated with fresh 50-mL hexane to wash residual grease from the collected particles. Tests demonstrated more than 95% recovery of particles collected with the grid.

An appropriate settling time, t_a, was selected using Stokes's Law:

$$t_a = \frac{18\,\mu_f h}{(\rho_p - \rho_f) g\, D_p^2} \qquad (2.2)$$

where μ_f is the fluid viscosity, h is the sedimentation height, ρ_p is the particle density, ρ_f is the fluid density, g is the gravitational constant, and D_p is the particle diameter. The time for a 5-μm glass sphere (ρ_p = 2.45 g cm^{-3}) to settle 1 cm in hexane ($\mu_f = 3.1 \times 10^{-3}$ g cm^{-1} s^{-1}, ρ_f = 0.66 g cm^{-3}) was calculated as two minutes.

c) Analysis

The total mass or the cumulative mass distribution of the recovered particles was analyzed for each sample. For total mass, approximately 25-mL methanol was used to transfer the dust to a vacuum filter holder (P/N K953750-5347, Fisher Scientific, Inc., Suwanee, GA 30024) containing a 47-mm, 2-μm pore filter (Zefluor, P5PJ047, VWR, International, West Chester, PA 19380). Before and after use, filters were conditioned in a vacuum oven at 60°C and 500 mm Hg for 8 hours and were weighed on a balance (M/N MT5, Mettler-Toledo, Greifensee, Switzerland) to the nearest microgram. Total mass was calculated as the difference between the filter weights. Filter blanks indicated that precision of the total mass measurements was ± 10 μg.

Alternatively, an Andreasen sedimentation pipette (P/N 14-232, Fisher Scientific, Inc., Suwanee, GA) was used to determine the cumulative mass distribution of the sampled dust by classifying particles according to their Stokes equivalent diameter. Settling times were calculated using Equation 2.2 for eight particle diameters. To convert Stokes equivalent diameter to aerodynamic diameter, the following relationship was used:

$$\sqrt{C_{ae}}D_{ae} = \sqrt{\frac{C_{Stk}\rho_p}{\chi\rho_0}}D_{Stk} \qquad (2.3)$$

where C_{ae} is the Cunningham correction factor for the particle of aerodynamic diameter, D_{ae}; C_{Stk} is the Cunningham correction factor for the particle of Stokes diameter, D_{Stk}; ρ_p is the density of the particle; χ is the shape factor of the particle; and ρ_0 is the unit density necessary for unit consistency (1000 kg m^{-3}). Because this work evaluated spherical particles, $\chi = 1$, and large particles with negligible Cunningham correction factors, $C_{ae} = C_{Stk} = 1$, Equation 2.3 reduced to:

$$D_{ae} = \sqrt{\frac{\rho_p}{\rho_0}}D_{Stk} \qquad (2.4)$$

For each sample, the particles recovered from the grid were wetted with 10-mL methanol and transferred into the pipette using approximately 250 mL of 40% ethylene glycol in deionized water. This solution was used to improve the sizing precision by slowing the settling of the glass spheres. The viscosity of the ethylene glycol solution at 22°C, determined by a falling ball viscometer (M/N B, S/N 91055, Haake, Dieselstrabe, Germany), was 2.0×10^{-2} g cm^{-1} s^{-1}, as compared to 1.1×10^{-2} g cm^{-1} s^{-1} for water alone. The pipette was then filled to a total volume of 511 mL by adding ethylene glycol solution. Aliquots were transferred into 20-mL capacity aluminum weighing dishes at times corresponding to aerodynamic particle sizes of 121 µm, 90 µm, 67 µm, 51 µm, 38 µm, 28 µm, 21 µm, and 16 µm. The mass of particles contained in each aliquot was determined using the procedures for total mass above. These measurements provided a direct measure of the particle cumulative mass distribution by aerodynamic particle size.

d) Velocity and Particle Concentration Profiles

Velocity profiles were measured with horizontal and vertical ten-point, equal-area traverses in a plane perpendicular to the airflow and 20-cm upstream of the bend. At each traverse position, a pitot tube (M/N 166-12, Dwyer Instruments, Inc., Michigan City, IN) and an inclined manometer (M/N 400, Dwyer Instruments, Inc., Michigan City, IN) were used to measure velocity pressure, which was then converted to velocity. The two traverses were in good agreement with fully developed pipe flow (Tennekes and Lumley, 1972).

For particle concentration, a sampling grid was used to collect particles in the upstream position for 30 s. Particle number distribution was measured with an optical microscope at four locations on the grid: 5 cm from each of the top, outside, inside, and bottom edges of the sampling grid. As the particle number distributions were nearly identical at each location, a uniform particle distribution and concentration was assumed to enter the bend. Appendix B contains data from velocity and particle concentration profile experiments.

2. Evaluation of Sampling and Recovery Procedures

To evaluate the precision and accuracy of the sampling and recovery procedures, grids were exposed to particle-laden air upstream of the bend for 30 s, 60 s, 80 s, 180 s, and 300 s. Three replicate samples were taken for each time period. The total mass collected by the grid was determined for each sample. The grid-measured particle surface loading, SL_{GRID}, was calculated as:

$$SL_{GRID} = \frac{M_g}{FCA_g * A_d} \tag{2.5}$$

where A_d is the cross-sectional area of the duct. This value was compared with the generator-estimated particle surface loading, SL_{GEN}, which was calculated as:

$$SL_{GEN} = \frac{G \cdot t_s}{FCA_g * A_d} \tag{2.6}$$

where G is the generator output rate and t_s is the sampling time.

3. Effectiveness of the Bend Surface Coating

The grease coating on the bend walls was evaluated for its effectiveness in preventing particle bounce as a function of cumulative mass input. First, the bend was coated with a fresh application of grease, and three successive 60-s samples were collected with the sampling grids in the downstream position. Then, the bend was exposed to the particle-laden air for 1380 s, after which an additional three successive 60-s downstream samples were taken. All samples were analyzed for total mass. For each sample, deposition in the bend for all particle sizes combined, $\eta_{dep,tot}$, was calculated as:

$$\eta_{dep,tot} = \left(\frac{M_{up} - M_{down}}{M_{up}} \right) * 100\% \qquad (2.7)$$

where M_{up} was the mass of particles upstream and M_{down} was the mass of particles downstream of the bend during the sampling event. M_{up} was estimated as $G * t_s$. M_{down} was calculated using Equation 2.1.

4. Deposition by Particle Size

Deposition by particle size was determined for the conditions specified in Table 2.2. Sampling grids were used to collect particles upstream (U) and downstream (D) of the bend for 100 s in a U-D-U-D-U-D pattern. As previously mentioned, this alternating pattern avoided disruption of airflow in the bend by the upstream grid while the downstream sampling occurred; it also minimized variation due to fluctuations in generator output. The grease coating on the bend walls was reapplied prior to each downstream measurement. For each sampling location, particles from the three grids were pooled into a single container. These procedures were repeated to obtain three sets of data; each set contained an upstream and downstream sample.

The sedimentation pipette was used to determine the cumulative mass distributions of each sample. Cumulative mass distributions were fitted with a log-normal distribution. Differential mass, dM, was calculated from the fitted cumulative mass distribution, CM, as:

$$dM_i = CM_i - CM_{i-1} \qquad (2.8)$$

Table 2.2: Experimental details: values of duct, fluid, and particle parameters.

	Parameter	Value
Bend	Diameter, cm	20.3
	Bend Angle	90°
	Curvature Ratio	3
	Surface Features	Smooth upper and lower sections joined with an axial seam along the outer and inner walls
	Orientation	Horizontal
	Interior Surface Coating	Grease
Fluid (Air)	Velocity, m s^{-1}	27.4
	Temperature, °C	20
	Pressure, mmHg	760
	Reynolds Number	368,000
Particle	Type	Glass Beads
	Size, μm	$5 < D_p < 150$
	Density, g cm^{-3}	2.45
	Shape	Spherical

where i is the interval associated with a given aerodynamic diameter as determined by the sedimentation pipette. Deposition for each interval, $\eta_{dep,i}$, was calculated as:

$$\eta_{dep,i} = \left(1 - \frac{dM_{i,down}}{dM_{i,up}}\right) * 100\% \quad (2.9)$$

where $dM_{i,down}$ is the downstream and $dM_{i,up}$ is the upstream interval mass. The differential mass distribution and deposition were plotted using the logarithmic average aerodynamic diameter for the interval.

D. Results and Discussion

1. Evaluation of Sampling and Recovery Procedures

For particle surface loadings on the sampling grid less than 0.7 mg cm^{-2}, Figure 2.2 shows that the grid-measured loading matched the generator-based loading. Paired t-tests accepted the hypothesis of equal grid and generator mean loading ($p = 0.41$, $p = 0.25$, $p = 0.36$). This agreement shows excellent precision and accuracy of both the sampling and the recovery procedures, thereby demonstrating that the sampling grid technique can be used to obtain representative samples of large solid particles in a fast moving, turbulent air stream.

For loadings greater than 0.7 mg cm^{-2}, the grid-measured loading became progressively lower than the generator-based loading. Paired t-tests rejected the equality of grid and generator mean loadings ($p = 0.03$, $p = 0.006$). These findings suggested a failure of the grease treatment at higher loadings. Using a stereomicroscope, collected particles on the sampling grid exhibited no indication of particle blow-off and were restricted predominately to the greased surface. Thus, poor retention at higher loadings was attributed to overloading (Marple and Rubow, 1986). When overloaded, a significant number of incoming particles probably struck previously deposited particles and bounced back into the airflow. A less stiff grease or wax might promote deeper penetration into the grease layer and improve retention (Turner and Hering, 1987).

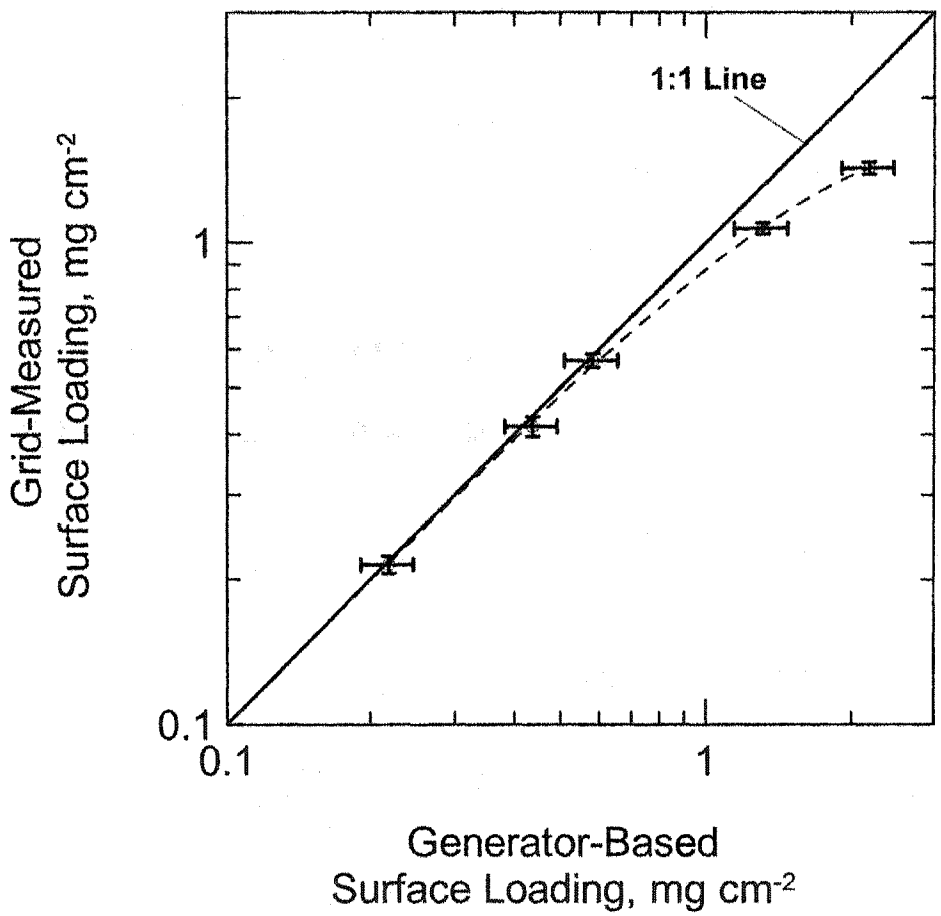

Figure 2.2: Loading capacity of a greased sampling grid. Error bars represent one standard deviation.

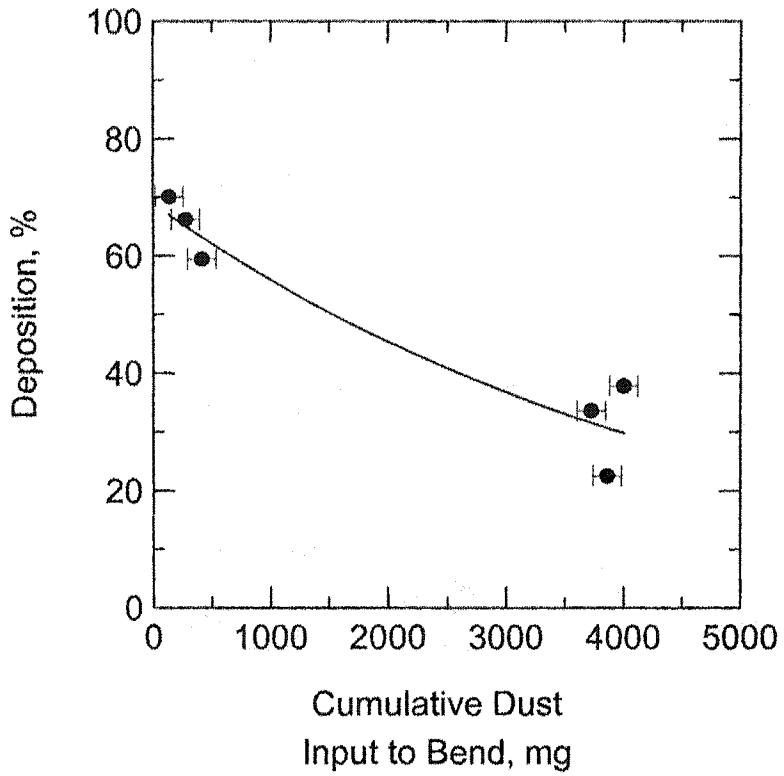

Figure 2.3: Particle deposition of a grease-coated bend as a function of cumulative mass of particles input. X-error bars represent the low and high values of cumulative dust during the sampling event. Y-error bars represent one standard deviation.

2. Effectiveness of the Bend Surface Coating

Figure 2.3 shows that the deposition of particles in the bend was sensitive to overloading. Deposition dropped from the initial 70% to 60% and 30% after 500 mg and 4000 mg were input to the bend, respectively. The decay in coating effectiveness was attributed to particle overload in the grease that coated the bend walls. Again, an alternative wax or grease that is less stiff at room temperature might improve retention (Turner and Hering, 1987). To avoid this problem, the interior of the bend was recoated frequently and cumulative mass input to the bend was limited to less than 100 mg between coatings.

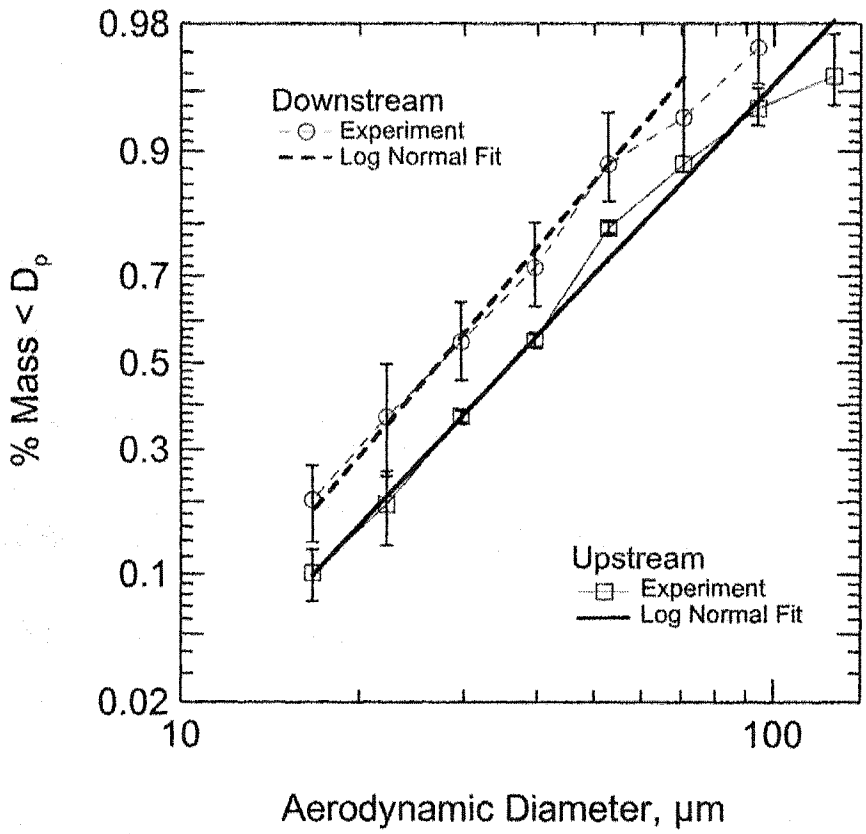

Figure 2.4: Cumulative mass distributions of particles collected upstream and downstream of the bend. Error bars represent one standard deviation.

3. Deposition in a Bend by Particle Size

Figure 2.4 provides cumulative mass distributions for the dust sampled upstream and downstream of the bend. Table 2.3 summarizes data from individual runs. Appendix C (identified as Test #7) presents raw experimental data. The r^2 values, all greater than 0.95, showed that the log-normal distribution fit the experimental data well. The mass median diameter was 27 µm downstream and 36 µm upstream of the bend, indicating preferential deposition of large particles. Consequently, the mean mass concentration downstream, 0.87 mg m^{-3}, was substantially less than the upstream concentration, 2.5 mg m^{-3}. The mean particle deposition for all combined particle sizes was 66%. This value is similar to that measured for the freshly grease-coated bend, as shown in Figure 2.3. The low variability associated with total mass concentration measurements, shown in Table 2.3, provided evidence of good accuracy and precision of sampling and recovery procedures.

Table 2.3: Summary of measurements made upstream and downstream of the bend.

Sampling Location	Replicate Number	MMAD µm	GSD	r^2	Mass Concentration mg m^{-3}
Upstream	1	35	1.84	0.99	2.5
	2	36	1.82	0.99	2.6
	3	38	1.81	0.96	2.5
	Mean =	36	1.83	0.98	2.5
	St. Dev. =	2	0.01	0.02	0.1
Downstream	1	23	2.00	0.95	0.90
	2	29	1.66	0.99	0.89
	3	28	1.64	0.96	0.82
	Mean =	27	1.76	0.97	0.87
	St. Dev. =	3	0.20	0.02	0.04
Overall Particle Deposition	1				64.8%
	2				65.3%
	3				66.8%
	Mean =				66%
	St. Dev. =				1.0%

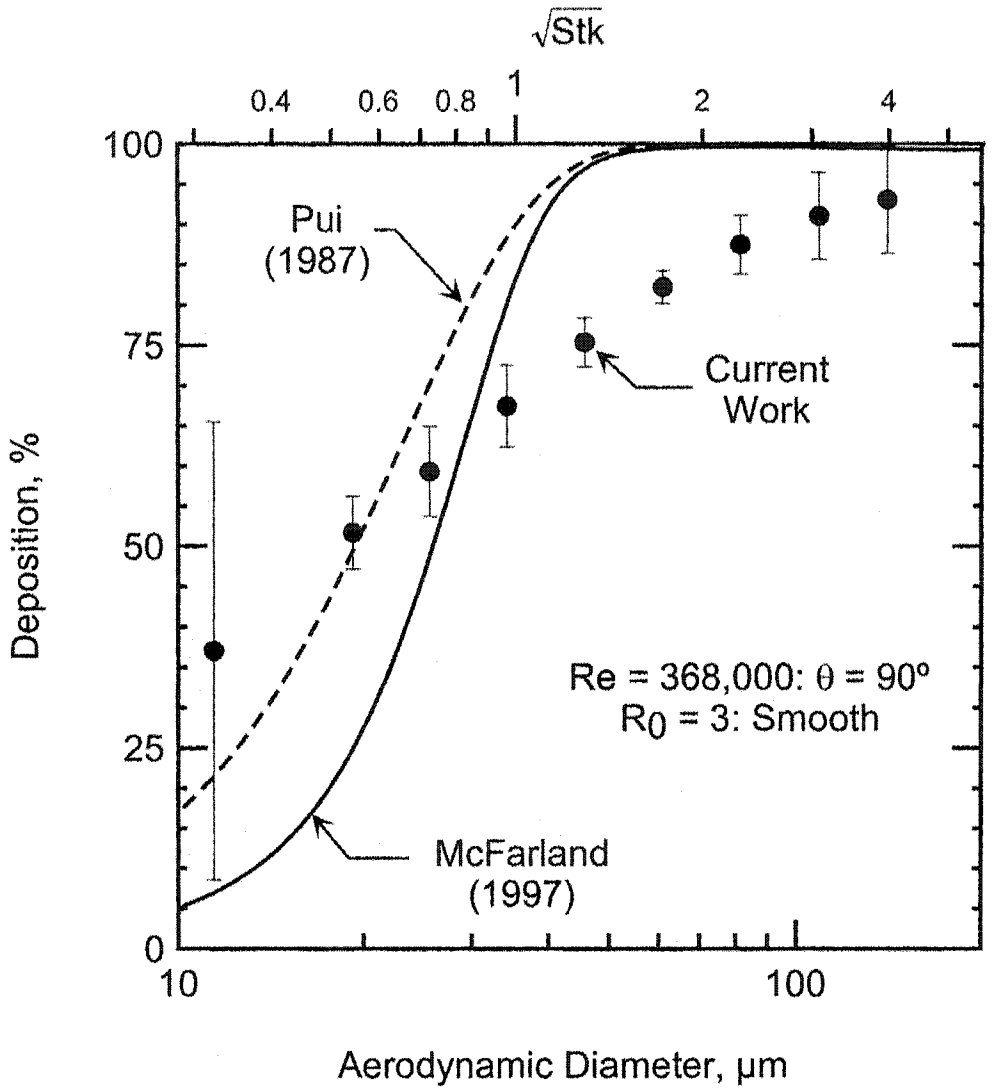

Figure 2.5: Deposition by size in a 90° bend measured experimentally and estimated using published models. Error bars represent one standard deviation.

Figure 2.5 shows particle deposition by size in the bend. Deposition increased from 35% for 15-μm particles to nearly 100% for 100-μm particles. Although the current test condition substantially departed from the experimental conditions used in constructing the Pui et al. (1987) and the McFarland et al. (1997) models, these results compared reasonably well with the two models. This agreement suggested that particle inertia, the basis for these models, was dominant over other flow features present in industrial bends at high Reynolds number.

Because the sampling and recovery procedures were highly reproducible, the variability in deposition measurements was attributed primarily to the sedimentation pipette analysis. This analysis introduced error in four processing steps (sedimentation, sample transfer, filtration, and weighing) and was then magnified through two mathematical operations (Equations 2.8 and 2.9). Although the sedimentation pipette offers a simple, direct, and inexpensive means of analysis, an alternative technique that directly measures particle differential mass without extra processing steps might be better suited for this purpose.

E. Summary and Conclusions

A new method is presented to measure particle deposition in industrial ducts. Greased wire sampling grids captured particles *in situ* upstream and downstream of a bend. Particles were recovered from the grid using a hexane extraction procedure. Cumulative mass distributions of the recovered particles were determined using a sedimentation pipette and were then used to calculate deposition by particle size. These procedures were compatible for solid particles only; to compare results obtained with this method to published models for bends, droplet behavior was simulated by coating the interior surface of the bend with grease to prevent particle bounce.

For particle surface loadings on the sampling grid less than 0.7 mg cm^{-2}, the total mass of collected samples was representative of particles in the duct and was highly reproducible. For greater surface loadings, the grease coating on the sampling grid became overloaded and caused an underestimation of particle mass. Similarly, the grease on the interior of the bend became less effective in capturing particles with increasing cumulative particle mass input. However, overloading was avoided by reapplying grease on the bend before a total of 100 mg input.

Particle deposition by size was measured in a 20.3-cm, 90° bend with an inlet velocity of 27.4 m s^{-1} to yield a Reynolds number of 368,000. Deposition increased from 35% for 15-μm particles to nearly 100% for 100-μm particles. For this limited comparison, the data generally agreed with published models for droplets in bends that were based on small diameter sampling tubes.

Although particle inertia impedes extractive sampling techniques, the method presented here leverages inertial properties of large particles to allow the measurement of particle deposition by size in industrial ducts. The method is simple, spatially integrated, and inexpensive. Moreover, sampling grids are adaptable to ducts of various sizes and shapes and can be used in field studies.

III. PARTICLE DEPOSITION IN INDUSTRIAL DUCT BENDS

A. Abstract

This work presents a study of particle deposition in industrial duct bends that have geometries and flow conditions similar to those used in industrial ventilation. As the interior surface of the duct bend was greased to prevent particle bounce, the results are applicable to liquid drops and solid particles where duct walls are sticky. Factors investigated were: (1) flow Reynolds number [Re = 203,000, 368,000]; (2) particle Reynolds number [$10 \leq Re_{p\infty} \leq 200$]; (3) particle Stokes number [$0.08 \leq Stk \leq 16$]; (4) bend angle [$\theta = 45°, 90°, 180°$]; (5) bend curvature ratio [$1.7 \leq R_0 \leq 12$]; (6) orientation [horizontal-to-horizontal and horizontal-to-vertical]; and (7) construction technique [smooth, gored, segmented]. Measured deposition was compared with models developed for bends in small diameter sampling lines ($Re < 20,000$; $Re_{p\infty} < 13$).

Whereas deposition measured in this work generally agreed with that estimated with models for particles smaller than 30 μm ($Stk < 0.7$), it was significantly less than that estimated for larger particles. The flow around larger particles was outside the Stokes regime; here, the models under-represented drag forces and over-estimated deposition. For particles larger than 20 μm, deposition was slightly greater in the horizontal-to-horizontal orientation than in the horizontal-to-vertical orientation due to gravitational settling. Penetration was not a multiplicative function of bend angle as theory predicts, due to the developing nature of turbulent flow in bends. Deposition in a smooth bend was similar to that in a gored bend; however, a tight radius segmented bend ($R_0 = 1.7$) exhibited much lower deposition. For more gradual bends ($3 \leq R_0 \leq 12$), curvature ratio had negligible effect on deposition.

B. Introduction

Particle deposition in ducts is important in situations ranging from the pneumatic transport of materials and icing of aircraft intakes to bioterrorist attacks. In occupational hygiene, the airflow velocity required to prevent particle deposition in ducts, commonly called the criterion of minimum transport velocity, serves as the basis for exhaust system design (ACGIH, 1998). Acceptable values for this criterion are available for solid particles that bounce upon contact with duct walls and are then re-entrained into the highly turbulent airflow of an industrial exhaust system (Baliff et al., 1948; DallaValle, 1932; Rajahns and Thompkins, 1967). However, the criterion of minimum transport velocity is not suited for liquid particles, especially oil droplets that adhere to the duct walls upon impact. Deposited droplets and particles can restrict airflow in branch lines, create fire hazards, cause failure of overhead supports, and present growth media for biological contaminants (Gregory et al., 1991; May and Berard, 1987).

This work focuses on the fate of droplets or solid particles where duct walls are sticky in bends of industrial ducts. The objectives are: (1) to measure deposition in industrial bends; and (2) to compare these measurements with estimates from published models.

C. Background

A bend introduces several scales of curvilinear motion to duct flow. The largest of these motions occurs as the bend reorients the direction of the airflow: its radius is of the size of the bend radius, R_b. As centrifugal force drives the central air core toward the outer wall, a smaller secondary flow develops perpendicular to the main flow. The size of the secondary flow is of the size of the duct radius, a (Ito, 1987), and its strength is characterized by the Dean number, De (Berger and Talbot, 1983): $De = Re/(R_0)^{1/2}$ where, R_0 is the radius of the bend divided by the radius of the duct ($R_0 = R_b/a$). For laminar flows ($De \leq 370$), flow rapidly becomes fully developed with a single pair of counter-rotating vortices (Berger and Talbot, 1983).

For turbulent flows ($De > 370$), experiments show that airflow continually develops throughout a 180° bend (Anwer et al., 1989; Azzola et al., 1986; Enayet et

al., 1982; Rowe, 1970). In this flow regime, further vortical structures can develop at various locations in the bend (Boersma and Nieuwstadt, 1996). For tight bends ($R_0 < 3$) with turbulent flow, separation can occur at the inner wall causing the replacement of the secondary flow with a single circulation pattern that switches direction at low frequency (Tunstall and Harvey, 1968). Rütten et al. (2001) characterized this phenomenon with the dimensionless Strouhal number.

Several mechanisms, including Brownian diffusion, gravitational setting, and electrostatic forces, can cause particles to deposit in ducts. In bends, the mechanism of inertial impaction dominates deposition for particles larger than 10 μm (Brockmann, 2001). Given sufficient inertial force, a particle will deviate from airflow streamlines and hit the bend wall. Deposition will occur if the adhesive forces are greater than the rebound forces (Hinds, 1999).

Particle deposition in bends has been characterized with the following dimensionless parameters: (1) particle Stokes number ($Stk = \tau U_0/a$); (2) particle free-stream Reynolds number ($Re_{p\infty} = D_p U_0/\nu$); (3) flow Reynolds number ($Re = D_{duct} U_0/\nu$), (4) De, and (5) R_0 (Cheng and Wang, 1975; Pui et al., 1987). All researchers have used Stk to describe results, but use of parameters such as R_0 and Re have been debated (Cheng and Wang, 1981; Crane and Evans, 1977; Pui et al., 1987).

For laminar flows ($De < 900$; $Re < 3000$), Tsai and Pui (1990) claimed increased deposition with increased secondary flow strength (De high and R_0 small) and used Stk, Re, De, and R_0 to describe their results. For moderately turbulent flows, Pui et al. (1987) used Stk alone to describe experimental measurements ($R_0 = 5.7$; $Re = 10{,}000$ and $6{,}000$; and $Re_{p\infty} < 13$) as: $\eta_{dep} = (1-10^{-0.963\,Stk})*100\%$. Brockmann (1993) modified this formula to include the bend angle in radians (θ):

$$\eta_{dep} = [1-\exp(-1.412\,Stk\,\theta)]*100\% \qquad (3.1)$$

McFarland et al. (1997) used Stk, θ, and R_0 to describe the fraction of particles penetrating a bend. Their correlation can be re-written in terms of deposition as:

$$\eta_{dep} = 100\% - \exp\left(\frac{4.61 + a_m \theta Stk}{1 + b_m \theta Stk + c_m \theta Stk^2 + d_m \theta^2 Stk}\right) \qquad (3.2)$$

where, a_m, b_m, c_m, and d_m are coefficients found using a curve-fitting program. However, an error appears in the published coefficient for the second term in the numerator of coefficient d_m. Equation 13 of McFarland et al. (1997) should read:

$$a_m = -0.9526 - 0.05686 R_0$$
$$b_m = \frac{-0.297 - 0.0174 R_0}{1 - 0.07 R_0 + 0.0171 R_0^2}$$
$$c_m = -0.306 + \frac{1.895}{\sqrt{R_0}} - \frac{2.0}{R_0} \qquad (3.3)$$
$$d_m = \frac{0.131 - 0.0132 R_0 + 0.000383 R_0^2}{1 - 0.129 R_0 + 0.0136 R_0^2}$$

For highly turbulent flow, Hacker et al. (1953) investigated deposition of water drops entering aircraft intakes (700,000 ≤ Re ≤ 3,700,000). Using a two-dimensional potential flow simulation, they demonstrated that $Re_{p\infty}$ strongly influenced deposition. Crane and Evans (1977) suggested that $Re_{p\infty}$ could affect deposition to a greater extent than R_0. Their analysis estimated that for Stk = 0.7 and R_0 = 4 deposition would decrease from 58% for $Re_{p\infty}$ of 0, to 52% for $Re_{p\infty}$ of 5, and to 26% for $Re_{p\infty}$ of 450.

In industrial ventilation ducts, recommended minimum transport velocity ranges from 10 m s^{-1} for welding fumes to 30 m s^{-1} for heavy or moist dusts (Alden and Kane, 1982). Given a transport velocity of 20 m s^{-1}, the flow Re increases from 130,000 to 1,300,000 as the diameter of industrial duct increases from 0.1 m to 1 m. Typical values of R_0 are between 3 and 5; cost factors generally limit the use of bends with large R_0, and high pressure drop prevents widespread use of bends with small R_0 (ACGIH, 1998). Given these restrictions, De in industry is approximately 30,000 to 500,000. For particles of unit density, Stk ranges from 0.01 to 4, and $Re_{p\infty}$ ranges from 1 to 300 for particles of 10 μm to 100 μm, respectively.

Previous work is inadequate to describe particle behavior in industrial bends. The correlation models of Pui et al. (1987) and McFarland et al. (1997) were constructed using experimental data atypical of industry: small particles (D_p < 10 μm), small diameter tubes (D_{duct} < 1.6 cm), and moderately turbulent flow (Re < 19,000). The theoretical studies of Hacker et al. (1953) and Crane and Evans (1977) are useful in a qualitative sense, but are difficult to apply to a new set of

conditions and have no experimental backing. Moreover, past research has been limited to bends with smooth interior walls, when in reality, the interior of industrial bends is rarely smooth because of the manner in which they are constructed. Thus, the experiments presented in the current work are the first to be directly applicable to industrial bends.

D. Methods

1. Particle Deposition

Particle deposition by size was measured with the methods presented by Peters and Leith (Peters and Leith, in press); a brief overview of this method is provided here. Figure 3.1 illustrates the experimental set-up. Upstream of the test bend, an aerosol generator introduced polydisperse glass spheres that ranged in size from 5 μm to 150 μm. To capture and retain particles that hit the wall, the interior of the bend was coated with petroleum jelly. Circular sampling grids were cut from welded-wire mesh, coated with petroleum jelly, and alternately inserted into the duct upstream and downstream of the bend. Upstream velocity profiles were characteristic of fully developed pipe flow (Tennekes and Lumley, 1972), and particle profiles were uniform in concentration and size distribution.

After sampling, the collected particles were recovered from the grids using a hexane extraction procedure and then sized using a sedimentation pipette (Silverman et al., 1971). Cumulative mass distributions were fitted with a log-normal distribution; all distributions were fit with $r^2 > 0.8$. From these distributions, deposition was calculated for each size interval (i) as:

$$\eta_{dep,i} = \left(1 - \frac{dM_{i,down}}{dM_{i,up}}\right) \tag{3.4}$$

where $dM_{i,down}$ is the downstream and $dM_{i,up}$ is the upstream interval mass associated with the log-normal fit.

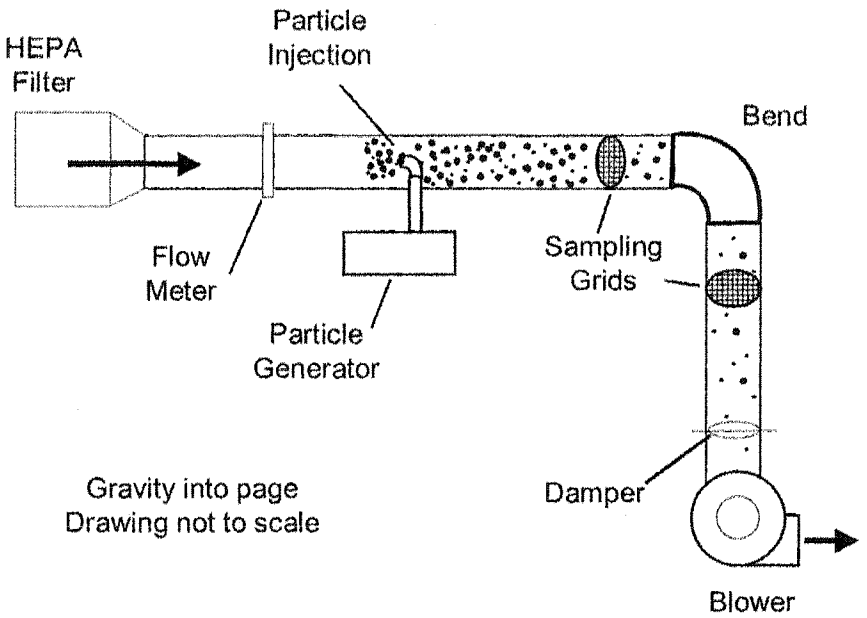

Figure 3.1: Experimental set-up.

2. Experiments

Table 3.1 lists the eight test conditions investigated. A base condition was selected as: Re = 203,000; R_0 = 5; construction = smooth; and orientation = horizontal-to-horizontal (H-H). Re of 203,000 was achieved in a 0.152 m duct at an average velocity of 20.0 m s^{-1}. Given these conditions, $Re_{p\infty}$ ranged from 10 to 150, Stk ranged from 0.1 to 16, and De was 91,000. The base conditions were modified to evaluate how duct orientation, bend angle, and bend construction affect particle deposition. For the last two conditions in Table 3.1, Re was 368,000 in a 0.203 m duct with an average velocity of 27.1 m s^{-1}. All tests were conducted in a H-H orientation except for one test, where the air entered the bend horizontally and exited vertically (H-V). Deposition by size was measured three times for each test condition.

Figure 3.2 depicts the bend construction types investigated. Smooth bends (Figure 3.2a) were manufactured by bending straight tubing or fabricated by welding together two stamped halves. The gored bend (Figure 3.2b) was constructed by welding sections of sheet metal together. The interior surface of the gored bend deviated from a smooth bend in that: (1) the welded seams protruded into the duct

Table 3.1: Test conditions investigated. Bold, italic font identifies parameters that deviate from the base condition.

Test Description	Re (De)	θ	R_0	Construction	Orientation
Base[a]	203,000 (91,000)	90°	5	Smooth	H-H
Base + Orientation[a]	203,000 (91,000)	90°	5	Smooth	***H-V***
Base + Bend Angle[b]	203,000 (91,000)	***180°***	5	Smooth	H-H
Base – Bend Angle[c]	203,000 (91,000)	***45°***	5	Smooth	H-H
Base + Construction[d]	203,000 (91,000)	90°	5	***Gored***	H-H
Base – Construction[e]	203,000 (156,000)	90°	***1.7***	***Segmented***	H-H
High Re, Small R_0[f]	***368,000 (212,000)***	90°	***3***	Smooth	H-H
High Re, Large R_0[g]	***368,000 (106,000)***	90°	***12***	Smooth	H-H

[a] H-P Products, Louisville, OH; P/N EL-602-Z
[b] two 90° bends as specified in footnote a butted together to form a 180° bend
[c] H-P Products; P/N EL-601-Z
[d] McGill Airflow Corp., Groveport, OH; Custom 5-piece, Gored, 6-inch, 90° bend
[e] McMaster-Carr, Atlanta, GA; P/N 1766K34
[f] W.H. Brady, Inc., Elkton, MD; P/N 90S, 8-inch diameter
[g] H-P Products; P/N 14-800321-Z

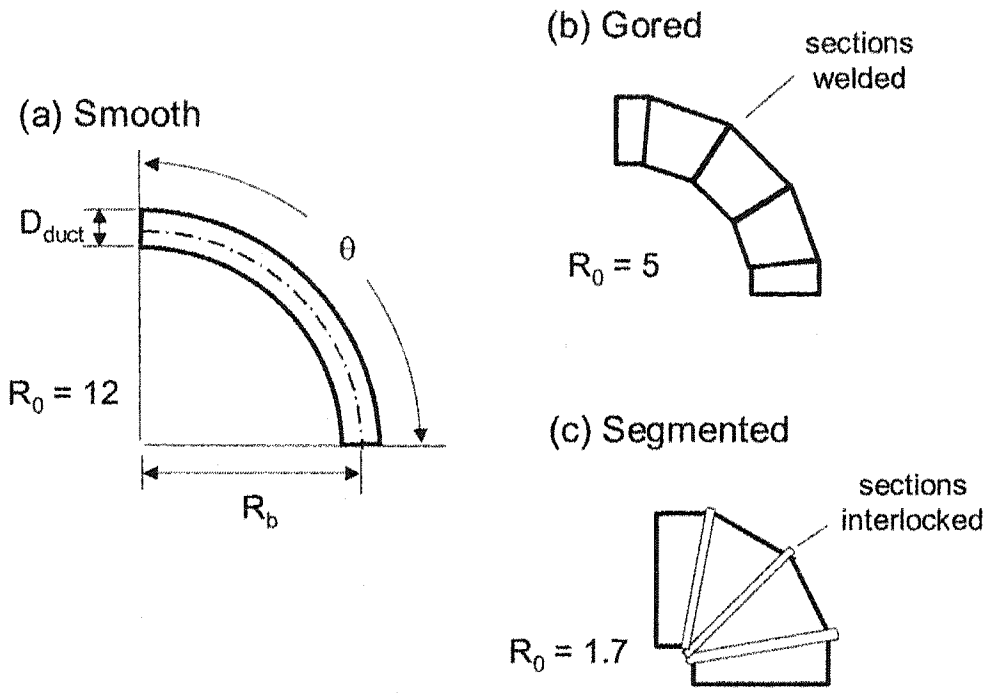

Figure 3.2: Industrial bends and identification of key dimensions.

perpendicular to the main direction of airflow; and (2) the bend's sectional construction presented flat surfaces to the airflow. The segmented bend (Figure 3.2c) was joined by interlocking sheet-metal sections. Most segmented bends have small R_0; the bend tested in this work had an R_0 of 1.7.

3. Statistical Analysis

The combined data from the three runs for each test condition were fitted with a cumulative log-normal function (Cooper, 1982). The cutpoint (D_{50}), or the particle size associated with 50% deposition, and the geometric standard deviation (GSD), a descriptor of the shape of the deposition curve, were estimated from the fitted function. The parameter estimates of the fitted function were used to investigate the similarity in deposition by size for different test conditions.

Table 3.2: Fit results.

Test Conditions	r^2	D_{50}, µm	GSD
Base	0.94	18.1	2.3
Base + Orientation (H-V)	0.94	20.5	2.9
Base + Bend Angle (θ = 180)	0.76	12.5	2.3
Base - Bend Angle (θ = 45)	0.92	105.4	24.9
Base + Construction (Gored)	0.97	18.2	2.9
Base – Construction (Segmented; R_0=1.7)	0.61	39.5	2.7
High Re; Small R_0	0.88	21.4	3.0
High Re; Large R_0	0.80	19.5	3.7

4. Model Comparison

For each test condition, experimental results were compared with deposition estimated with the Pui et. al (1987) model, Equation 3.1, and the McFarland et. al (1997) model, Equation 3.2.

E. Results

Table 3.2 provides the fit r^2 value, D_{50}, and GSD for each test condition. Appendix C provides all raw experimental data. The cumulative log-normal distribution explained greater than 76% of the variability in the experimental data for seven of the eight test conditions. The lowest r^2 value (0.61) was observed for the test with the segmented bend.

Figure 3.3 compares deposition by size for the base condition (H-H orientation) to H-V orientation and to model estimates from Equation 3.1 and 3.2. The deposition curve was slightly steepter in the H-H orientation than in the H-V orientation (p= 0.001). The deposition curves for both H-H and H-V orientations were shallower than those estimated with either model. For particles smaller than

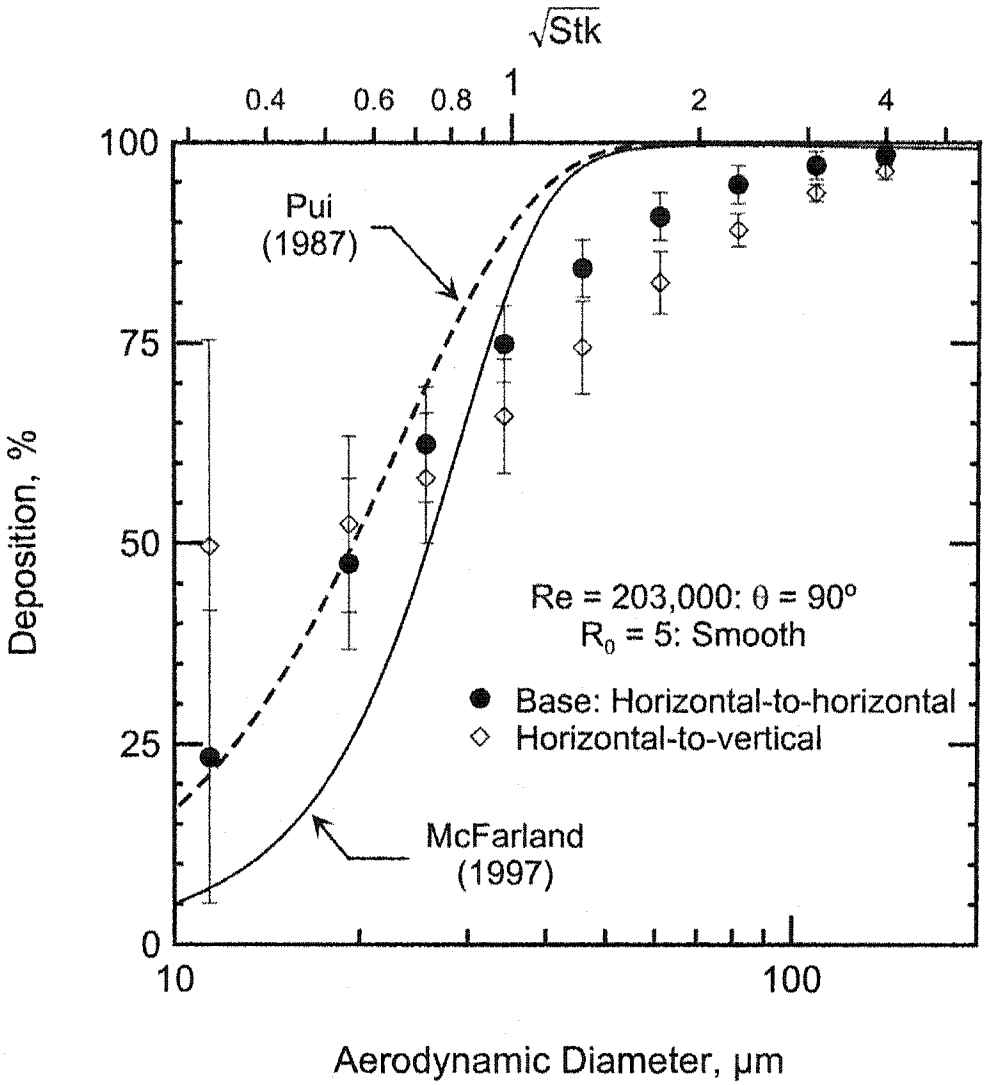

Figure 3.3: Deposition by particle size: orientation varied.

30 µm, the experimental data overlapped with Pui et al. (1987) model estimates, but measured deposition was substantially greater than that estimated with the McFarland et al. (1997) model. For larger particles, measured deposition was substantially less than that estimated with either model.

Figure 3.4 shows deposition by size as a function of bend angle. For a given particle size, deposition increased with bend angle. For $\theta = 45°$, deposition increased from 15% at 10 µm to 45% at 80 µm. For larger bend angles, deposition neared 100% for 100 µm particles.

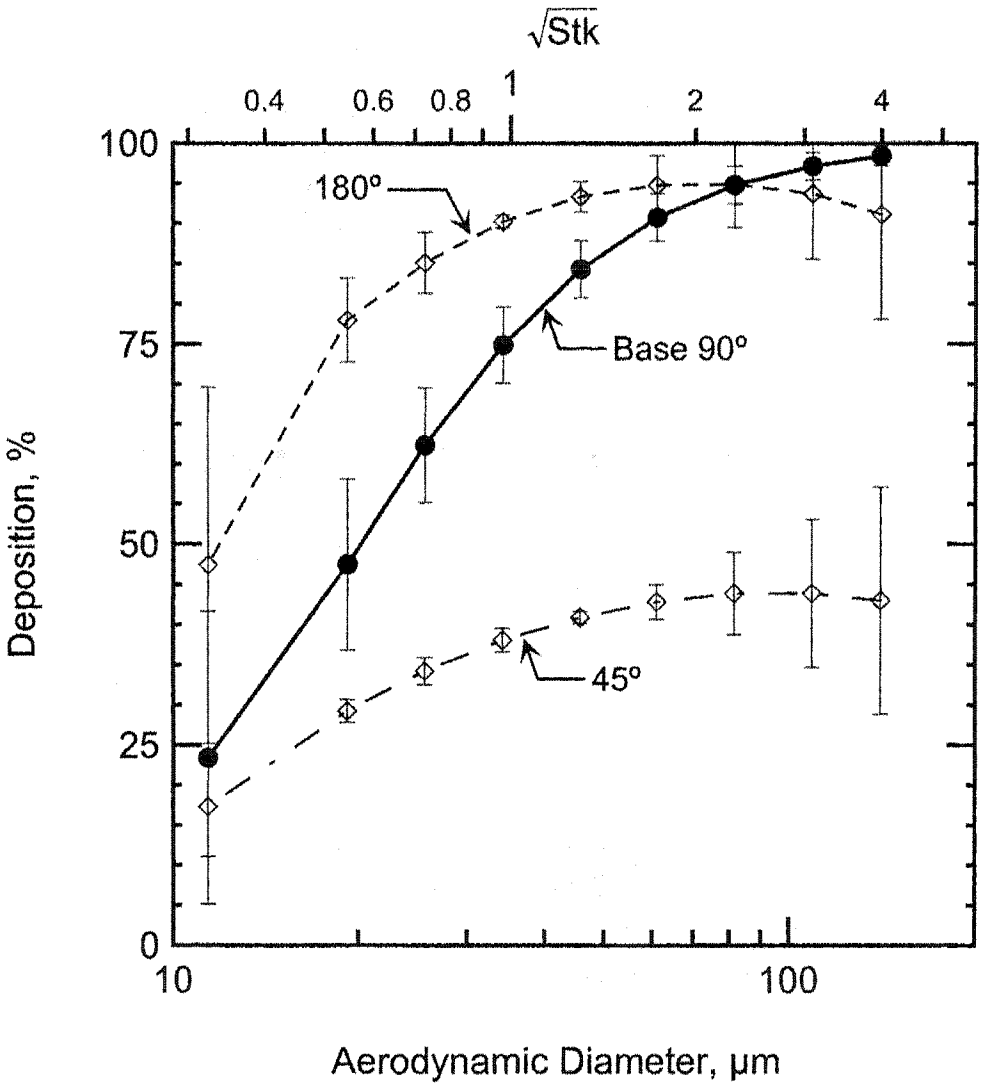

Figure 3.4: Deposition by particle size: bend angle varied.

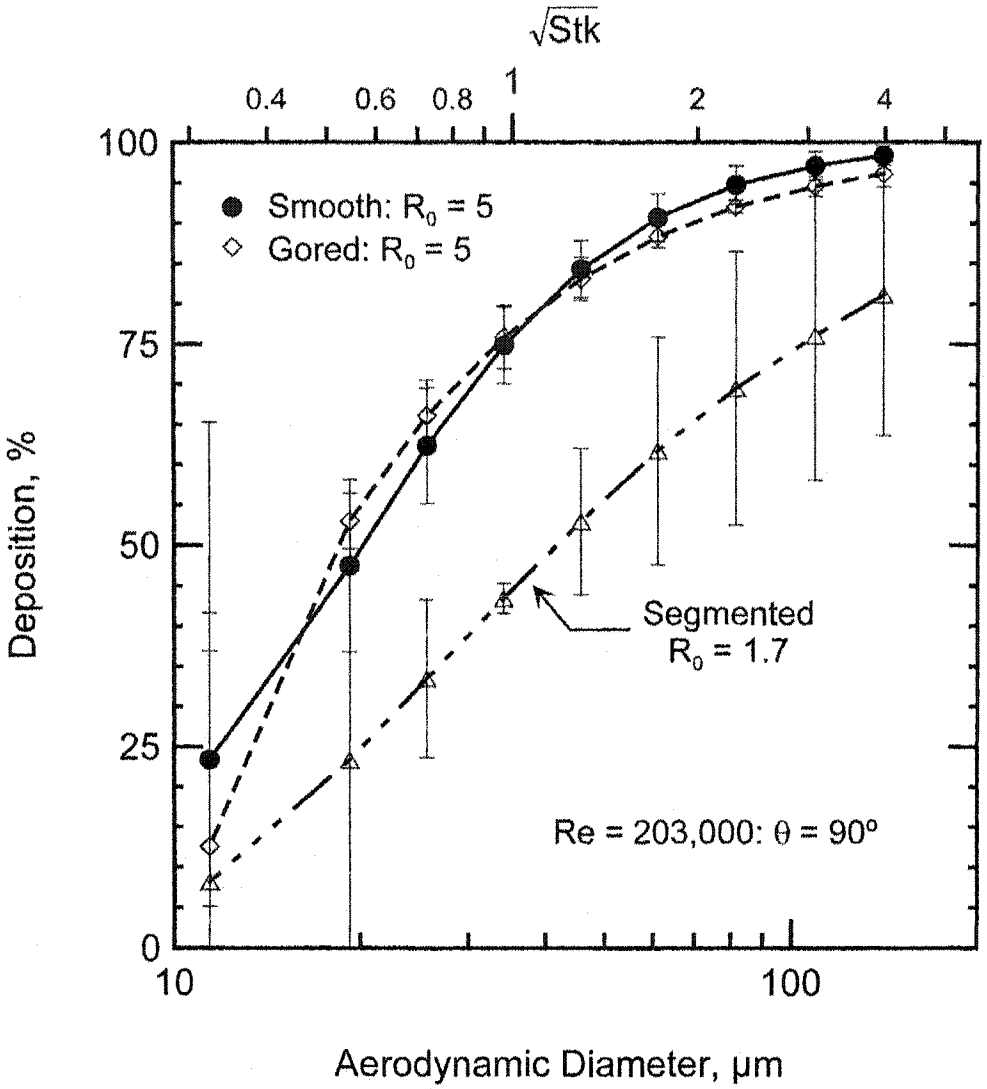

Figure 3.5: Deposition by particle size: bend construction varied.

Figure 3.5 presents deposition by size for bends of different construction. Deposition in the smooth bend was similar to that in the gored bend, but was substantially and significantly greater than that in the segmented bend. The deposition cutpoint for the segmented bend (D_{50} = 39.5 µm) was significantly larger than that for the smooth bend (18.1 µm, $p < 0.001$).

Figure 3.6 compares deposition by size measured in bends with two curvature ratios to that estimated with the models. Deposition measured in the tight bend (R_0 = 3) was statistically equivalent to that in the gradual bend (R_0 = 12): $p = 0.53$ for D_{50} values and $p = 0.23$ for GSD values. Whereas the experimental results compared favorably with Pui et al. (1987) model estimates for particles smaller than

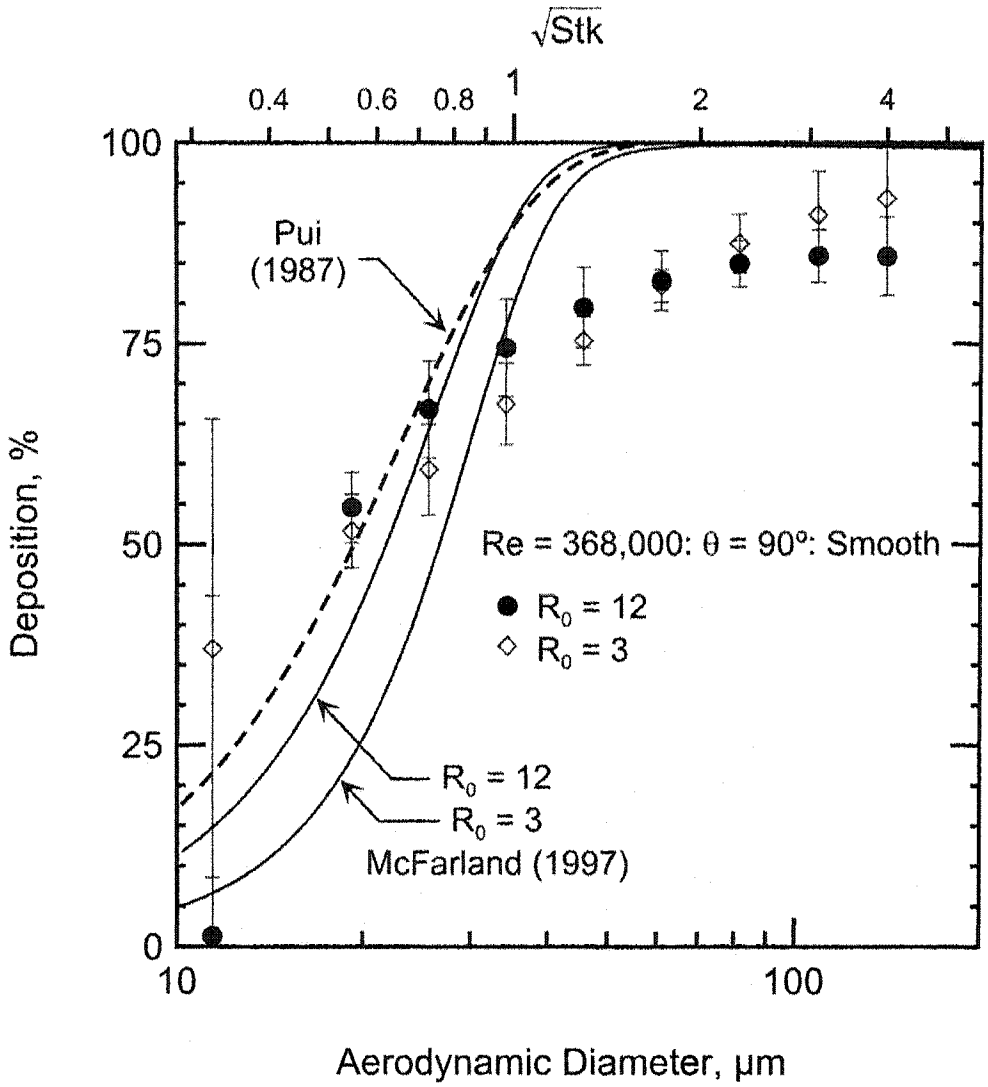

Figure 3.6: Deposition by particle size: curvature ratio varied.

30 µm, measured deposition was greater than that estimated with the McFarland et al. (1997) model. For particles larger than 30 µm, measured deposition was substantially lower than that estimated with either model.

F. Discussion

As shown in Figures 3.3 and 3.6, deposition by size in industrial bends was not fully described by models developed for small sampling tubes. Whereas the experimental data in this work compared favorably with Pui et al. (1987) model estimates for particles smaller than 30 µm (Stk < 0.7), it was substantially lower than

that estimated for larger particles. Moreover, the differences between measurement and models became greater when the flow Reynolds number increased from Re = 203,000 (Figure 3.3) to Re = 368,000 (Figure 3.6).

For relatively small particles, the agreement between the deposition measured here and that estimated with the Pui et al. (1987) model illustrates the importance of Stk in estimating deposition in bends. Furthermore, the agreement suggests that deposition is dominated by large-scale curvilinear motion as opposed to the more subtle airflow features. The region where models over-estimated deposition is consistent with non-Stokesian drag effects and airflow turbulence.

Some data associated with the smallest particle size (near 10 μm) had relatively large error bars and did not follow expected trends. For example, in Figure 3.3, the difference in deposition between orientations should diminish as particle size becomes smaller and gravity becomes less important; this trend was observed for all but the smallest diameter particle where the error bars were large. As discussed in (Peters and Leith, accepted), the sedimentation pipette was optimized to size large particles, and thus, suffered from greater uncertainty for the smallest particle size measured. The analysis technique might be optimized for smaller particles, or perhaps more practical, alternative real-time, in-situ methods might be used to determine deposition for particles of this size and smaller.

Figure 3.7 compares Re_{pr} by particle size for the current experiments to that used to build the models. Re_{pr} was calculated as: $Re_{pr} = D_p V_r / \nu$, where V_r is the radial velocity of the particle. V_r was estimated from a balance of outward centrifugal forces and drag forces for a particle in the centerline of the bend. Plug flow was assumed in this estimation and calculations were carried out in an iterative routine in a spreadsheet macro (see Appendix D). For the Pui et al. (1987) and McFarland et al. (1997) data, V_r was estimated from conditions they reported. For conditions in the current work where Re_{pr} was less than that of the models (i.e., $Re_{pr} < 3$ for particle sizes smaller than 30 μm), the models acceptably represented drag forces and experiments done here agreed with the model estimates. However, as Re_{pr} became progressively greater than 3, (i.e., particles larger than 30 μm), the models increasingly under-represented drag forces and over-estimated deposition.

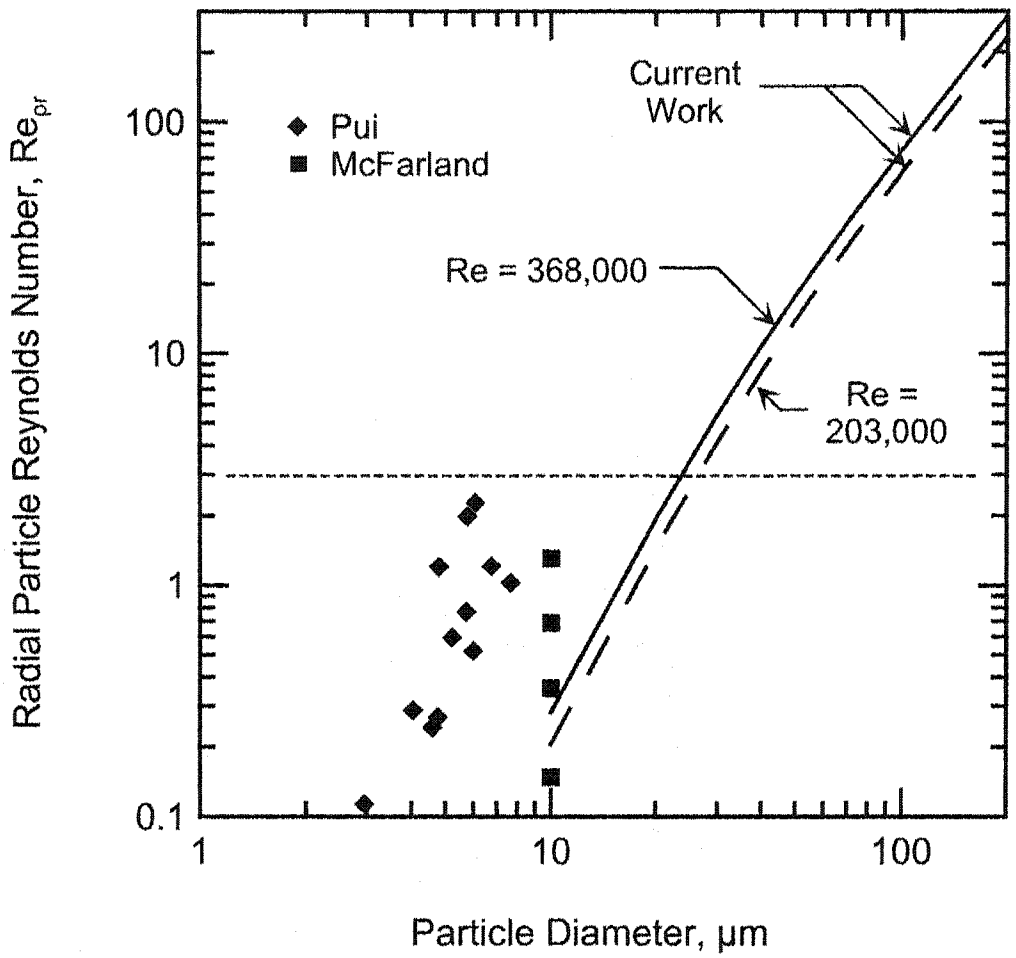

Figure 3.7: Particle radial Reynolds number by size in this work and the experimental work used to develop the models of Pui et al. (1987) and McFarland et al. (1997).

Airflow turbulence might also explain some model over-estimates. Torobin and Gauvin (1961) showed that free-stream turbulence decreases the critical Reynolds number where the flow over a particle transitions from laminar to turbulent. Thus, drag forces were further under-represented in the models. Crowe et al. (1998) provided equations to account for this behavior that might be useful in future modeling efforts.

As shown in Figure 3.3, the deposition curve for an H-H oriented bend was steeper than that for an H-V oriented bend. When oriented H-H, gravity caused particles to settle throughout the length of the bend. As gravitational settling is

proportional to the square of particle size, deposition in the H-H orientation was greater than that in the H-V orientation for particles larger than about 20 μm.

Theory predicts that percent particle penetration, $P_{\%} = 100\% - \eta_{dep}$, is a multiplicative function of bend angle. Thus, deposition in the 90° and 180° bends can be estimated as $100\% - P_{\%,45}^2$ and $100\% - P_{\%,45}^4$, respectively. This relationship generally holds for particles smaller than 20 μm, but not for larger particles (Figure 3.4). As turbulent flow in a bend develops continuously, sufficient curvilinear motion to deposit large particles was not established by a bend angle of 45°. Better agreement was observed between deposition measured in the 180° bend and that estimated as $100\% - P_{\%,90}^2$, suggesting that most flow development had occurred by a bend angle of 90°.

As shown in Figure 3.5, deposition by size was nearly identical for the smooth and gored bends; however, it was substantially lower and exhibited the greatest variability in the segmented bend. Relatively clean laboratory air might have leaked into the segmented bend through its interlocking joints, providing a clean air sheath at the bend walls that reduced deposition. As the interior of the bend was recoated with grease when sampling was switched from the upstream to the downstream position, the leaks through the interlocking joints might have changed between runs, explaining the relatively high variability in measurements for this test condition. Alternatively, the segmented bend had a very tight curvature ratio ($R_0 = 1.7$) compared to the other bends tested ($R_0 > 3$). As noted by Tunstall and Harvey (1968) and Rütten et al. (2001), drastically different airflow patterns are anticipated in a tight bend at these flow conditions due to flow separation at the inner wall; these differing airflow patterns may account for reduced deposition.

For more gradual bends ($3 \leq R_0 \leq 12$), deposition by particle size was relatively unaffected by curvature ratio (Figure 3.6). Deposition was slightly greater in the gradual bend ($R_0 = 12$) as compared to that in the tight bend ($R_0 = 3$). Although estimates made with the McFarland et al. (1997) model qualitatively agree with this trend, the difference in estimated deposition was greater than that observed in the experiments.

The major limitation of the present work was that the inlet profiles were uniform in terms of the velocity, particle size distribution, and particle concentration. In industrial settings, deviations from such uniform conditions often occur. More work is required to evaluate how deposition changes as inlet conditions become non-uniform.

G. Conclusion

This work explored particle deposition by particle size in industrial duct bends. Because the interior surface of the duct bend was greased to prevent particle bounce, the results are applicable to liquid drops and solid particles where duct walls are sticky. These experiments are the first of their kind for conditions typical of industry. As such, they should be useful to construct models appropriate for industrial conditions and to benchmark computer simulations.

A new model is required to describe particle deposition in industrial bends adequately. The high radial velocity that large particle experience in industrial bends represents a substantial departure from conditions in small diameter sampling lines, for which the models of Pui et. al (1987) and McFarland et. al (1997) were developed. Thus, these models under-represent drag forces and over-estimate deposition in industrial bends. Further, the current work suggests that gravitational settling causes differences in deposition with orientation. Bend angle is important in estimating deposition for particles larger than 30 μm. In contrast, curvature ratio is relatively unimportant for R_0 between 3 and 12.

IV. MODELING PARTICLE DEPOSITION IN INDUSTRIAL DUCT BENDS

A. Abstract

A new model is presented to describe particle deposition in 90° bends of industrial ducts. This model accounts for non-Stokes particle motion and for variable deposition patterns as a function of particle Stokes number. Estimates made with the new model and with two models previously published were compared to measurements of deposition in bends with geometries, particle characteristics, and airflow conditions similar to those found in industry: large duct diameters (15.4 cm and 20.3 cm); large particle sizes (5 μm to 150 μm); and turbulent airflow (Re = 203,000 and Re = 368,000). Whereas the two models published previously explain 30% or less of the variability in the data, the new model explains 85%. The mean residual with the new model, 0.6%, is nearer to zero than that of the two other models, 3.6% and 9.8%. The new model is applicable to mists and to solid particles that stick to bend walls.

B. Introduction

Industrial ducts are prevalent in modern buildings; they supply conditioned air and exhaust contaminated air. When particles deposit in these ducts, problems can arise that range from sick building syndrome in office buildings (Muhic and Butala, 2004) to fires in restaurant kitchens (Gerstler, 2002). In factories, particles that deposit in exhaust ducts can restrict airflow, create fire hazards, cause failure of overhead supports, and present growth media for biological contaminants (Gregory et al., 1991; May and Berard, 1987).

Models are available to estimate particle deposition as a function of duct geometry, airflow conditions, and particle characteristics. Generally, the deposition of particles smaller than 20 μm from laminar airflow is well understood (Brockmann, 2001). However, industrial ducts commonly transport particles larger than 20 μm in

highly turbulent airflow (100,000 < Reynolds number, Re < 1,000,000). Although Sippola and Nazaroff (2003) provide a model to estimate particle deposition in straight, rectangular ducts at high Re, models remain unavailable to estimate the deposition of large particles in bends under turbulent airflow conditions.

For moderately turbulent flow (Re < 10,000), Pui et al. (1987) used a well-mixed model to describe particle deposition in small-diameter bends. McFarland et al. (1997) empirically modeled numerical simulations of particle impaction in bends for Re up to 19,800. Peters and Leith (accepted) identified inadequacies in these models when applied to round bends in industrial exhaust systems. Specifically, they showed that these models under-represent drag force and over-estimate deposition when particle motion is outside the Stokes regime. Further, they identified small but significant differences in particle deposition with changes in bend orientation.

The present work develops a new model to describe particle deposition in round, 90° bends for conditions typical of industry.

C. Methods

1. Data Set

The data used here were taken from Peters and Leith (accepted) for tests in which the bend angle was 90° (Table 4.1). In each test, particle deposition was measured versus particle size in triplicate. In Test #1, they identified a base condition as: Re = 203,000, smooth internal walls (Figure 4.1a), curvature ratio (R_0) of 5, and orientation such that air entered and exited the bend horizontally (H-H). In Test #2, they modified the base condition so that air entered the bend horizontally and exited vertically (H-V), and in Test #3, so that the construction of the bend was gored (Figure 4.1b). They conducted the remaining tests with Re = 368,000: in Test #4 the bend curved tightly (R_0 = 3) and in Test #5 the bend curved gradually (R_0 = 12). Appendix C presents detailed experimental data from these tests.

Table 4.1: Test conditions for 90° bends. Bold, italic font identifies parameters that deviate from the base condition.

Test	Test Description	Re (De)	R_0	Construction	Orientation
1	Base	203,000 [a] (91,000)	5	Smooth	H-H
2	Base + Orientation	203,000 (91,000)	5	Smooth	***H-V***
3	Base + Construction	203,000 (91,000)	5	***Gored***	H-H
4	High Re, Small R_0	***368,000*** [b] ***(212,000)***	***3***	Smooth	H-H
5	High Re, Large R_0	***368,000*** ***(106,000)***	**12**	Smooth	H-H

[a] $U_0 = 20.0$ m s^{-1}; $D_{duct} = 0.152$ m.
[b] $U_0 = 27.1$ m s^{-1}; $D_{duct} = 0.203$ m.

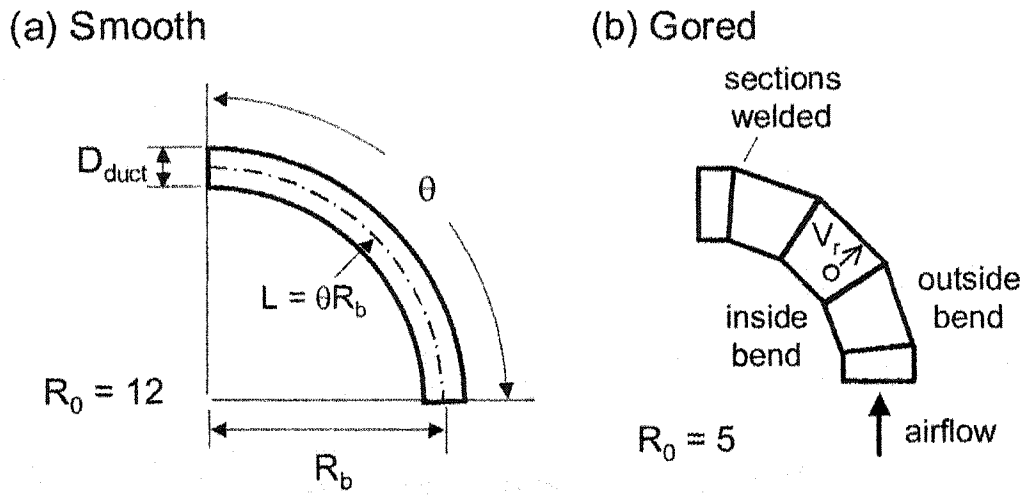

Figure 4.1: Schematic diagram of bends: (a) Smooth; and (b) Gored.

2. Model Formulation

The new model considered particle deposition due to gravitational settling and inertial impaction. The fraction of particles that penetrate through a duct due to gravitational settling, P_{grav}, was estimated as:

$$P_{grav} = \exp\left(-\frac{4V_{ts}L}{\pi D_{duct}U_0}\right) \quad (4.1)$$

where V_{ts} is the terminal settling velocity of the particle, L is the length through which gravity contributes to deposition, D_{duct} is the duct diameter, and U_0 is the airflow velocity entering the bend (Brockmann, 2001). In comparison to inertial impaction, gravitational settling was relatively unimportant for particle sizes up to 140 μm. Thus, the effect of gravity was not included in the model developed.

For inertial impaction, the assumption of well-mixed conditions allows the fraction of particles that penetrates a bend (P) to be expressed as:

$$P = \exp\left(-\frac{A_e V_r}{Q}\right) = \exp\left(-\frac{A_e V_r}{\pi a^2 U_0}\right) \quad (4.2)$$

where V_r is velocity with which the particle moves radially toward the outer wall of the bend, A_e is the effective deposition surface area, Q is the airflow rate, a is the duct radius, and U_0 is the inlet air velocity (Pui et al., 1987). Assuming negligible

particle acceleration time and rotational airflow, the centrifugal force was balanced with the Newtonian drag force to estimate V_r as:

$$V_r = \sqrt{\frac{4D_p\rho_p U_0^2}{3R_b\rho_f C_D}} \tag{4.3}$$

where D_p is the particle diameter, ρ_p is the particle density, R_b is the centerline radius of curvature of the bend, ρ_f is the fluid density, and C_D is the coefficient of drag. C_D is a function of particle Reynolds number (Re_p), which is a function of V_r. According to Hinds (1999), V_r can be estimated by iterating Equation 4.3 and the following equation:

$$C_D = \frac{24}{Re_p}\left(1 + \frac{Re_p^{2/3}}{6}\right) \tag{4.4}$$

Secondary airflow in a bend causes the effective deposition area term, A_e, in Equation 4.2 to be a fraction of the total internal surface area of the bend, f:

$$A_e = f\,2\,\pi\,a\,L = f\,2\,\pi\,a\,R_b\,\theta \tag{4.5}$$

where L is the axial length of the bend, and θ is the angle in radians through which the bend sweeps. With substitutions, Equation 4.2 becomes:

$$P = \exp\left(-2f\frac{V_r R_b \theta}{aU_0}\right) \tag{4.6}$$

In industrial ducts, particle motion is often outside the Stokes regime; thus, a transition Stokes number (Stk_T) was formulated as:

$$Stk_T = \frac{\text{distance traveled by particle}}{\text{distance required to hit wall}} = \frac{V_r t}{a} = \frac{V_r R_b \theta}{aU_0} \tag{4.7}$$

where t is the time for the air to pass through the bend. And, penetration is:

$$P = \exp(-2\,f\,Stk_T) \tag{4.8}$$

Whereas Stk_T is easily estimated from experimental conditions, the factor f requires more consideration.

As depicted in Figure 4.2, the value of f depends on particle Stokes number. For small Stokes numbers, particles are easily entrained by the secondary flow and particle deposits occur over a relatively large surface area (Figure 4.2a). Thus,

$$\lim_{Stk_T \to 0}(f) = 1 \tag{4.9}$$

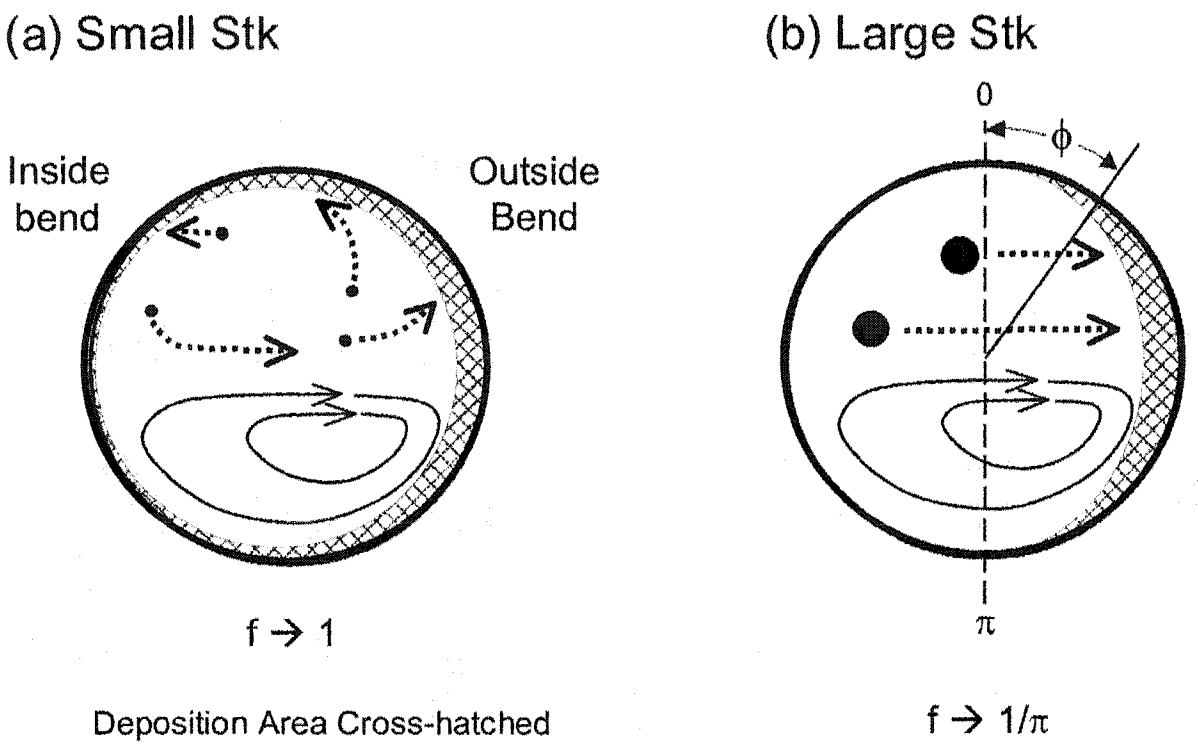

Figure 4.2: Duct cross-section showing the secondary flow (lower half of duct) and particles entrained in this flow (upper half of duct) for: (a) Small Stk; and (b) Large Stk.

For large Stokes numbers, particles are relatively unaffected by the secondary flow and the vector of outward radial velocity is directed solely towards the outside wall (Figure 4.2b). Here, f is the integrated component of outward radial velocity normal to the outside wall, $V_r \sin(\phi)$, divided by V_r and the duct circumference in radians:

$$f = \frac{V_r \int_0^{\pi} \sin(\phi) d\phi}{V_r\, 2\pi} = \frac{-\cos(\phi)|_0^{\pi}}{2\pi} = \frac{1}{\pi} \qquad (4.10)$$

Thus,

$$\lim_{Stk_T \to \infty} (f) = \frac{1}{\pi} \qquad (4.11)$$

A semi-empirical relationship was developed to describe f between these limits. Equation 4.8 was rearranged as:

$$f = -\frac{\ln(P_x)}{2\, Stk_T} \qquad (4.12)$$

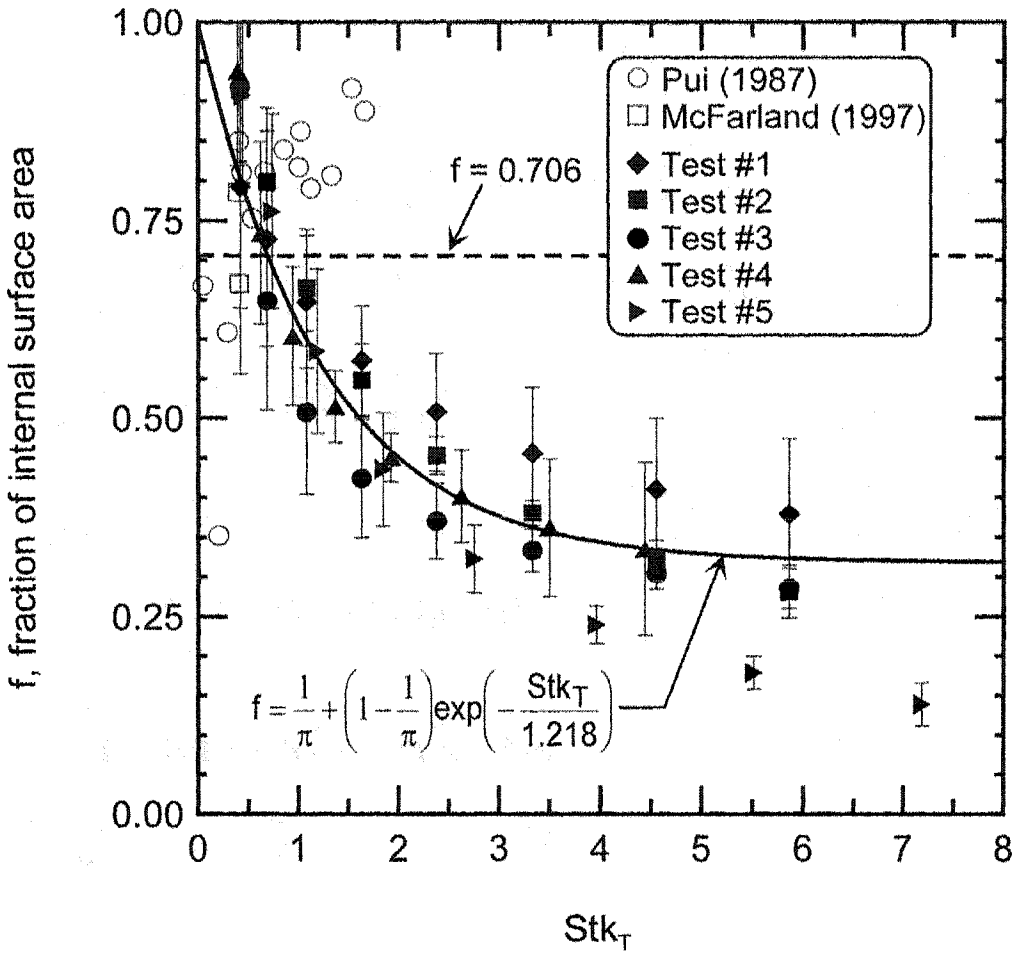

Figure 4.3: Fraction of total internal surface area where particles deposit, f, versus Stk_T.

where P_x is fractional penetration from the data set. As shown in Figure 4.3, f values approached the limits discussed above for small and large Stk_T. These data were fit with the following three-parameter model:

$$f = \frac{1}{\pi} + \left(1 - \frac{1}{\pi}\right)\exp\left(-\frac{Stk_T}{1.218}\right) \qquad (4.13)$$

Two of the three parameters in Equation 4.13 came from the limits for f: the first term from Equation 4.11 and the coefficient of the second term from Equation 4.9. The factor of 1.218 came from a least squares fit between Equation 4.13 and the data.

To use the new model to determine deposition in a duct bend for a particle of given size: (1) iteratively calculate V_r with Equation 4.3 and Equation 4.4; (2) calculate Stk_T with Equation 4.7; (3) calculate f with Equation 4.13; (4) calculate

P with Equation 4.8; and (5) calculate the percentage of particles that deposits in the bend, η_{dep}, as:

$$\eta_{dep} = (1-P)*100\% \quad (4.14)$$

In this work, all calculations were carried out in a spreadsheet (Excel, Microsoft, Redmond, WA). A macro within the spreadsheet was written to estimate V_r by iterating Equations 4.3 and 4.4. For example, a 30-μm spherical glass particle (ρ_p = 2450 kg m^{-3}, aerodynamic diameter = 50 μm) in Test #1 yielded the following values for each step above: (1) V_r = 4.5 m s^{-1}; (2) Stk_T = 1.76; (3) f = 0.48; (4) P = 0.185; and (5) η_{dep} = 81.5%.

3. Model Comparisons

Estimates made with the new model were compared with three other models. The first of these, published by McFarland et al. (1997), expresses fractional penetration as:

$$P = \exp\left(\frac{4.61 + a_m \theta Stk}{1 + b_m \theta Stk + c_m \theta Stk^2 + d_m \theta^2 Stk}\right) x \frac{1}{100\%} \quad (4.15)$$

where a_m, b_m, c_m, and d_m are coefficients found using a curve-fitting program, and Stk is the particle Stokes number assuming laminar conditions (Stk = $\tau U_0/a$). An error appears in the published coefficient for the second term in the numerator of coefficient d_m. Equation 13 of McFarland et al. (1997) should read:

$$a_m = -0.9526 - 0.05686 R_0$$

$$b_m = \frac{-0.297 - 0.0174 R_0}{1 - 0.07 R_0 + 0.0171 R_0^2}$$

$$c_m = -0.306 + \frac{1.895}{\sqrt{R_0}} - \frac{2.0}{R_0} \quad (4.16)$$

$$d_m = \frac{0.131 - 0.0132 R_0 + 0.000383 R_0^2}{1 - 0.129 R_0 + 0.0136 R_0^2}$$

The second model, originally published by Pui et al. (1987) and later modified to include bend angle by (Brockmann, 1993), is:

$$P = \exp[-(2)(0.706)\ \ Stk\ \ \theta] \quad (4.17)$$

where the constant, 0.706, was determined by Pui et al. (1987) as the average of the f values determined in their experiments. For the third comparison, the model of

Table 4.2: Fit results for each model.

Model Name	r^2	F (p value)	Mean Residual, %	St. Dev. Residual, %
McFarland et al. (1997)	0.04	5 (0.02)	3.6	14.5
Pui et al. (1987)	0.29	48 (< 0.001)	9.8	8.3
Corrected Pui	0.62	190 (< 0.001)	5.1	7.9
New Model	0.85	699 (< 0.001)	0.6	5.8

Pui et al. (1987) was corrected for particle motion outside the Stokes regime by substituting Stk_T for Stk θ in Equation 4.17. In all comparisons, percentage depositions were calculated from fractional penetrations using Equation 4.14.

For each model, the method of least squares was used to calculate the square of the correlation coefficient, r^2, and the F statistic. The mean residual and the standard deviation of the residual were also calculated. The experimental variability associated with the smallest particle diameter in the experiments obscured model evaluation; thus, statistical analyses were limited to data where particle diameter was between 19 μm and 140 μm.

D. Results

Table 4.2 presents results for each model. The r^2 value ranged from 0.04 for the model of McFarland et al. (1997) to 0.85 for the new model. The F value was much larger for the new model, F = 699, than for the McFarland et al. (1997) model, F = 5, the Pui et al. (1987) model, F = 48, or for the corrected Pui model, F = 190. Mean residual, an indicator of systematic bias, was greatest for the Pui et al. (1987) model, 9.8%, and least for the new model, 0.6%. Standard deviations of the residuals were greatest for the McFarland et al. (1997) model, 14.5%, and least for the new model, 5.8%.

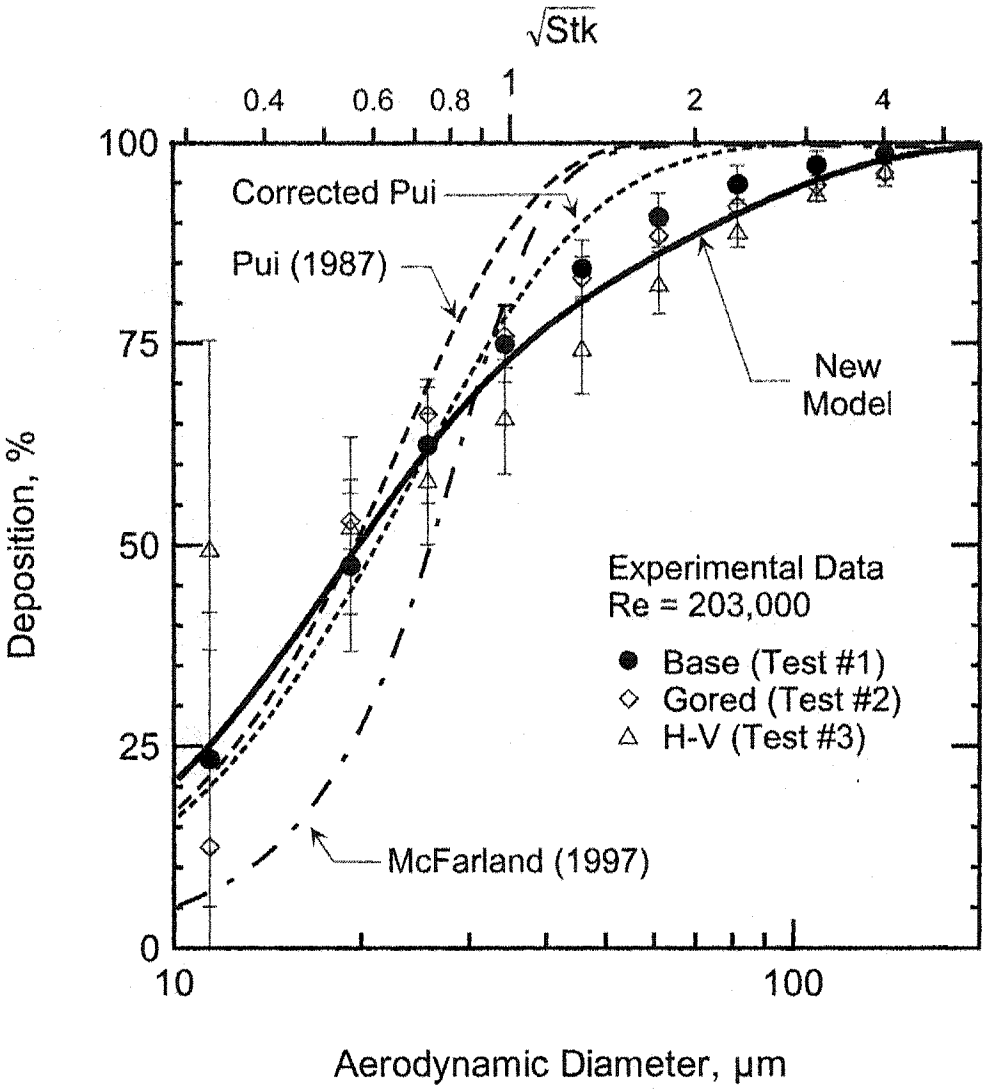

Figure 4.4: Deposition versus particle size estimated with models and measured experimentally for tests where Re = 203,000.

Figure 4.4 compares model estimates for deposition by particle size to the data for tests where Re = 203,000 (Test #1, Test #2, and Test #3). For particles smaller than 30 µm, the Pui et al. (1987) model estimates agreed well with the data but the McFarland et al. (1997) model estimates were lower than the data. For larger particles, both earlier models over-estimated deposition. Estimates made with the new model agreed relatively well with the data for all particle sizes.

Figure 4.5 compares new model estimates and corrected Pui model estimates to the data for tests where Re = 368,000 (Test #4 and Test #5). For particles smaller than 30 µm, estimates made with the new model and the corrected Pui model were

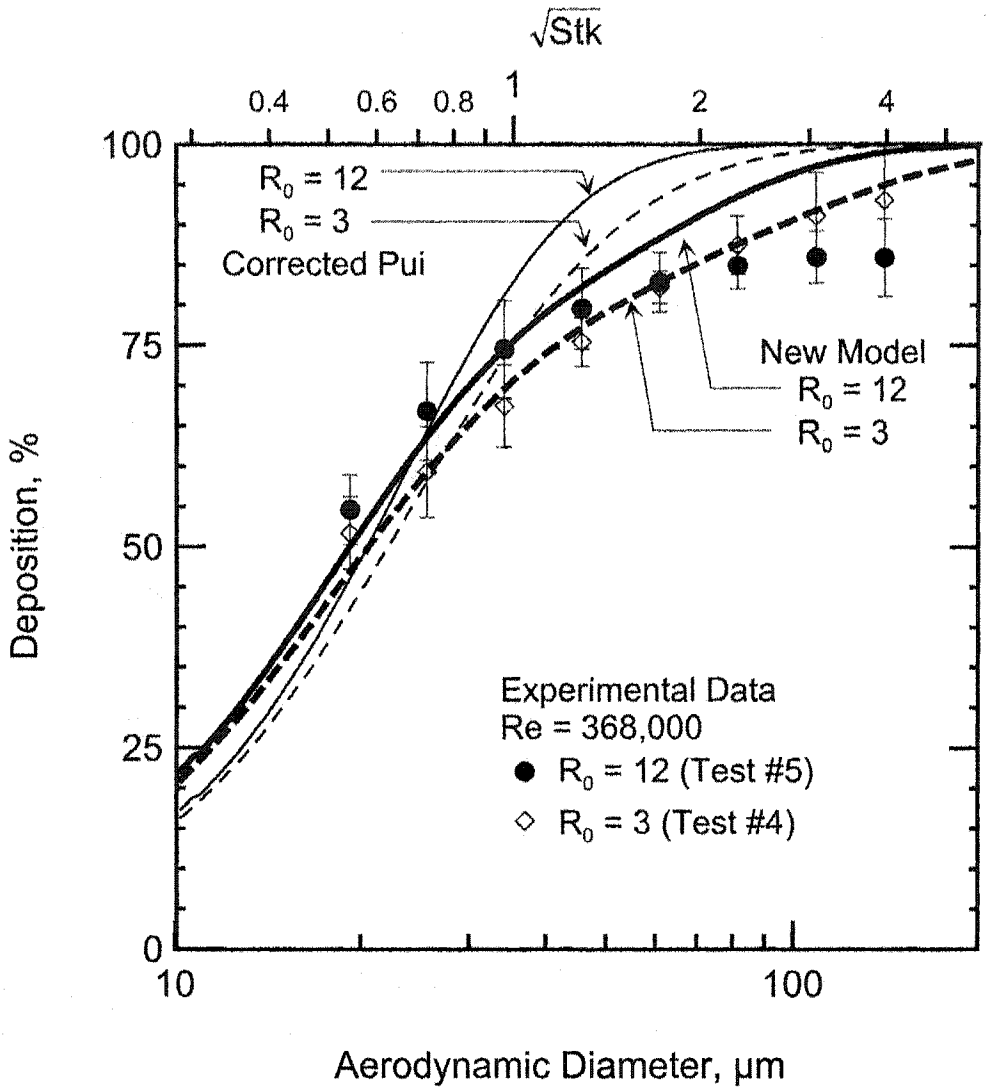

Figure 4.5: Deposition versus particle size estimated with models and measured experimentally for tests where Re = 368,000.

similar and generally agreed with the data. For larger particles, the corrected Pui model over-estimated deposition. The new model estimates agreed with the data somewhat better. For both models and for all particle sizes, deposition estimates were greater for the gradual bend (R_0 = 12) than for the tight bend (R_0 = 3).

E. Discussion

Estimates of particle deposition made with the two earlier models did not agree particularly well with experimental data from industrial bends, especially for particles larger than about 30 µm in diameter. These models were developed using data from

experiments where particle motion was within, or nearly within, the Stokes regime, $Re_p < 3$. Thus, they under-estimated drag forces and over-estimated deposition for larger particles in industrial bends, where Re_p ranged up to 200. Consequently, as shown in Table 4.2, these models fit the data used here with relatively low r^2, low F, high mean residual, and high standard deviation of the residual.

The corrected Pui model, which takes into account particle motion outside the Stokes region, explained more than twice the variability in the experimental data than did the original Pui et al. (1987) model. This observation illustrates the importance of correcting the drag force when particle motion is outside the Stokes regime. However, the corrected Pui model still over-estimated deposition for particles larger than about 30 μm.

Estimates of particle deposition made with the new model agreed well with the experimental data for all particle sizes. Whereas the new model uses the semi-empirical relationship for f given in Equation 4.13, the Pui et al. (1987) model and the corrected Pui model use a constant value for f of 0.706. Thus, where f calculated with Equation 4.13 was less than 0.706 (i.e., Stk_T greater than 0.7), new model estimates were lower than the corrected Pui model estimates and agreed better with the data. Because the data used to develop the new model and the data used to compare the models were the same, the relatively good fit with the new model was not unexpected.

For $Stk_T > 2$, some values of f calculated from the data deviated from those estimated from Equation 4.13, see Figure 4.3. In Test #1, experimental f values were consistently greater than Equation 4.13 estimates. However, in Test #5 for $Stk_T > 3$, the experimental f values were consistently lower than the estimates, and lower than the theoretical limit identified in Equation 4.11. The longer time required to pass through the gradual bend of Test #5 might have allowed gravity settling to alter deposition patterns in a manner slightly different from those in the other tests.

As shown in Figure 4.3 for $Stk_T < 2$, f values computed from industrial bends are generally consistent with those from Pui et al. (1987) and McFarland et al. (1997). However, f values from Pui et al. (1987) exhibited a trend opposite that of the data used here. Perhaps particle behavior in a large diameter bend with highly turbulent

airflow is different from that in the small diameter bends with moderately turbulent airflow studied by Pui et al. (1987).

Consistent with the data in Figure 4.5 for particles between 30 μm and 60 μm, new model estimates of particle deposition were slightly greater for the gradual bend (Test #5, R_0 = 12) than for the tight bend (Test #4, R_0 = 3). As the duct radius was the same for both tests, the bend radius, R_b, was larger for the bend with the larger R_0. Outward radial velocity is inversely proportional to $R_b^{1/2}$ (Equation 4.3), but the time for the air to pass through the bend is directly proportional to R_b (Equation 4.6). Thus, Stk_T is proportional to $R_b^{1/2}$, and model estimates are greater when the bend curves more gradually.

Although the new model offers improvement over other models, it does not explain some features in the data. For particles larger than 60 μm, Figure 4.5 shows that new model estimates were less for the tight bend than for the gradual bend, but the data show an opposite trend. Further, as gravity was assumed to be negligible, the new model does not account for the differences in particle deposition between orientations (i.e., H-H vs. H-V) shown in Figure 4.4.

F. Conclusion

This work presents a new model to estimate particle deposition in round, 90° duct bends with highly turbulent airflows. The new model accounts for particle motion outside the Stokes regime and for variable deposition patterns as a function of particle Stokes number. The model is applicable to deposition of droplets or solid particles where duct walls are sticky.

APPENDIX A: STANDARD OPERATING PROCEDURES

The following pages provide standard operating procedures used in tests described in Chapters II and III. The table below provides a directory for these procedures.

Standard Operating Procedures: Master List

Reference Number	Title
SOP 1500	Procedures to measure particle deposition by size in industrial ducts
SOP 1600	Measurement of duct velocity profile
SOP 1610	Measurement of duct particle concentration profile
SOP 1700	Collection of integrated particle samples in industrial ducts
SOP 1800	Measurement of particle mass distribution using the Andreasen sedimentation pipette

SOP 1500 – PROCEDURES TO MEASURE PARTICLE DEPOSITION BY SIZE IN INDUSTRIAL DUCTS

1.0 Purpose and Applicability

The following procedure is used to determine particle deposition by size in industrial ducts. Behavior of droplets can be studied by greasing interior duct walls. As outlined in Figure A-1, this standard operating procedure requires several other procedures.

2.0 Safety and Operating Precautions

Solvents used in the extraction procedures should be used under an approved safety hood.

3.0 Equipment, Materials, and Supplies

3.1 Equipment

Dust generator to produce solid particle cloud
Others as listed in linked procedures

3.2 Materials

Refer to linked procedures

3.3 Supplies

Petroleum jelly (Eckerd Drug, FL3109B)

4.0 Methods

4.1 Preparation

1. Prepare test component – to simulate droplet behavior, coat interior surface with petroleum jelly
2. Set up the desired duct configuration
3. Adjust airflow conditions to the desired conditions and record the pressure drop across the orifice
4. Measure velocity (SOP 1600) and particle concentration (SOP 1610) profiles

4.2 Sample collection

1. Prepare grids for sample collection following SOP 1700
2. Collect samples alternately upstream and downstream of the test component
3. Repeat steps 1 and 2 until three replicates are collected

4.3 Sample analysis

Analyze all samples following SOP 1700

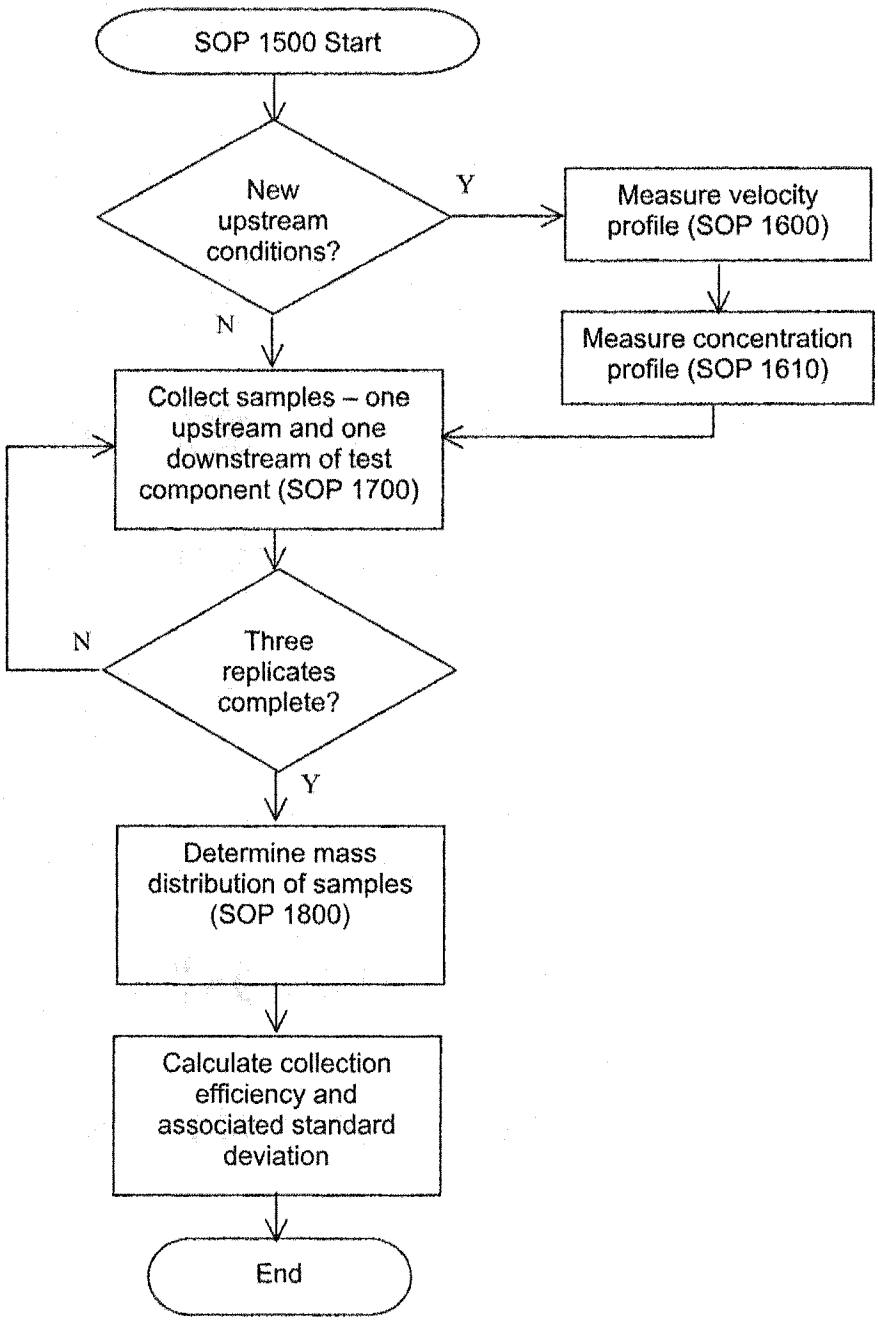

Figure A-1. Flowchart outlining steps to measure deposition by size.

SOP 1600 – Measurement of Duct Velocity Profile

1.0 Purpose and Applicability

This procedure is used to determine the velocity profile entering the test component.

2.0 Safety and Operating Precautions

None

3.0 Equipment, Materials, and Supplies

3.1 Equipment

1. Pitot tube
2. Pitot tube traverse mechanism
3. Manometer (Dwyer Instruments, Inc., Michigan City, IN 4360, M/N 400)

3.2 Materials

1. Red gauge oil
2. Tygon tubing

3.3 Supplies

None required

4.0 Methods

4.1 Preparation (refer to Figure C-2)

1. Drill two 0.5-inch holes in duct using a level perpendicular to each other – document orientation of traverse positions relative to upstream or downstream components
2. Select the appropriate pitot tube traverse mechanism for the duct under investigation
3. Place piece of duct tape over the hole and make a small hole, slightly smaller than the diameter of the pitot tube, in the center.
4. Install the pitot tube through the hole in the duct tape and secure the traverse mechanism to the duct
5. Set the slider on the traverse mechanism so that the pitot tube is zero reading
6. Level and zero manometer
7. Connect flexible tubing between the total and static pressure ports to the manometer

4.2 Velocity Measurement

1. Move pitot tube to traverse position
2. Wait approximately 20 seconds and then record the manometer reading
3. Move to the next position and go to step 2 until done with all points.

SOP 1610 – Measurement of Duct Particle Concentration Profile

1.0 Purpose and Applicability

This procedure is used to document the particle concentration profile upstream of a test component.

2.0 Safety and Operating Precautions

None

3.0 Equipment, Materials, and Supplies

3.1 Equipment

1. Microscope (Olympus America, Inc., Melville, NY 11747, M/N BH, S/N 205042)
2. Porton graticule (Olympus America, Inc., Melville, NY 11747, M/N WF.10X)

3.2 Materials

None

3.3 Supplies

None

4.0 Methods

4.1 Sample collection

1. Grease sample collection grid (see SOP 1700) in locations where particle size distribution information is desired
2. Insert into duct following SOP 1700
3. Collect particles at test airflow conditions for a given time. Note, sample time should be short enough so that particles do not overlap

4.2 Microscope Analysis

1. Place grid under microscope
2. Focus on center of coated area
3. Count particles in one field – one of six rectangular sections on the Porton graticule – use of the black filled circles of the Porton graticule is recommended if measuring glass beads on a stainless steel grid
4. Move slightly and repeat steps 2 and 3 until a minimum of 100 particles are counted
5. Repeat steps 1 though 4 for each greased area

SOP 1700 – COLLECTION OF INTEGRATED PARTICLE SAMPLES IN INDUSTRIAL DUCTS

1.0 Purpose and Applicability

This procedures describes a method to sample solid particles in industrial ducts. Samples are collected *in situ* using a greased, stainless steel wire-mesh grid. A subsequent extraction procedure is used to isolate the collected particles from the greased grid, resulting in a dry dust sample representative of the material in the duct.

2.0 Safety and Operating Precautions

Use a hood during the extraction process. Properly dispose of hexane through health and safety department.

3.0 Equipment, Materials, and Supplies

3.1 Equipment

1. Hotplate (Thermolyne Corporation, Dubuque, Iowa, M/N, S/N 30602462)
2. Vacuum source for aspiration

3.2 Materials

1. Two squirt bottles, one with water and one with hexane
2. Water, deionized water
3. Grid material (McMaster-Carr, Atlanta, GA, P/N 93322T41)
4. Aspiration flask (Pyrex, 500 mL filter flask, 5340)

3.3 Supplies

1. Hexanes (Fisher Scientific, H291-4)
2. Petroleum jelly (Eckerd Drug, FL3109B)
3. Solvent-proof containers

4.0 Methods

4.1 Preparation

1. Cut grid to fit into duct leaving four tabs for handling (see Figure C-3)
2. Rinse both grid and sample container with the following: water, methanol, hexane x 3
3. Coat each grid with grease
   - 3.1 Set the hotplate to a setting of 8
   - 3.2 Melt petroleum jelly ("grease") in a clean metal pan on the hotplate
   - 3.3 Dip grid into melted grease
   - 3.4 Remove grid, hold vertically over pan, and gently rap ten times so that excess grease drips back into the pan
   - 3.5 Place grid on cooling rack for approximately five minutes

4.2 Sample collection

1. Insert grid into duct
   - 1.1 Disconnect the duct at desired location
   - 1.2 Insert grid into position ensuring a tight fit using the positioning tabs
   - 1.3 Reconnect duct and tape joint
2. Expose grid to particles
   - 2.1 Turn power on to blower
   - 2.2 Adjust to desired flow conditions
   - 2.3 Turn on particle generator

2.4 Collect particles for a time such that the grid is not coated with more than a monolayer of particles – this ensures that particle bounce will not be a problem
2.5 Turn off particle generator
2.6 Turn off power to blower

3. Remove grid from duct and place in sample container

4.3 Sample extraction

1. Relocate samples to a hood to prevent hexane exposure
2. Remove grease and glass beads from grid – wash one
   2.1 Add sufficient quantity of hexane to the container so that the grid is totally immersed, excluding the four positioning tabs
   2.2 Cover the container so that the hexane does not evaporate – note that the cover should have a small hole so that pressure does not become excessive
   2.3 Place the container on the hotplate at a setting of 5
   2.4 Heat sample until hexane boils
   2.5 Remove from hotplate
   2.6 Grab grid by the positioning tabs and gently immerse and remove the grid from the heated hexane mixture five times
   2.7 Place the grid on a drying rack
   2.8 Tip the container 30 degrees to maximize the height of the hexane
   2.9 Use a hexane wash bottle to push any particles in the dry section of the container into the original hexane wash solution
   2.10 Wait 1 minute to allow glass beads to settle to bottom
   2.11 Slowly turn container 180 while maintaining the 30 tilt
   2.12 Wait 1 minute
   2.13 Aspirate the hexane to waste
   2.14 Repeat steps 2.9 to 2.13 two more times
3. Rinse glass beads – wash two and three
   3.1 Repeat step 2.9 through step 2.13 two times
   3.2 Sample is now ready for analysis

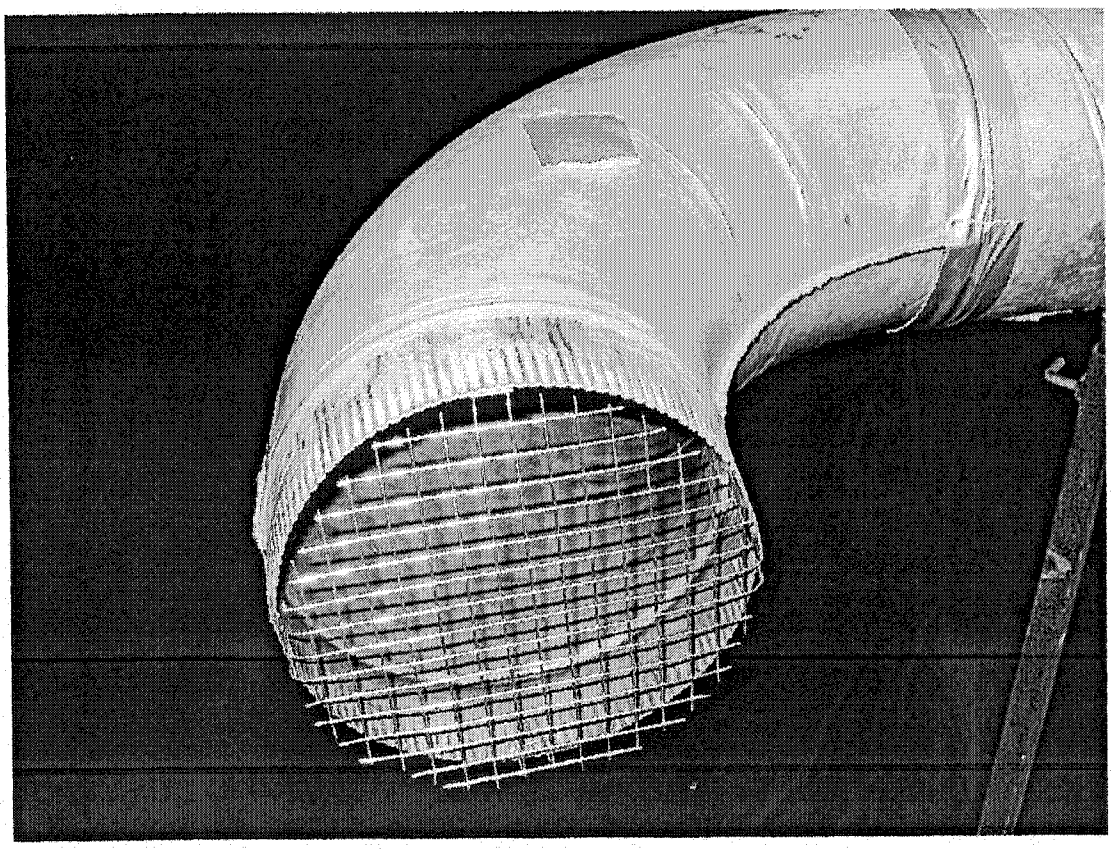

Figure C-1. Sampling grid installed upstream of a test bend.

SOP 1800 – MEASUREMENT OF PARTICLE MASS DISTRIBUTION USING THE ANDREASEN SEDIMENTATION PIPETTE

1.0 Purpose and Applicability

This procedure describes measurement of a particle size distribution using the Andreasen sedimentation pipette.

2.0 Safety and Operating Precautions

Ethylene glycol is a poison and should be disposed of through health and safety.

3.0 Equipment, Materials, and Supplies

3.1 Equipment

1. Microbalance with ± 1 µg resolution (Mettler Toledo, Greifensee, Switzerland, M/N MT5, S/N 1114410420)
2. Top loader balance (Mettler Toledo, Greinfensee, Switzerland, M/N PM 34-K, S/N M44686)
3. Vacuum oven (National Appliance Company, M/N 5830, S/N 4A66)
4. Glass vacuum filter holder (Ultra-Ware 47 mm micro filtration assembly available through Fisher Scientific, P/N K953750-5347)

3.2 Materials

1. Borosilicate glass fiber filters (Pall Corp., Ann Arbor, MI 48103, Type A/E, P/N 61652)
2. Ethylene glycol (Fisher Scientific, CAS 107-21-1, E178-1)
3. Deionized water

3.3 Supplies

1. Tweezers for handling of filters
2. Pipette bulb
3. 47-mm Zefluor filters (P5PJ047)

4.0 Methods

4.1 Preparation

1. Prepare 40% by mass ethylene glycol solution in DI water
   - 1.1 Dispense 10 L DI water into a 20 L container with a volumetric flask
   - 1.2 Weigh 4 kg of ethylene glycol on the top loader balance
   - 1.3 Slowly pour the ethylene glycol into the 20 L container holding the DI water
   - 1.4 Thoroughly mix the solution
   - 1.5 Allow solution to temperature equilibrate for a minimum of 24 hours in the room where pipette measurements will be conducted
2. Condition and preweigh filters
   - 2.1 Place 12 filters into aluminum weighing dishes
   - 2.2 Label samples x0 to x8, xT, xDI, and xBlk
   - 2.3 Place labeled samples into vacuum oven for 24 hours minimum at a temperature of 80°C and greater than 20 inHg vacuum
   - 2.4 Remove from conditioning oven
   - 2.5 Allow to equilibrate in weighing room for 1 hour
   - 2.6 Weigh filters to the nearest µg using the microbalance
   - 2.7 Separate the filters from the aluminum weighing dishes

3. Transfer the dry dust sample (collected according to SOP 1700) into the sedimentation pipette
   3.1 Wet the dry dust with 10 mL of methanol using a squirt bottle to reduce the surface adhesion forces between the dry powder and the container
   3.2 Use a wash bottle containing 40% ethylene glycol in DI water to push all of the collected dust into the liquid
   3.3 Transfer the dust in liquid solution into the sedimentation pipette using a clean funnel
   3.4 Repeat step 3.2 and step 3.3 until three rinses are complete
   3.5 Fill pipette to the 20 cm mark with 40% ethylene glycol solution

4.2 Sedimentation Pipette Operation

1. Thouroughly mix sample
   1.1 Plug holes in nylon stopper with toothpicks
   1.2 Repeatedly invert the pipette 10 times 180 degrees to vertical – motion should take approximately two seconds to complete one repetition
2. Take the total sample
   2.1 Immediately waste the first 10 mL sample
   2.2 Repeat step 1 to mix sample
   2.3 Transfer the total sample to the aluminum weighing dish labeled XT
3. Take the remaining samples
   3.1 Repeat step 1 to mix sample
   3.2 Start the sedimentation pipette timer program
   3.3 Take samples X8 through X1 at the times indicated by the program by transferring the 10 mL sample from the sedimentation pipette to the appropriate aluminum weighing dish

4.3 Post Pipette Procedures

1. Filter the liquid samples --- for each sample:
   1.1 Rinse the upper section of the glass vacuum filter holder with DI water
   1.2 Place the appropriate filter into the filter holder
   1.3 Rinse filter with methanol
   1.4 Clamp the upper and lower sections together
   1.5 Pour the liquid in the aluminum weighing dish that is matched with the filter into the upper section of the filter holder
   1.5 Rinse the dish with methanol three times, pouring the rinse liquid into the upper section of the filter holder
   1.6 Rinse the interior of the upper section of the filter holder with methanol
   1.7 Transfer the filter back into the clean aluminum weighing dish
   1.8 Repeat step 1.1 to step 1.8 for all samples; the recommended order is from low to high concentration; thus, the solution blank (XDI) first, then low to high mass samples (X1 to X8), and finally the total sample (XT)
2. Filter the remaining liquid to recover all dust
   2.1 Follow step 1.1 to step 1.4 above to install filter X0 into the filter holder
   2.2 Remove the sampling tube from the sedimentation pipette
   2.3 Filter the liquid remaining in the sedimentation pipette down to the 0 cm mark
   2.4 Shake the remaining liquid to disperse the solid particles on the bottom of the pipette and filter
   2.5 Rinse the pipette three times with DI water, filtering the rinse liquid
   2.6 Rinse the upper section of the filter holder with methanol
3. Condition and postweigh filters
   3.1 Filters and aluminum weighing dishes into vacuum oven for 24 hours minimum at a temperature of 80°C and greater than 20 inHg vacuum
   3.2 Remove from conditioning oven
   3.3 Allow to equilibrate in weighing room for 1 hour
   3.4 Weigh filters to the nearest µg using the microbalance

APPENDIX B: UNIFORMITY TEST DATA

The following pages provide data from the particle concentration and velocity uniformity tests. The tests labeled 8" duct are associated with Chapter II and Chapter III experiments. The tests labeled 6" duct are associated with Chapter III experiments. Two pages of data are presented for each duct diameter tested. The first page provides particle concentration data, and the second page provides velocity data.

Particle Concentration Uniformity

Date	12/3/2002	Configuration: Damper Slightly Under 1/2 Open	
Orifice	> 6 inch orifice		
Orifice ΔP	3.25 inH20		
Duct Diameter	8 in	0.2032 m	
Duct Area	0.349 ft2		
Measurement Plane:	20 cm upstream of bend		

TOTALS **Counts From 4 Fields**

Porton Number	Top Dp, µm	Top	Out	Bot	In	Total Count	Mean Counts	StDev Counts
7	**50**	3	2	3	3	**11**	2.8	0.5
6	**35**	16	20	20	18	**74**	18.5	1.9
5	**24**	34	39	38	29	**140**	35.0	4.5
4	**17**	33	42	41	30	**146**	36.5	5.9
3	**12**	17	24	17	15	**73**	18.3	3.9
2	**8**	0	1	3	0	**4**	1.0	1.4
	Total Count	**103**	**128**	**122**	**95**	**448**		

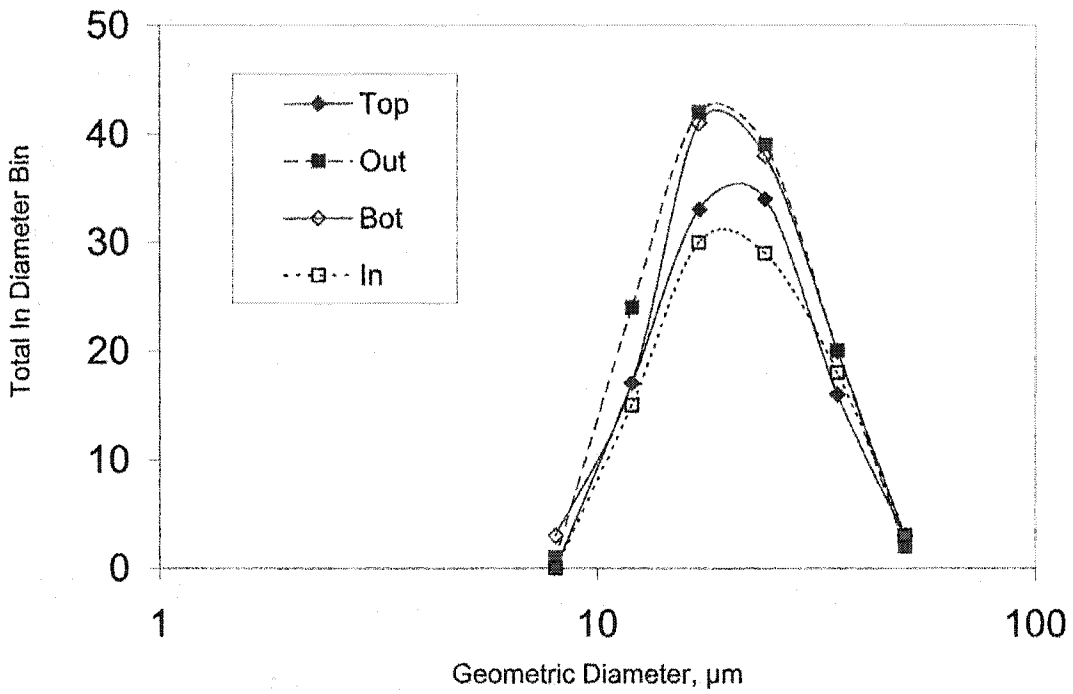

Velocity Uniformity

Date 12/3/2002 Configuration: Damper Full Open
Orifice > 6 inch orifice
Orifice ΔP 3.25 inH20
Duct Diameter 8 in 0.2032 m
Duct Area 0.349 ft2
Measurement Plane: 20 cm upstream of bend

		Horizontal Traverse			Vertical Traverse		
Traverse Position Number	Distance From Wall, inch		Velocity Pressure, inH20	Velocity, fpm		Velocity Pressure, inH20	Velocity, fpm
1	0.21	out	1.45	4823	top	1.1	4200
2	0.66		1.7	5222		1.6	5066
3	1.17		2	5664		1.85	5447
4	1.81		2.25	6008		2.1	5804
5	2.74		2.4	6205		2.3	6074
6	5.48		2.1	5804		2.3	6074
7	6.19		1.9	5521		2.1	5804
8	6.83		1.7	5222		1.9	5521
9	7.34		1.5	4905		1.7	5222
10	7.79	in	1.1	4200	bottom	1.25	4478
			Average =	5357		Average =	5369

Average Velocity = 5363 fpm 27.2 m/s
Flowrate = 1871 cfm
Reynolds No = 365,021

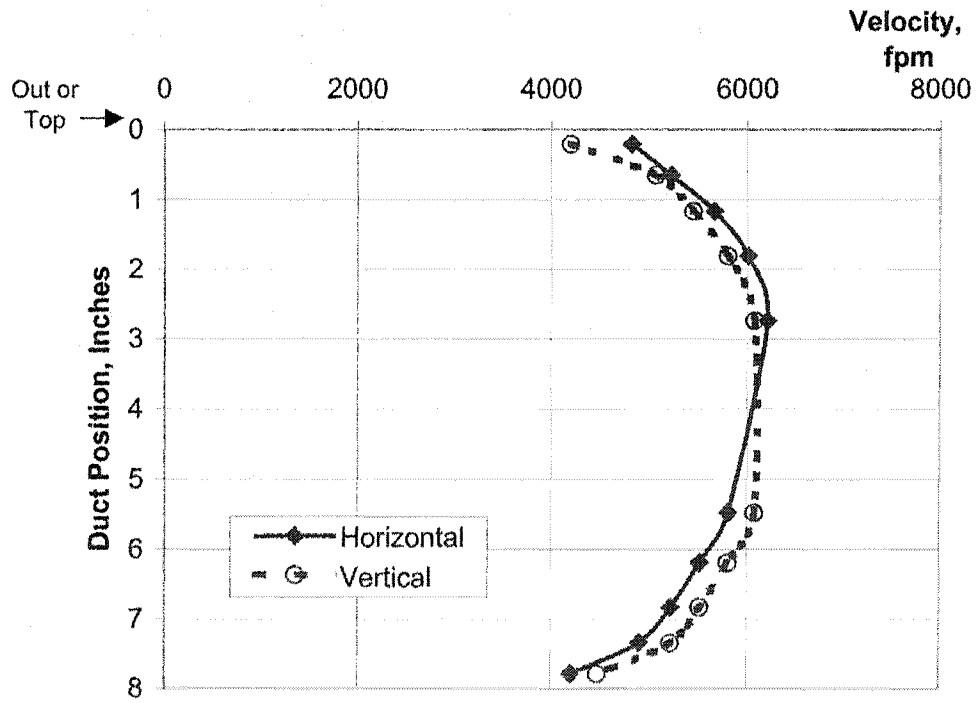

Particle Concentration Uniformity

Date 5/24/2003 Configuration: Damper Slightly Under 1/2 Open
Orifice > 6 inch orifice
Orifice ΔP 0.52 inH20
Duct Diameter 6 in 0.1524 m Fx --- indicates field number
Duct Area 0.196 ft2
Measurement Plane: 20 cm upstream of bend

TOTALS **Counts From 10 Fields**

Porton Number	Top Dp, µm	Top	Out	Bot	In	Total Count	Mean Count	StDev Count
7	**50**	1	0	2	1	**4**	1.0	0.8
6	**35**	10	7	9	8	**34**	8.5	1.3
5	**24**	28	27	31	23	**109**	27.3	3.3
4	**17**	43	57	45	42	**187**	46.8	6.9
3	**12**	52	51	51	56	**210**	52.5	2.4
2	**8**	33	23	19	25	**100**	25.0	5.9
1	**5**	1	2	0	0	**3**	0.8	1.0
	Total Count	**168**	**167**	**157**	**155**	**647**		

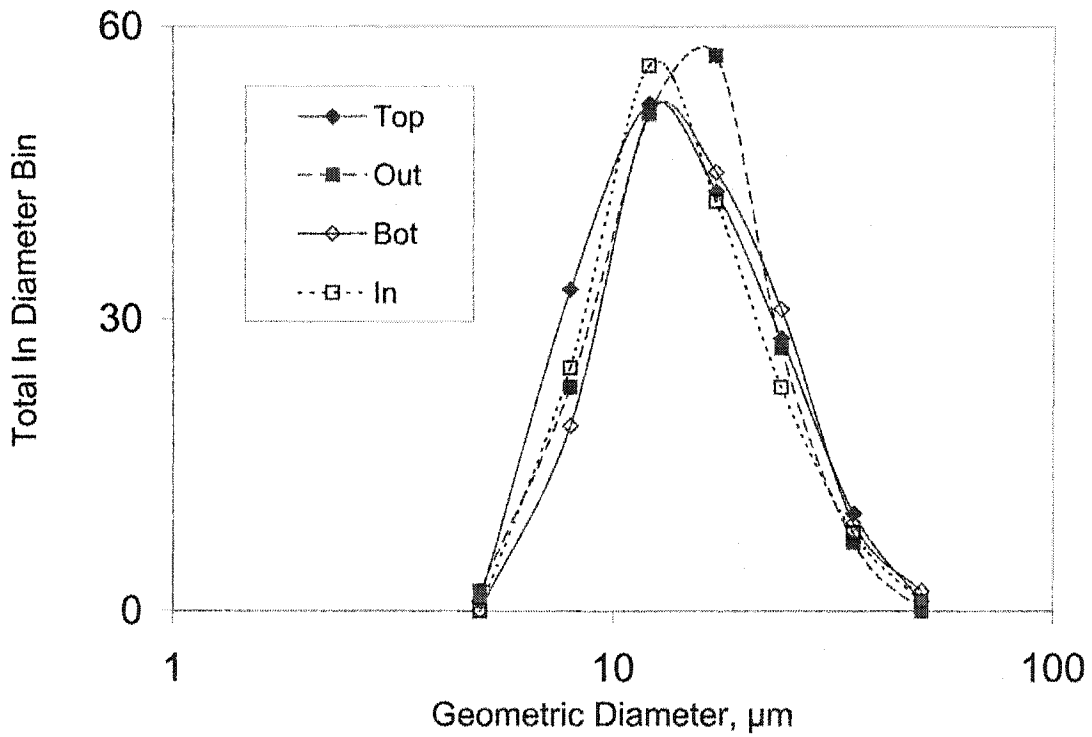

Velocity Uniformity

Date 5/23/2003 Configuration: Damper Slightly Under 1/2 Open
Orifice > 6 inch orifice
Orifice ΔP 0.52 inH20
Duct Diameter 6 in 0.1524 m
Duct Area 0.196 ft2
Measurement Plane: 20 cm upstream of bend

		Horizontal Traverse			Vertical Traverse		
Traverse Position Number	Distance From Wall, inch		Velocity Pressure, inH20	Velocity, fpm		Velocity Pressure, inH20	Velocity, fpm
1	0.16	out	0.85	3692	top	0.72	3398
2	0.49		0.85	3692		0.78	3537
3	0.88		0.98	3965		0.9	3799
4	1.36		1.1	4200		0.98	3965
5	2.05		1.2	4387		1.1	4200
6	4.11		1.35	4653		1.2	4387
7	4.64		1.25	4478		1.1	4200
8	5.12		1.1	4200		1	4005
9	5.51		0.91	3821		0.9	3799
10	5.84	in	0.54	2943	bottom	0.7	3351
			Average =	4003		Average =	3864

Average Velocity = 3934 fpm 20.0 m/s
Flowrate = 772 cfm
Reynolds No = 200,806

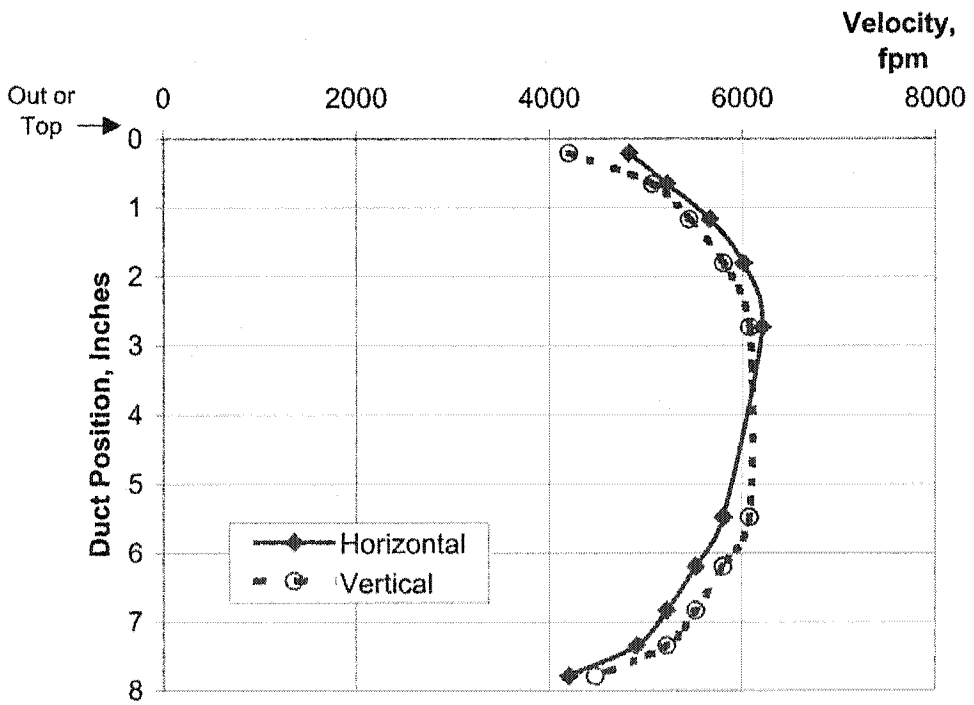

APPENDIX C: DEPOSITION BY SIZE DATA

The following pages provide data from the tests referred to in Chapters II, III, and IV. The table below provides test numbers. The experiment described in Chapter II is labeled as Test #7 below. Chapter III presented data from all experiments. Chapter IV modeled data where bend angle was 90°.

Three pages of data are presented for each test. The first page displays experimental conditions, collection information, deposition versus size, and summary statistics. The second and third pages provide raw filter weights and size distribution calculations for the upstream and downstream samples, respectively.

							Chapter		
Test #	**Test Description**	**Re (De)**	**θ**	**R_0**	**Construction**	**Orient**	**II**	**III**	**IV**
1	Base	203,000 (91,000)	90°	5	Smooth	H-H		X	Test 1
2	Base + Bend Angle	203,000 (91,000)	***180°***	5	Smooth	H-H		X	
3	Base – Bend Angle	203,000 (91,000)	***45°***	5	Smooth	H-H		X	
4	Base + Construction	203,000 (91,000)	90°	5	***Gored***	H-H		X	Test 3
5	Base – Construct	203,000 (156,000)	90°	***1.7***	***Segmented***	H-H		X	
6	Base + Orient	203,000 (91,000)	90°	5	Smooth	***H-V***		X	Test 2
7	High Re, Small R_0	***368,000 (212,000)***	90°	***3***	Smooth	H-H	X	X	Test 4
8	High Re, Large R_0	***368,000 (106,000)***	90°	***12***	Smooth	H-H		X	Test 5

Test #1: Base

Duct Conditions:

Duct Diameter	6 in	Start Date	6/13/03
	0.152 m	End Date	6/15/03
Bend Surface	Smooth	**Collection Details:**	
Curvature Ratio, Ro	5	# Grids / Sample	6
Bend Angle	90 deg	Sample Time / Grid	50 sec
Flow Setpoint, DP	0.52 in H20		
Duct Velocity	3942 fpm		
	20.0 m/s		
Flow Rate	774.0 cfm		
	0.365 m3/s		
Reynolds Number	203,055		
Dean Number	90,809		

Deposition vs. size

Sed Pip Chan	Geo Mid Dp, µm	Aero Mid Dp, µm	Mid Stk	η-1, %	η-2, %	η-3, %	Mean η, %	StDev η, %
Total	89.8	140.5	15.9	99.7	98.2	97.3	98.4	1.2
8	69.6	109.0	9.6	99.1	96.5	95.8	97.1	1.7
7	52.0	81.5	5.4	97.5	93.5	93.3	94.7	2.4
6	39.0	61.0	3.0	94.0	88.4	89.6	90.7	3.0
5	29.2	45.7	1.7	87.7	80.6	84.5	84.3	3.5
4	21.9	34.2	0.95	77.8	69.4	77.4	74.9	4.7
3	16.4	25.7	0.53	64.8	54.3	68.0	62.4	7.2
2	12.3	19.2	0.30	51.0	35.5	55.9	47.5	10.6
1	7.3	11.4	0.11	40.0	3.9	26.2	23.4	18.3

Summary statistics for particles sampled upstream and downstream of the bend

Sample ID	MMAD, µm	GSD	Cm, mg/m3	R2		
Up-1	30.7	1.95	5.10	0.96		
Up-2	31.2	1.70	4.86	0.98		
Up-3	32.6	1.93	5.46	1.00		
Up-Mean	**31.5**	**1.86**	**5.14**	**0.98**	Overall η-1, %	69.2
Up-StDev	**1.0**	**0.14**	**0.30**	**0.02**	Overall η-2, %	63.0
					Overall η-3, %	71.0
Down-1	19.8	1.66	1.57	0.91	Overall η-mean, %	**67.7**
Down-2	22.2	1.62	1.79	0.79	Overall η-stdev, %	**4.2**
Down-3	20.2	1.85	1.58	0.87		
Down-Mean	**20.7**	**1.71**	**1.65**	**0.86**		
Down-StDev	**1.3**	**0.12**	**0.13**	**0.06**		

Test #1: Base

Sample ID: Up-1

Chan	Aero HiD, µm	LnHi	PreWt, mg	PostWt, mg	Cum Mass, ΔWt, mg	Frac < HiD	Mass Probits	dM, mg	Fit Mass Probits	Fit Cum Mass, mg	Fit dM, mg
Total	156.5	5.1	286.505	288.561	2.056				2.441	2.041	0.020
8	126.1	4.8	251.156	253.111	1.955	0.951	1.653	0.000	2.117	2.021	0.060
7	94.2	4.5	290.213	292.223	2.010	0.978	2.007	0.145	1.679	1.960	0.123
6	70.5	4.3	285.013	286.878	1.865	0.907	1.323	0.225	1.245	1.837	0.209
5	52.8	4.0	261.196	262.836	1.640	0.798	0.833	0.280	0.813	1.628	0.295
4	39.6	3.7	288.223	289.583	1.360	0.661	0.417	0.394	0.380	1.333	0.348
3	29.6	3.4	278.016	278.982	0.966	0.470	-0.076	0.335	-0.053	0.985	0.340
2	22.2	3.1	261.060	261.691	0.631	0.307	-0.505	0.238	-0.485	0.645	0.276
1	16.6	2.8	292.702	293.095	0.393	0.191	-0.874	0.393	-0.918	0.369	0.369
	Remaining Wt		1411.493	1513.333	101.840						
	Soln Blank		287.887	287.857	-0.030						
	Blank		262.118	262.103	-0.015						

Sample ID: Up-2

Chan	Aero HiD, µm	LnHi	PreWt, mg	PostWt, mg	Cum Mass, ΔWt, mg	Frac < HiD	Mass Probits	dM, mg	Fit Mass Probits	Fit Cum Mass, mg	Fit dM, mg
Total	156.5	5.1	258.127	259.955	1.828				3.050	1.826	0.005
8	126.1	4.8	274.853	276.687	1.834	0.990	2.326	0.000	2.640	1.820	0.026
7	94.2	4.5	293.973	295.807	1.834	0.990	2.326	0.158	2.088	1.794	0.079
6	70.5	4.3	259.474	261.150	1.676	0.917	1.384	0.175	1.540	1.715	0.180
5	52.8	4.0	256.758	258.259	1.501	0.821	0.920	0.370	0.993	1.535	0.305
4	39.6	3.7	283.863	284.994	1.131	0.619	0.302	0.417	0.447	1.230	0.388
3	29.6	3.4	287.616	288.330	0.714	0.391	-0.278	0.226	-0.099	0.842	0.368
2	22.2	3.1	258.323	258.811	0.488	0.267	-0.622	0.152	-0.646	0.474	0.261
1	16.6	2.8	283.292	283.628	0.336	0.184	-0.901	0.336	-1.192	0.213	0.213
	Remaining Wt		1432.381	1530.363	97.982						
	Soln Blank		284.382	284.388	0.006						
	Blank		278.415	278.396	-0.019						

Sample ID: Up-3

Chan	Aero HiD, µm	LnHi	PreWt, mg	PostWt, mg	Cum Mass, ΔWt, mg	Frac < HiD	Mass Probits	dM, mg	Fit Mass Probits	Fit Cum Mass, mg	Fit dM, mg
Total	156.5	5.1	273.387	275.520	2.133				2.380	2.115	0.024
8	126.1	4.8	279.896	281.991	2.095	0.982	2.101	0.101	2.052	2.090	0.072
7	94.2	4.5	272.684	274.678	1.994	0.935	1.513	0.124	1.610	2.018	0.143
6	70.5	4.3	268.582	270.452	1.870	0.877	1.159	0.162	1.170	1.875	0.237
5	52.8	4.0	277.944	279.652	1.708	0.801	0.844	0.447	0.733	1.638	0.324
4	39.6	3.7	273.386	274.647	1.261	0.591	0.231	0.313	0.295	1.314	0.369
3	29.6	3.4	263.475	264.423	0.948	0.444	-0.140	0.376	-0.143	0.945	0.346
2	22.2	3.1	276.546	277.118	0.572	0.268	-0.618	0.219	-0.581	0.599	0.270
1	16.6	2.8	279.811	280.164	0.353	0.165	-0.972	0.353	-1.019	0.329	0.329
	Remaining Wt		1402.293	1512.224	109.931						
	Soln Blank		262.385	262.366	-0.019						
	Blank		291.326	291.297	-0.029						

Average Upstream

Chan	Aero HiD, µm	LnHi	Mean Probits	StDev Probits	Fit Probits
Total	156.5	5.1			
8	126.1	4.8	2.027	0.343	2.270
7	94.2	4.5	1.949	0.410	1.792
6	70.5	4.3	1.289	0.117	1.318
5	52.8	4.0	0.866	0.047	0.846
4	39.6	3.7	0.316	0.094	0.374
3	29.6	3.4	-0.164	0.103	-0.098
2	22.2	3.1	-0.582	0.067	-0.570
1	16.6	2.8	-0.916	0.051	-1.043

	Mean, mg	StDev, mg
Remaining Wt	103.251	6.10
Soln Blank	-0.014	0.02
Blank	-0.021	0.01

Test #1: Base

Sample ID: Down-1

Chan	Aero HiD, µm	LnHi	PreWt, mg	PostWt, mg	Cum Mass, ΔWt, mg	Frac < HiD	Mass Probits	dM, mg	Fit Mass Probits	Fit Cum Mass, mg	Fit dM, mg
Total	156.5	5.1	296.579	297.185	0.606				4.072	0.606	0.000
8	126.1	4.8	285.330	285.967	0.637	0.990	2.326	0.034	3.646	0.606	0.001
7	94.2	4.5	290.427	291.030	0.603	0.995	2.579	0.000	3.071	0.605	0.003
6	70.5	4.3	253.757	254.400	0.643	0.990	2.326	0.058	2.499	0.602	0.012
5	52.8	4.0	290.915	291.500	0.585	0.965	1.816	0.013	1.931	0.590	0.036
4	39.6	3.7	298.509	299.081	0.572	0.944	1.588	0.136	1.362	0.554	0.077
3	29.6	3.4	264.239	264.675	0.436	0.719	0.581	0.094	0.793	0.476	0.120
2	22.2	3.1	290.576	290.918	0.342	0.564	0.162	0.128	0.224	0.357	0.135
1	16.6	2.8	289.904	290.118	0.214	0.353	-0.377	0.214	-0.345	0.221	0.221
	Remaining Wt		1404.538	1435.285	30.747						
	Soln Blank		287.314	287.309	-0.005						
	Blank		249.438	249.421	-0.017						

Sample ID: Down-2

Chan	Aero HiD, µm	LnHi	PreWt, mg	PostWt, mg	Cum Mass, ΔWt, mg	Frac < HiD	Mass Probits	dM, mg	Fit Mass Probits	Fit Cum Mass, mg	Fit dM, mg
Total	156.5	5.1	255.945	256.691	0.746				4.050	0.746	0.000
8	126.1	4.8	281.847	282.607	0.760	0.990	2.326	0.049	3.602	0.746	0.001
7	94.2	4.5	290.463	291.174	0.711	0.953	1.676	0.026	2.997	0.745	0.005
6	70.5	4.3	255.614	256.299	0.685	0.918	1.393	0.000	2.395	0.740	0.021
5	52.8	4.0	297.105	297.845	0.740	0.992	2.407	0.099	1.797	0.719	0.059
4	39.6	3.7	291.124	291.765	0.641	0.859	1.077	0.134	1.198	0.660	0.119
3	29.6	3.4	289.771	290.278	0.507	0.680	0.467	0.111	0.599	0.541	0.168
2	22.2	3.1	259.208	259.604	0.396	0.531	0.077	0.101	0.000	0.373	0.168
1	16.6	2.8	272.878	273.173	0.295	0.395	-0.265	0.295	-0.598	0.205	0.205
	Remaining Wt		1406.792	1441.640	34.848						
	Soln Blank		297.281	297.269	-0.012						
	Blank		285.742	285.717	-0.025						

Sample ID: Down-3

Chan	Aero HiD, µm	LnHi	PreWt, mg	PostWt, mg	Cum Mass, ΔWt, mg	Frac < HiD	Mass Probits	dM, mg	Fit Mass Probits	Fit Cum Mass, mg	Fit dM, mg
Total	156.5	5.1	268.831	269.475	0.644				3.325	0.644	0.001
8	126.1	4.8	281.432	282.063	0.631	0.980	2.050	0.025	2.974	0.643	0.003
7	94.2	4.5	276.278	276.884	0.606	0.941	1.563	0.000	2.500	0.640	0.010
6	70.5	4.3	270.118	270.747	0.629	0.977	1.990	0.088	2.030	0.630	0.025
5	52.8	4.0	275.382	275.923	0.541	0.840	0.995	0.000	1.561	0.606	0.050
4	39.6	3.7	271.242	271.812	0.570	0.885	1.201	0.045	1.093	0.556	0.083
3	29.6	3.4	269.922	270.447	0.525	0.815	0.897	0.181	0.624	0.472	0.111
2	22.2	3.1	268.988	269.332	0.344	0.534	0.086	0.109	0.155	0.362	0.119
1	16.6	2.8	263.095	263.330	0.235	0.365	-0.345	0.235	-0.314	0.243	0.243
	Remaining Wt		1418.401	1449.283	30.882						
	Soln Blank		269.706	269.733	0.027						
	Blank		271.485	271.466	-0.019						

Average Downstream

Chan	Aero HiD, µm	LnHi	Mean Probits	StDev Probits	Fit Probits
Total	156.5	5.1			
8	126.1	4.8	2.234	0.160	3.407
7	94.2	4.5	1.939	0.557	2.856
6	70.5	4.3	1.903	0.473	2.308
5	52.8	4.0	1.739	0.709	1.763
4	39.6	3.7	1.289	0.267	1.218
3	29.6	3.4	0.648	0.223	0.672
2	22.2	3.1	0.108	0.047	0.126
1	16.6	2.8	-0.329	0.058	-0.419

	Mean, mg	StDev, mg
Remaining Wt	32.159	2.33
Soln Blank	0.003	0.02
Blank	-0.020	0.00

Test #2: Base + Bend Angle

Duct Conditions:

Duct Diameter	6	in	
	0.152	m	
Bend Surface	Smooth		
Curvature Ratio, Ro	5		
Bend Angle	180	deg	
Flow Setpoint, DP	0.52	in H20	
Duct Velocity	3942	fpm	
	20.0	m/s	
Flow Rate	774.0	cfm	
	0.365	m3/s	
Reynolds Number	203,055		
Dean Number	90,809		

Start Date	7/9/03
End Date	7/10/03

Collection Details:

# Grids / Sample	6
Sample Time / Grid	50 sec

Deposition vs. size

Sed Pip Chan	Geo Mid Dp, µm	Aero Mid Dp, µm	Mid Stk	η-1, %	η-2, %	η-3, %	Mean η, %	StDev η, %
Total	89.8	140.5	15.9	100.0	76.2	97.1	91.1	13.0
8	69.6	109.0	9.6	99.9	84.5	96.7	93.7	8.1
7	52.0	81.5	5.4	99.5	88.9	96.1	94.8	5.4
6	39.0	61.0	3.0	98.2	90.9	95.1	94.7	3.7
5	29.2	45.7	1.7	95.1	91.4	93.4	93.3	1.9
4	21.9	34.2	0.95	89.3	90.6	90.7	90.2	0.8
3	16.4	25.7	0.53	80.9	88.3	86.1	85.1	3.8
2	12.3	19.2	0.30	72.7	83.2	78.0	78.0	5.2
1	7.3	11.4	0.11	72.6	38.8	30.8	47.4	22.2

Summary statistics for particles sampled upstream and downstream of the bend

Sample ID	MMAD, µm	GSD	Cm, mg/m3	R2		
Up-1	31.6	2.04	5.05	0.98		
Up-2	30.2	1.77	5.19	0.88		
Up-3	35.7	1.90	4.92	0.97		
Up-Mean	**32.5**	**1.90**	**5.05**	**0.95**	Overall η-1, %	85.9
Up-StDev	**2.9**	**0.13**	**0.13**	**0.05**	Overall η-2, %	83.1
					Overall η-3, %	84.6
Down-1	19.7	1.59	0.71	0.96	Overall η-mean, %	**84.5**
Down-2	17.2	2.38	0.88	0.88	Overall η-stdev, %	**1.4**
Down-3	17.1	2.14	0.76	0.92		
Down-Mean	**18.0**	**2.03**	**0.78**	**0.92**		
Down-StDev	**1.5**	**0.41**	**0.08**	**0.04**		

Test #2: Base + Bend Angle

Sample ID: Up-1

Chan	Aero HiD, µm	LnHi Dp	PreWt, mg	PostWt, mg	Cum Mass, ΔWt, mg	Frac < HiD	Mass Probits	dM, mg	Fit Mass Probits	Fit Cum Mass, mg	Fit dM, mg
Total	156.5	5.1	282.787	284.957	2.170				2.252	2.144	0.029
8	126.1	4.8	266.134	268.242	2.108	0.971	1.902	0.131	1.948	2.114	0.079
7	94.2	4.5	249.419	251.396	1.977	0.911	1.347	0.111	1.537	2.035	0.146
6	70.5	4.3	258.148	260.014	1.866	0.860	1.080	0.037	1.129	1.889	0.229
5	52.8	4.0	265.276	267.105	1.829	0.843	1.006	0.405	0.723	1.660	0.305
4	39.6	3.7	249.881	251.305	1.424	0.656	0.402	0.408	0.317	1.355	0.347
3	29.6	3.4	263.507	264.523	1.016	0.468	-0.080	0.366	-0.089	1.008	0.335
2	22.2	3.1	254.873	255.523	0.650	0.300	-0.526	0.287	-0.495	0.673	0.275
1	16.6	2.8	263.090	263.453	0.363	0.167	-0.965	0.363	-0.902	0.398	0.398
	Remaining Wt		1300.645	1400.731	100.086						
	Soln Blank		272.149	272.161	0.012						
	Blank		272.434	272.435	0.001						

Sample ID: Up-2

Chan	Aero HiD, µm	LnHi Dp	PreWt, mg	PostWt, mg	Cum Mass, ΔWt, mg	Frac < HiD	Mass Probits	dM, mg	Fit Mass Probits	Fit Cum Mass, mg	Fit dM, mg
Total	156.5	5.1	245.441	247.536	2.095				2.876	2.091	0.009
8	126.1	4.8	236.891	238.781	1.890	0.902	1.294	0.000	2.499	2.082	0.036
7	94.2	4.5	256.682	258.740	2.058	0.982	2.105	0.181	1.989	2.046	0.096
6	70.5	4.3	266.265	268.142	1.877	0.896	1.259	0.081	1.483	1.950	0.199
5	52.8	4.0	238.537	240.333	1.796	0.857	1.068	0.393	0.979	1.752	0.322
4	39.6	3.7	238.430	239.833	1.403	0.670	0.439	0.367	0.475	1.430	0.407
3	29.6	3.4	259.279	260.315	1.036	0.495	-0.014	0.420	-0.030	1.022	0.401
2	22.2	3.1	259.729	260.345	0.616	0.294	-0.542	0.280	-0.534	0.621	0.308
1	16.6	2.8	262.369	262.705	0.336	0.160	-0.993	0.336	-1.038	0.313	0.313
	Remaining Wt		1302.815	1406.388	103.573						
	Soln Blank		246.115	246.145	0.030						
	Blank		274.036	274.043	0.007						

Sample ID: Up-3

Chan	Aero HiD, µm	LnHi Dp	PreWt, mg	PostWt, mg	Cum Mass, ΔWt, mg	Frac < HiD	Mass Probits	dM, mg	Fit Mass Probits	Fit Cum Mass, mg	Fit dM, mg
Total	156.5	5.1	262.866	264.936	2.070				2.310	2.048	0.029
8	126.1	4.8	261.790	263.814	2.024	0.978	2.010	0.183	1.972	2.020	0.084
7	94.2	4.5	283.699	285.540	1.841	0.889	1.223	0.094	1.517	1.936	0.164
6	70.5	4.3	261.656	263.403	1.747	0.844	1.011	0.058	1.064	1.772	0.261
5	52.8	4.0	271.625	273.314	1.689	0.816	0.900	0.446	0.613	1.511	0.343
4	39.6	3.7	277.712	278.955	1.243	0.600	0.255	0.436	0.162	1.168	0.369
3	29.6	3.4	257.954	258.761	0.807	0.390	-0.280	0.440	-0.289	0.799	0.324
2	22.2	3.1	290.096	290.463	0.367	0.177	-0.926	0.080	-0.740	0.475	0.234
1	16.6	2.8	267.002	267.289	0.287	0.139	-1.086	0.287	-1.191	0.242	0.242
	Remaining Wt		1331.707	1430.180	98.473						
	Soln Blank		283.471	283.499	0.028						
	Blank		297.735	297.740	0.005						

Average Upstream

Chan	Aero HiD, µm	LnHi	Mean Probits	StDev Probits	Fit Probits
Total	156.5	5.1			
8	126.1	4.8	1.735	0.386	2.140
7	94.2	4.5	1.558	0.477	1.681
6	70.5	4.3	1.117	0.128	1.225
5	52.8	4.0	0.991	0.085	0.771
4	39.6	3.7	0.365	0.098	0.318
3	29.6	3.4	-0.124	0.138	-0.136
2	22.2	3.1	-0.664	0.226	-0.590
1	16.6	2.8	-1.015	0.064	-1.044

	Mean, mg	StDev, mg
Remaining Wt	100.711	2.61
Soln Blank	0.023	0.01
Blank	0.004	0.00

Test #2: Base + Bend Angle

Sample ID: Down-1

Chan	Aero HiD, µm	LnHi Dp	PreWt, mg	PostWt, mg	Cum Mass, ΔWt, mg	Frac < HiD	Mass Probits	dM, mg	Fit Mass Probits	Fit Cum Mass, mg	Fit dM, mg
Total	156.5	5.1	277.271	277.576	0.305				4.501	0.305	0.000
8	126.1	4.8	268.114	268.420	0.306	0.990	2.326	0.000	4.032	0.305	0.000
7	94.2	4.5	259.118	259.426	0.308	0.990	2.326	0.004	3.398	0.305	0.001
6	70.5	4.3	265.825	266.129	0.304	0.997	2.719	0.000	2.769	0.304	0.004
5	52.8	4.0	278.966	279.282	0.316	0.990	2.326	0.046	2.142	0.300	0.015
4	39.6	3.7	260.359	260.629	0.270	0.885	1.202	0.031	1.516	0.285	0.037
3	29.6	3.4	242.797	243.036	0.239	0.784	0.784	0.039	0.888	0.248	0.064
2	22.2	3.1	233.077	233.277	0.200	0.656	0.401	0.080	0.262	0.184	0.075
1	16.6	2.8	241.316	241.436	0.120	0.393	-0.270	0.120	-0.365	0.109	0.109
	Remaining Wt		1307.916	1321.567	13.651						
	Soln Blank		264.256	264.243	-0.013						
	Blank		266.672	266.672	0.000						

Sample ID: Down-2

Chan	Aero HiD, µm	LnHi Dp	PreWt, mg	PostWt, mg	Cum Mass, ΔWt, mg	Frac < HiD	Mass Probits	dM, mg	Fit Mass Probits	Fit Cum Mass, mg	Fit dM, mg
Total	156.5	5.1	269.225	269.620	0.395				2.549	0.393	0.002
8	126.1	4.8	244.432	244.791	0.359	0.909	1.334	0.000	2.300	0.391	0.006
7	94.2	4.5	239.694	240.066	0.372	0.942	1.570	0.000	1.963	0.385	0.011
6	70.5	4.3	269.428	269.801	0.373	0.944	1.592	0.039	1.629	0.375	0.018
5	52.8	4.0	252.232	252.566	0.334	0.846	1.018	0.000	1.296	0.356	0.028
4	39.6	3.7	236.564	236.906	0.342	0.866	1.107	0.042	0.963	0.329	0.038
3	29.6	3.4	245.175	245.475	0.300	0.759	0.705	0.036	0.629	0.290	0.047
2	22.2	3.1	272.647	272.911	0.264	0.668	0.435	0.085	0.296	0.244	0.052
1	16.6	2.8	265.487	265.666	0.179	0.453	-0.118	0.179	-0.037	0.192	0.192
	Remaining Wt		1293.643	1310.360	16.717						
	Soln Blank		271.394	271.416	0.022						
	Blank		273.424	273.427	0.003						

Sample ID: Down-3

Chan	Aero HiD, µm	LnHi Dp	PreWt, mg	PostWt, mg	Cum Mass, ΔWt, mg	Frac < HiD	Mass Probits	dM, mg	Fit Mass Probits	Fit Cum Mass, mg	Fit dM, mg
Total	156.5	5.1	244.699	245.043	0.344				2.921	0.343	0.001
8	126.1	4.8	286.368	286.712	0.344	0.990	2.326	0.046	2.636	0.343	0.003
7	94.2	4.5	262.102	262.400	0.298	0.866	1.109	0.000	2.251	0.340	0.006
6	70.5	4.3	290.622	290.949	0.327	0.951	1.651	0.002	1.869	0.333	0.013
5	52.8	4.0	265.484	265.809	0.325	0.945	1.596	0.051	1.489	0.321	0.023
4	39.6	3.7	242.875	243.149	0.274	0.797	0.829	0.003	1.108	0.298	0.034
3	29.6	3.4	262.365	262.636	0.271	0.788	0.799	0.058	0.727	0.264	0.045
2	22.2	3.1	285.801	286.014	0.213	0.619	0.303	0.026	0.347	0.219	0.051
1	16.6	2.8	275.505	275.692	0.187	0.544	0.110	0.187	-0.034	0.167	0.167
	Remaining Wt		1330.943	1345.330	14.387						
	Soln Blank		289.472	289.504	0.032						
	Blank		267.900	267.909	0.009						

Average Downstream

Chan	Aero HiD, µm	LnHi	Mean Probits	StDev Probits	Fit Probits
Total	156.5	5.1			
8	126.1	4.8	1.995	0.573	2.989
7	94.2	4.5	1.668	0.615	2.537
6	70.5	4.3	1.987	0.634	2.089
5	52.8	4.0	1.647	0.656	1.642
4	39.6	3.7	1.046	0.194	1.195
3	29.6	3.4	0.763	0.051	0.748
2	22.2	3.1	0.380	0.068	0.302
1	16.6	2.8	-0.093	0.191	-0.145

	Mean, mg	StDev, mg
Remaining Wt	14.918	1.60
Soln Blank	0.014	0.02
Blank	0.004	0.00

Test #3: Base - Bend Angle

Duct Conditions:

Duct Diameter	6 in	Start Date	7/10/03
	0.152 m	End Date	7/14/03
Bend Surface	Smooth	**Collection Details:**	
Curvature Ratio, Ro	5	# Grids / Sample	6
Bend Angle	45 deg	Sample Time / Grid	50 sec
Flow Setpoint, DP	0.52 in H20		
Duct Velocity	3942 fpm		
	20.0 m/s		
Flow Rate	774.0 cfm		
	0.365 m3/s		
Reynolds Number	203,055		
Dean Number	90,809		

Deposition vs. size

Sed Pip Chan	Geo Mid Dp, µm	Aero Mid Dp, µm	Mid Stk	η-1, %	η-2, %	η-3, %	Mean η, %	StDev η, %
Total	89.8	140.5	15.9	46.4	27.4	55.1	43.0	14.1
8	69.6	109.0	9.6	45.8	33.9	52.0	43.9	9.2
7	52.0	81.5	5.4	44.5	38.5	48.6	43.8	5.1
6	39.0	61.0	3.0	42.6	40.8	45.1	42.8	2.1
5	29.2	45.7	1.7	40.1	41.2	41.5	40.9	0.8
4	21.9	34.2	0.95	36.8	39.7	37.8	38.1	1.4
3	16.4	25.7	0.53	32.7	36.0	34.0	34.3	1.7
2	12.3	19.2	0.30	27.6	30.0	30.2	29.3	1.4
1	7.3	11.4	0.11	16.5	11.5	23.9	17.3	6.3

Summary statistics for particles sampled upstream and downstream of the bend

Sample ID	MMAD, µm	GSD	Cm, mg/m3	R2		
Up-1	33.0	1.81	5.20	0.94		
Up-2	35.4	1.84	5.35	0.95		
Up-3	35.1	1.86	5.42	0.99		
Up-Mean	**34.5**	**1.84**	**5.32**	**0.96**	Overall η-1, %	36.1
Up-StDev	**1.3**	**0.03**	**0.12**	**0.03**	Overall η-2, %	33.1
					Overall η-3, %	36.7
Down-1	30.5	1.83	3.32	1.00	Overall η-mean, %	**35.3**
Down-2	33.4	1.93	3.58	1.00	Overall η-stdev, %	**2.0**
Down-3	32.4	1.86	3.43	0.98		
Down-Mean	**32.1**	**1.87**	**3.44**	**0.99**		
Down-StDev	**1.5**	**0.05**	**0.13**	**0.01**		

Test #3: Base - Bend Angle

Sample ID: Up-1

Chan	Aero HiD, µm	LnHi Dp	PreWt, mg	PostWt, mg	Cum Mass, ΔWt, mg	Frac < HiD	Mass Probits	dM, mg	Fit Mass Probits	Fit Cum Mass, mg	Fit dM, mg
Total	156.5	5.1	242.072	244.279	2.207				2.626	2.197	0.017
8	126.1	4.8	240.401	242.487	2.086	0.945	1.600	0.000	2.261	2.181	0.059
7	94.2	4.5	245.793	247.967	2.174	0.985	2.171	0.132	1.769	2.122	0.136
6	70.5	4.3	239.734	241.776	2.042	0.925	1.441	0.275	1.281	1.986	0.250
5	52.8	4.0	231.498	233.265	1.767	0.801	0.844	0.400	0.794	1.736	0.365
4	39.6	3.7	238.268	239.635	1.367	0.619	0.304	0.438	0.308	1.370	0.424
3	29.6	3.4	270.988	271.917	0.929	0.421	-0.200	0.404	-0.180	0.946	0.389
2	22.2	3.1	283.004	283.529	0.525	0.238	-0.713	0.192	-0.666	0.558	0.283
1	16.6	2.8	287.730	288.063	0.333	0.151	-1.033	0.333	-1.153	0.275	0.275
	Remaining Wt		1432.003	1535.337	103.334						
	Soln Blank		287.858	287.872	0.014						
	Blank		262.084	262.088	0.004						

Sample ID: Up-2

Chan	Aero HiD, µm	LnHi Dp	PreWt, mg	PostWt, mg	Cum Mass, ΔWt, mg	Frac < HiD	Mass Probits	dM, mg	Fit Mass Probits	Fit Cum Mass, mg	Fit dM, mg
Total	156.5	5.1	290.469	292.841	2.372				2.442	2.355	0.026
8	126.1	4.8	278.401	280.547	2.146	0.905	1.309	0.000	2.087	2.328	0.084
7	94.2	4.5	275.989	278.256	2.267	0.956	1.703	0.249	1.607	2.244	0.178
6	70.5	4.3	293.731	295.749	2.018	0.851	1.040	0.226	1.130	2.066	0.301
5	52.8	4.0	297.096	298.888	1.792	0.755	0.692	0.486	0.656	1.765	0.408
4	39.6	3.7	292.237	293.543	1.306	0.551	0.127	0.469	0.182	1.357	0.445
3	29.6	3.4	280.119	280.956	0.837	0.353	-0.378	0.339	-0.293	0.913	0.387
2	22.2	3.1	285.888	286.386	0.498	0.210	-0.807	0.179	-0.767	0.525	0.271
1	16.6	2.8	289.272	289.591	0.319	0.134	-1.105	0.319	-1.242	0.254	0.254
	Remaining Wt		1439.123	1545.733	106.610						
	Soln Blank		284.420	284.402	-0.018						
	Blank		278.379	278.381	0.002						

Sample ID: Up-3

Chan	Aero HiD, µm	LnHi Dp	PreWt, mg	PostWt, mg	Cum Mass, ΔWt, mg	Frac < HiD	Mass Probits	dM, mg	Fit Mass Probits	Fit Cum Mass, mg	Fit dM, mg
Total	156.5	5.1	292.084	294.411	2.327				2.403	2.308	0.027
8	126.1	4.8	302.009	304.301	2.292	0.985	2.169	0.150	2.056	2.281	0.085
7	94.2	4.5	302.668	304.810	2.142	0.920	1.408	0.115	1.586	2.196	0.175
6	70.5	4.3	294.716	296.743	2.027	0.871	1.132	0.218	1.120	2.021	0.290
5	52.8	4.0	292.352	294.161	1.809	0.777	0.763	0.538	0.656	1.731	0.391
4	39.6	3.7	291.843	293.114	1.271	0.546	0.116	0.410	0.192	1.340	0.427
3	29.6	3.4	298.945	299.806	0.861	0.370	-0.332	0.373	-0.273	0.913	0.377
2	22.2	3.1	296.058	296.546	0.488	0.210	-0.807	0.147	-0.737	0.536	0.269
1	16.6	2.8	279.007	279.348	0.341	0.147	-1.051	0.341	-1.202	0.267	0.267
	Remaining Wt		1423.722	1531.970	108.248						
	Soln Blank		262.396	262.408	0.012						
	Blank		291.281	291.283	0.002						

Average Upstream

Chan	Aero HiD, µm	LnHi	Mean Probits	StDev Probits	Fit Probits
Total	156.5	5.1			
8	126.1	4.8	1.693	0.437	2.135
7	94.2	4.5	1.761	0.385	1.654
6	70.5	4.3	1.204	0.210	1.177
5	52.8	4.0	0.766	0.076	0.702
4	39.6	3.7	0.182	0.105	0.227
3	29.6	3.4	-0.303	0.092	-0.249
2	22.2	3.1	-0.776	0.054	-0.724
1	16.6	2.8	-1.063	0.038	-1.199

	Mean, mg	StDev, mg
Remaining Wt	106.064	2.50
Soln Blank	0.003	0.02
Blank	0.003	0.00

Test #3: Base - Bend Angle

Sample ID: Down-1

Chan	Aero HiD, µm	LnHi Dp	PreWt, mg	PostWt, mg	Cum Mass, ΔWt, mg	Frac < HiD	Mass Probits	dM, mg	Fit Mass Probits	Fit Cum Mass, mg	Fit dM, mg
Total	156.5	5.1	289.568	291.016	1.448				2.695	1.443	0.009
8	126.1	4.8	296.243	297.546	1.303	0.900	1.281	0.000	2.339	1.434	0.032
7	94.2	4.5	293.311	294.615	1.304	0.901	1.285	0.018	1.857	1.402	0.076
6	70.5	4.3	275.680	276.966	1.286	0.888	1.217	0.111	1.379	1.327	0.144
5	52.8	4.0	289.302	290.477	1.175	0.811	0.883	0.207	0.904	1.183	0.219
4	39.6	3.7	284.559	285.527	0.968	0.669	0.436	0.246	0.428	0.964	0.268
3	29.6	3.4	278.969	279.691	0.722	0.499	-0.003	0.309	-0.049	0.696	0.262
2	22.2	3.1	293.544	293.957	0.413	0.285	-0.567	0.180	-0.525	0.434	0.205
1	16.6	2.8	293.824	294.057	0.233	0.161	-0.991	0.233	-1.001	0.230	0.230
	Remaining Wt		1441.030	1506.709	65.679						
	Soln Blank		290.311	290.375	0.064						
	Blank		249.398	249.401	0.003						

Sample ID: Down-2

Chan	Aero HiD, µm	LnHi Dp	PreWt, mg	PostWt, mg	Cum Mass, ΔWt, mg	Frac < HiD	Mass Probits	dM, mg	Fit Mass Probits	Fit Cum Mass, mg	Fit dM, mg
Total	156.5	5.1	286.965	288.513	1.548				2.342	1.533	0.019
8	126.1	4.8	293.174	294.669	1.495	0.966	1.822	0.000	2.014	1.514	0.056
7	94.2	4.5	288.361	289.856	1.495	0.966	1.822	0.200	1.571	1.458	0.110
6	70.5	4.3	290.477	291.772	1.295	0.837	0.980	0.135	1.132	1.349	0.178
5	52.8	4.0	283.927	285.087	1.160	0.749	0.672	0.215	0.694	1.171	0.240
4	39.6	3.7	287.953	288.898	0.945	0.610	0.281	0.274	0.257	0.931	0.268
3	29.6	3.4	287.878	288.549	0.671	0.433	-0.168	0.265	-0.182	0.662	0.248
2	22.2	3.1	279.999	280.405	0.406	0.262	-0.636	0.181	-0.619	0.415	0.190
1	16.6	2.8	289.058	289.283	0.225	0.145	-1.057	0.225	-1.057	0.225	0.225
	Remaining Wt		1435.855	1507.097	71.242						
	Soln Blank		283.464	283.492	0.028						
	Blank		285.713	285.711	-0.002						

Sample ID: Down-3

Chan	Aero HiD, µm	LnHi Dp	PreWt, mg	PostWt, mg	Cum Mass, ΔWt, mg	Frac < HiD	Mass Probits	dM, mg	Fit Mass Probits	Fit Cum Mass, mg	Fit dM, mg
Total	156.5	5.1	283.656	285.100	1.444				2.549	1.436	0.012
8	126.1	4.8	280.954	282.348	1.394	0.965	1.817	0.000	2.199	1.424	0.041
7	94.2	4.5	293.463	294.881	1.418	0.982	2.097	0.110	1.727	1.383	0.090
6	70.5	4.3	302.699	304.007	1.308	0.906	1.315	0.151	1.268	1.293	0.159
5	52.8	4.0	304.879	306.036	1.157	0.801	0.846	0.278	0.791	1.134	0.229
4	39.6	3.7	285.560	286.439	0.879	0.609	0.276	0.250	0.324	0.905	0.266
3	29.6	3.4	295.980	296.609	0.629	0.436	-0.162	0.296	-0.143	0.640	0.249
2	22.2	3.1	291.460	291.793	0.333	0.231	-0.737	0.082	-0.610	0.391	0.188
1	16.6	2.8	276.759	277.010	0.251	0.174	-0.939	0.251	-1.077	0.203	0.203
	Remaining Wt		1438.354	1506.641	68.287						
	Soln Blank		274.230	274.224	-0.006						
	Blank		271.438	271.446	0.008						

Average Downstream

Chan	Aero HiD, µm	LnHi	Mean Probits	StDev Probits	Fit Probits
Total	156.5	5.1			
8	126.1	4.8	1.640	0.311	2.184
7	94.2	4.5	1.734	0.413	1.719
6	70.5	4.3	1.171	0.172	1.256
5	52.8	4.0	0.801	0.113	0.796
4	39.6	3.7	0.331	0.091	0.336
3	29.6	3.4	-0.111	0.093	-0.125
2	22.2	3.1	-0.647	0.085	-0.585
1	16.6	2.8	-0.995	0.059	-1.045

	Mean, mg	StDev, mg
Remaining Wt	68.403	2.78
Soln Blank	0.029	0.04
Blank	0.003	0.01

Test #4: Base + Construction

Duct Conditions:

Duct Diameter	6 in	Start Date	6/19/03
	0.152 m	End Date	6/20/03
Bend Surface	Gored	**Collection Details:**	
Curvature Ratio, Ro	5	# Grids / Sample	6
Bend Angle	90 deg	Sample Time / Grid	50 sec
Flow Setpoint, DP	0.52 in H20		
Duct Velocity	3942 fpm		
	20.0 m/s		
Flow Rate	774.0 cfm		
	0.365 m3/s		
Reynolds Number	203,055		
Dean Number	90,809		

Deposition vs. size

Sed Pip Chan	Geo Mid Dp, µm	Aero Mid Dp, µm	Mid Stk	η-1, %	η-2, %	η-3, %	Mean η, %	StDev η, %
Total	89.8	140.5	15.9	94.2	97.0	97.1	96.1	1.6
8	69.6	109.0	9.6	93.2	95.0	95.5	94.6	1.2
7	52.0	81.5	5.4	91.5	91.7	93.0	92.1	0.8
6	39.0	61.0	3.0	89.0	86.8	89.3	88.4	1.4
5	29.2	45.7	1.7	85.1	80.1	84.2	83.1	2.7
4	21.9	34.2	0.95	79.0	71.5	77.2	75.9	3.9
3	16.4	25.7	0.53	69.2	61.1	68.1	66.1	4.4
2	12.3	19.2	0.30	53.0	49.6	56.5	53.0	3.5
1	7.3	11.4	0.11	-15.5	28.8	24.3	12.5	24.4

Summary statistics for particles sampled upstream and downstream of the bend

Sample ID	MMAD, µm	GSD	Cm, mg/m3	R2		
Up-1	34.6	1.82	5.16	0.97		
Up-2	32.5	2.22	5.26	0.93		
Up-3	34.7	2.17	5.11	0.94		
Up-Mean	**33.9**	**2.07**	**5.18**	**0.95**	Overall η-1, %	70.5
Up-StDev	**1.2**	**0.22**	**0.08**	**0.02**	Overall η-2, %	67.4
					Overall η-3, %	67.3
Down-1	19.8	1.94	1.52	0.94	Overall η-mean, %	**68.4**
Down-2	19.3	1.96	1.72	0.98	Overall η-stdev, %	**1.8**
Down-3	18.7	2.03	1.67	0.99		
Down-Mean	**19.3**	**1.98**	**1.64**	**0.97**		
Down-StDev	**0.6**	**0.05**	**0.10**	**0.03**		

Test #4: Base + Construction

Sample ID: Up-1

Chan	Aero HiD, µm	LnHi Dp	PreWt, mg	PostWt, mg	Cum Mass, ΔWt, mg	Frac < HiD	Mass Probits	dM, mg	Fit Mass Probits	Fit Cum Mass, mg	Fit dM, mg
Total	156.5	5.1	273.719	275.777	2.058				2.521	2.046	0.020
8	126.1	4.8	273.943	276.084	2.141	0.990	2.326	0.299	2.160	2.026	0.065
7	94.2	4.5	262.202	264.044	1.842	0.895	1.254	0.000	1.672	1.961	0.144
6	70.5	4.3	266.733	268.596	1.863	0.905	1.312	0.233	1.188	1.817	0.252
5	52.8	4.0	262.496	264.126	1.630	0.792	0.813	0.407	0.707	1.564	0.352
4	39.6	3.7	260.695	261.918	1.223	0.594	0.239	0.538	0.225	1.212	0.392
3	29.6	3.4	276.750	277.435	0.685	0.333	-0.432	0.239	-0.258	0.820	0.347
2	22.2	3.1	254.874	255.320	0.446	0.217	-0.783	0.117	-0.739	0.473	0.245
1	16.6	2.8	297.870	298.199	0.329	0.160	-0.995	0.329	-1.221	0.228	0.228
	Remaining Wt		1341.764	1445.546	103.782						
	Soln Blank		272.125	272.147	0.022						
	Blank		272.418	272.415	-0.003						

Sample ID: Up-2

Chan	Aero HiD, µm	LnHi Dp	PreWt, mg	PostWt, mg	Cum Mass, ΔWt, mg	Frac < HiD	Mass Probits	dM, mg	Fit Mass Probits	Fit Cum Mass, mg	Fit dM, mg
Total	156.5	5.1	269.708	271.807	2.099				1.975	2.048	0.042
8	126.1	4.8	278.004	280.092	2.088	0.995	2.560	0.270	1.703	2.006	0.098
7	94.2	4.5	277.839	279.657	1.818	0.866	1.108	0.045	1.336	1.909	0.157
6	70.5	4.3	271.346	273.119	1.773	0.845	1.014	0.109	0.972	1.751	0.222
5	52.8	4.0	255.197	256.861	1.664	0.793	0.816	0.363	0.609	1.530	0.276
4	39.6	3.7	273.674	274.975	1.301	0.620	0.305	0.399	0.246	1.254	0.302
3	29.6	3.4	274.323	275.225	0.902	0.430	-0.177	0.251	-0.117	0.952	0.289
2	22.2	3.1	260.048	260.699	0.651	0.310	-0.495	0.235	-0.480	0.663	0.243
1	16.6	2.8	284.451	284.867	0.416	0.198	-0.848	0.416	-0.843	0.419	0.419
	Remaining Wt		1306.585	1412.215	105.630						
	Soln Blank		246.072	246.101	0.029						
	Blank		274.027	274.025	-0.002						

Sample ID: Up-3

Chan	Aero HiD, µm	LnHi Dp	PreWt, mg	PostWt, mg	Cum Mass, ΔWt, mg	Frac < HiD	Mass Probits	dM, mg	Fit Mass Probits	Fit Cum Mass, mg	Fit dM, mg
Total	156.5	5.1	273.989	276.228	2.239				1.945	2.181	0.049
8	126.1	4.8	262.887	264.757	1.870	0.835	0.975	0.015	1.666	2.132	0.114
7	94.2	4.5	257.797	259.652	1.855	0.828	0.948	0.000	1.289	2.018	0.183
6	70.5	4.3	262.525	264.390	1.865	0.833	0.966	0.266	0.914	1.835	0.255
5	52.8	4.0	277.231	278.830	1.599	0.714	0.566	0.414	0.541	1.580	0.311
4	39.6	3.7	282.157	283.342	1.185	0.529	0.073	0.300	0.169	1.269	0.331
3	29.6	3.4	247.969	248.854	0.885	0.395	-0.266	0.266	-0.205	0.938	0.307
2	22.2	3.1	266.573	267.192	0.619	0.276	-0.593	0.179	-0.577	0.631	0.248
1	16.6	2.8	272.546	272.986	0.440	0.197	-0.854	0.440	-0.950	0.383	0.383
	Remaining Wt		1302.388	1404.590	102.202						
	Soln Blank		283.449	283.446	-0.003						
	Blank		297.730	297.731	0.001						

Average Upstream

Chan	Aero HiD, µm	LnHi	Mean Probits	StDev Probits	Fit Probits
Total	156.5	5.1			
8	126.1	4.8	1.954	0.856	1.843
7	94.2	4.5	1.103	0.153	1.432
6	70.5	4.3	1.097	0.188	1.025
5	52.8	4.0	0.732	0.144	0.619
4	39.6	3.7	0.206	0.119	0.213
3	29.6	3.4	-0.292	0.129	-0.193
2	22.2	3.1	-0.624	0.146	-0.599
1	16.6	2.8	-0.899	0.083	-1.005

	Mean, mg	StDev, mg
Remaining Wt	103.871	1.72
Soln Blank	0.016	0.02
Blank	-0.001	0.00

Test #4: Base + Construction

Sample ID: Down-1

Chan	Aero HiD, µm	LnHi Dp	PreWt, mg	PostWt, mg	Cum Mass, ΔWt, mg	Frac < HiD	Mass Probits	dM, mg	Fit Mass Probits	Fit Cum Mass, mg	Fit dM, mg
Total	156.5	5.1	278.031	278.698	0.667				3.122	0.666	0.001
8	126.1	4.8	274.991	275.600	0.609	0.913	1.360	0.000	2.795	0.665	0.004
7	94.2	4.5	265.491	266.148	0.657	0.985	2.170	0.000	2.354	0.661	0.012
6	70.5	4.3	271.394	272.051	0.657	0.985	2.170	0.053	1.916	0.649	0.028
5	52.8	4.0	268.558	269.162	0.604	0.906	1.314	0.042	1.480	0.621	0.053
4	39.6	3.7	268.621	269.183	0.562	0.843	1.005	0.020	1.044	0.568	0.082
3	29.6	3.4	273.951	274.493	0.542	0.813	0.887	0.172	0.607	0.486	0.107
2	22.2	3.1	278.444	278.814	0.370	0.555	0.138	0.117	0.171	0.379	0.115
1	16.6	2.8	262.968	263.221	0.253	0.379	-0.307	0.253	-0.265	0.264	0.264
	Remaining Wt		1320.006	1349.231	29.225						
	Soln Blank		264.175	264.191	0.016						
	Blank		266.657	266.659	0.002						

Sample ID: Down-2

Chan	Aero HiD, µm	LnHi Dp	PreWt, mg	PostWt, mg	Cum Mass, ΔWt, mg	Frac < HiD	Mass Probits	dM, mg	Fit Mass Probits	Fit Cum Mass, mg	Fit dM, mg
Total	156.5	5.1	253.488	254.212	0.724				3.104	0.723	0.001
8	126.1	4.8	262.841	263.502	0.661	0.913	1.359	0.000	2.784	0.722	0.005
7	94.2	4.5	269.743	270.501	0.758	0.990	2.326	0.032	2.350	0.717	0.013
6	70.5	4.3	267.256	267.982	0.726	0.990	2.326	0.063	1.920	0.704	0.029
5	52.8	4.0	270.940	271.603	0.663	0.916	1.377	0.032	1.492	0.675	0.055
4	39.6	3.7	274.280	274.911	0.631	0.872	1.134	0.076	1.064	0.620	0.086
3	29.6	3.4	272.457	273.012	0.555	0.767	0.728	0.135	0.635	0.534	0.113
2	22.2	3.1	253.982	254.402	0.420	0.580	0.202	0.134	0.206	0.421	0.123
1	16.6	2.8	272.591	272.877	0.286	0.395	-0.266	0.286	-0.222	0.298	0.298
	Remaining Wt		1293.583	1326.703	33.120						
	Soln Blank		259.960	260.001	0.041						
	Blank		273.409	273.411	0.002						

Sample ID: Down-3

Chan	Aero HiD, µm	LnHi Dp	PreWt, mg	PostWt, mg	Cum Mass, ΔWt, mg	Frac < HiD	Mass Probits	dM, mg	Fit Mass Probits	Fit Cum Mass, mg	Fit dM, mg
Total	156.5	5.1	264.861	265.529	0.668				3.006	0.667	0.001
8	126.1	4.8	276.140	276.895	0.755	0.990	2.326	0.042	2.700	0.666	0.005
7	94.2	4.5	265.367	266.080	0.713	0.990	2.326	0.049	2.287	0.661	0.013
6	70.5	4.3	276.206	276.870	0.664	0.994	2.513	0.040	1.876	0.648	0.027
5	52.8	4.0	283.166	283.790	0.624	0.934	1.507	0.071	1.468	0.621	0.049
4	39.6	3.7	283.279	283.832	0.553	0.828	0.946	0.042	1.059	0.571	0.076
3	29.6	3.4	263.093	263.604	0.511	0.765	0.722	0.116	0.650	0.496	0.098
2	22.2	3.1	275.194	275.589	0.395	0.591	0.231	0.102	0.242	0.398	0.108
1	16.6	2.8	289.563	289.856	0.293	0.439	-0.154	0.293	-0.167	0.290	0.290
	Remaining Wt		1330.473	1362.920	32.447						
	Soln Blank		276.326	276.330	0.004						
	Blank		271.300	271.300	0.000						

Average Downstream

Chan	Aero HiD, µm	LnHi	Mean Probits	StDev Probits	Fit Probits
Total	156.5	5.1			
8	126.1	4.8	1.682	0.558	2.759
7	94.2	4.5	2.274	0.090	2.330
6	70.5	4.3	2.336	0.172	1.904
5	52.8	4.0	1.399	0.099	1.480
4	39.6	3.7	1.028	0.096	1.056
3	29.6	3.4	0.779	0.094	0.631
2	22.2	3.1	0.190	0.048	0.206
1	16.6	2.8	-0.243	0.079	-0.218

	Mean, mg	StDev, mg
Remaining Wt	31.597	2.08
Soln Blank	0.020	0.02
Blank	0.001	0.00

Test #5: Base - Construction

Duct Conditions:

Duct Diameter	6 in	Start Date	5/26/03
	0.152 m	End Date	5/31/03
Bend Surface	Segmented	**Collection Details:**	
Curvature Ratio, Ro	5	# Grids / Sample	6
Bend Angle	90 deg	Sample Time / Grid	50 sec
Flow Setpoint, DP	0.52 in H20		
Duct Velocity	3942 fpm		
	20.0 m/s		
Flow Rate	774.0 cfm		
	0.365 m3/s		
Reynolds Number	203,055		
Dean Number	90,809		

Deposition vs. size

Sed Plp Chan	Geo Mid Dp, µm	Aero Mid Dp, µm	Mid Stk	η-1, %	η-2, %	η-3, %	Mean η, %	StDev η, %
Total	89.8	140.5	15.9	61.0	90.7	91.7	81.1	17.5
8	69.6	109.0	9.6	55.4	86.6	86.4	76.1	18.0
7	52.0	81.5	5.4	49.9	80.3	78.3	69.5	17.0
6	39.0	61.0	3.0	45.6	71.5	68.2	61.8	14.1
5	29.2	45.7	1.7	42.7	59.7	56.6	53.0	9.1
4	21.9	34.2	0.95	41.5	43.7	45.1	43.4	1.8
3	16.4	25.7	0.53	42.1	22.8	35.6	33.5	9.8
2	12.3	19.2	0.30	44.5	-4.3	29.8	23.3	25.0
1	7.3	11.4	0.11	50.0	-56.8	31.3	8.2	57.1

Summary statistics for particles sampled upstream and downstream of the bend

Sample ID	MMAD, µm	GSD	Cm, mg/m3	R2		
Up-1	41.6	1.68	4.89	0.93		
Up-2	41.4	1.75	5.02	0.97		
Up-3	39.0	1.75	5.34	0.98		
Up-Mean	**40.7**	**1.72**	**5.08**	**0.96**	Overall h-1, %	49.2
Up-StDev	**1.5**	**0.04**	**0.23**	**0.02**	Overall h-2, %	39.5
					Overall h-3, %	48.6
Down-1	40.7	1.63	2.48	0.97	Overall h-mean, %	**45.8**
Down-2	29.1	1.72	3.04	0.99	Overall h-stdev, %	**5.4**
Down-3	32.0	1.63	2.74	0.99		
Down-Mean	**33.9**	**1.66**	**2.75**	**0.99**		
Down-StDev	**6.0**	**0.05**	**0.28**	**0.01**		

Test #5: Base - Construction

Sample ID: Up-1

Chan	Aero HiD, µm	LnHi Dp	PreWt, mg	PostWt, mg	Cum Mass, ΔWt, mg	Frac < HiD	Mass Probits	dM, mg	Fit Mass Probits	Fit Cum Mass, mg	Fit dM, mg
Total	156.5	5.1	1300.965	1302.718	1.753				2.566	1.744	0.019
8	126.1	4.8	1320.500	1322.030	1.530	0.873	1.140	0.000	2.147	1.725	0.072
7	94.2	4.5	1316.841	1318.507	1.666	0.950	1.648	0.213	1.582	1.653	0.170
6	70.5	4.3	1321.538	1322.991	1.453	0.829	0.950	0.209	1.020	1.483	0.296
5	52.8	4.0	1322.608	1323.852	1.244	0.710	0.552	0.483	0.460	1.187	0.380
4	39.6	3.7	1300.892	1301.653	0.761	0.434	-0.166	0.402	-0.099	0.807	0.360
3	29.6	3.4	1307.338	1307.697	0.359	0.205	-0.825	0.194	-0.659	0.447	0.251
2	22.2	3.1	1306.759	1306.924	0.165	0.094	-1.316	0.056	-1.218	0.196	0.129
1	16.6	2.8	1314.215	1314.324	0.109	0.062	-1.537	0.109	-1.778	0.066	0.066
	Remaining Wt		1313.034	1414.137	101.103						
	Soln Blank		1336.342	1336.355	0.013						
	Blank		1345.457	1345.451	-0.006						

Sample ID: Up-2

Chan	Aero HiD, µm	LnHi Dp	PreWt, mg	PostWt, mg	Cum Mass, ΔWt, mg	Frac < HiD	Mass Probits	dM, mg	Fit Mass Probits	Fit Cum Mass, mg	Fit dM, mg
Total	156.5	5.1	1326.987	1329.269	2.282				2.371	2.262	0.033
8	126.1	4.8	1326.180	1328.361	2.181	0.956	1.703	0.235	1.986	2.228	0.109
7	94.2	4.5	1325.454	1327.400	1.946	0.853	1.048	0.021	1.466	2.119	0.228
6	70.5	4.3	1314.626	1316.551	1.925	0.844	1.009	0.223	0.949	1.891	0.367
5	52.8	4.0	1307.891	1309.593	1.702	0.746	0.661	0.477	0.434	1.524	0.456
4	39.6	3.7	1309.850	1311.075	1.225	0.537	0.092	0.502	-0.080	1.068	0.439
3	29.6	3.4	1310.159	1310.882	0.723	0.317	-0.477	0.433	-0.596	0.629	0.325
2	22.2	3.1	1343.004	1343.294	0.290	0.127	-1.140	0.200	-1.110	0.305	0.186
1	16.6	2.8	1318.928	1319.018	0.090	0.039	-1.757	0.090	-1.625	0.119	0.119
	Remaining Wt		1308.691	1408.863	100.172						
	Soln Blank		1336.464	1336.451	-0.013						
	Blank		1320.145	1320.156	0.011						

Sample ID: Up-3

Chan	Aero HiD, µm	LnHi Dp	PreWt, mg	PostWt, mg	Cum Mass, ΔWt, mg	Frac < HiD	Mass Probits	dM, mg	Fit Mass Probits	Fit Cum Mass, mg	Fit dM, mg
Total	156.5	5.1	1292.847	1294.997	2.150				2.493	2.136	0.024
8	126.1	4.8	1308.810	1310.843	2.033	0.946	1.603	0.052	2.106	2.112	0.084
7	94.2	4.5	1293.541	1295.522	1.981	0.921	1.415	0.110	1.583	2.028	0.187
6	70.5	4.3	1321.988	1323.859	1.871	0.870	1.127	0.257	1.063	1.841	0.320
5	52.8	4.0	1286.367	1287.981	1.614	0.751	0.677	0.456	0.545	1.521	0.422
4	39.6	3.7	1286.606	1287.764	1.158	0.539	0.097	0.522	0.028	1.099	0.428
3	29.6	3.4	1293.444	1294.080	0.636	0.296	-0.536	0.335	-0.490	0.671	0.334
2	22.2	3.1	1296.500	1296.801	0.301	0.140	-1.080	0.158	-1.007	0.337	0.201
1	16.6	2.8	1292.734	1292.877	0.143	0.067	-1.502	0.143	-1.525	0.137	0.137
	Remaining Wt		1292.389	1400.615	108.226						
	Soln Blank		1331.718	1331.677	-0.041						
	Blank		1326.166	1326.156	-0.010						

Average Upstream

Chan	Aero HiD, µm	LnHi	Mean Probits	StDev Probits	Fit Probits
Total	156.5	5.1			
8	126.1	4.8	1.482	0.301	2.080
7	94.2	4.5	1.370	0.302	1.543
6	70.5	4.3	1.029	0.091	1.010
5	52.8	4.0	0.630	0.068	0.480
4	39.6	3.7	0.008	0.150	-0.050
3	29.6	3.4	-0.613	0.186	-0.582
2	22.2	3.1	-1.179	0.122	-1.112
1	16.6	2.8	-1.599	0.138	-1.643

	Mean, mg	StDev, mg
Remaining Wt	103.167	4.41
Soln Blank	-0.014	0.03
Blank	-0.002	0.01

Test #5: Base - Construction

Sample ID: Down-1

Chan	Aero HiD, µm	LnHi Dp	PreWt, mg	PostWt, mg	Cum Mass, ΔWt, mg	Frac < HiD	Mass Probits	dM, mg	Fit Mass Probits	Fit Cum Mass, mg	Fit dM, mg
Total	156.5	5.1	1307.509	1308.477	0.968				2.744	0.965	0.007
8	126.1	4.8	1320.477	1321.411	0.934	0.965	1.810	0.089	2.303	0.958	0.032
7	94.2	4.5	1313.481	1314.326	0.845	0.873	1.140	0.000	1.708	0.926	0.085
6	70.5	4.3	1319.983	1320.843	0.860	0.888	1.218	0.096	1.118	0.840	0.161
5	52.8	4.0	1311.164	1311.928	0.764	0.789	0.804	0.219	0.530	0.679	0.218
4	39.6	3.7	1311.514	1312.059	0.545	0.563	0.159	0.220	-0.058	0.461	0.211
3	29.6	3.4	1312.350	1312.675	0.325	0.336	-0.424	0.268	-0.647	0.250	0.146
2	22.2	3.1	1321.158	1321.225	0.067	0.069	-1.482	0.064	-1.235	0.105	0.072
1	16.6	2.8	1328.632	1328.635	0.003	0.003	-2.737	0.003	-1.824	0.033	0.033
	Remaining Wt		1314.585	1365.181	50.596						
	Soln Blank		1318.605	1318.590	-0.015						
	Blank		1319.916	1319.889	-0.027						

Sample ID: Down-2

Chan	Aero HiD, µm	LnHi Dp	PreWt, mg	PostWt, mg	Cum Mass, ΔWt, mg	Frac < HiD	Mass Probits	dM, mg	Fit Mass Probits	Fit Cum Mass, mg	Fit dM, mg
Total	156.5	5.1	1310.664	1311.894	1.230				3.093	1.229	0.003
8	126.1	4.8	1297.540	1298.739	1.199	0.975	1.956	0.028	2.695	1.226	0.015
7	94.2	4.5	1291.139	1292.310	1.171	0.952	1.665	0.000	2.158	1.211	0.045
6	70.5	4.3	1288.971	1290.148	1.177	0.957	1.716	0.106	1.625	1.166	0.104
5	52.8	4.0	1293.984	1295.055	1.071	0.871	1.130	0.229	1.094	1.062	0.184
4	39.6	3.7	1310.637	1311.479	0.842	0.685	0.480	0.210	0.564	0.878	0.247
3	29.6	3.4	1310.880	1311.512	0.632	0.514	0.035	0.219	0.032	0.631	0.251
2	22.2	3.1	1298.141	1298.554	0.413	0.336	-0.424	0.235	-0.499	0.380	0.194
1	16.6	2.8	1285.842	1286.020	0.178	0.145	-1.059	0.178	-1.030	0.186	0.186
	Remaining Wt		1285.518	1345.855	60.337						
	Soln Blank		1306.912	1306.898	-0.014						
	Blank		1343.847	1343.823	-0.024						

Sample ID: Down-3

Chan	Aero HiD, µm	LnHi Dp	PreWt, mg	PostWt, mg	Cum Mass, ΔWt, mg	Frac < HiD	Mass Probits	dM, mg	Fit Mass Probits	Fit Cum Mass, mg	Fit dM, mg
Total	156.5	5.1	1291.794	1292.818	1.024				3.239	1.023	0.002
8	126.1	4.8	1294.123	1295.149	1.026	0.990	2.326	0.000	2.799	1.021	0.011
7	94.2	4.5	1279.904	1280.950	1.046	0.990	2.326	0.058	2.204	1.010	0.041
6	70.5	4.3	1270.729	1271.717	0.988	0.965	1.810	0.185	1.613	0.969	0.102
5	52.8	4.0	1290.243	1291.046	0.803	0.784	0.786	0.167	1.024	0.867	0.183
4	39.6	3.7	1285.430	1286.066	0.636	0.621	0.308	0.155	0.436	0.685	0.235
3	29.6	3.4	1275.203	1275.684	0.481	0.470	-0.076	0.257	-0.153	0.450	0.215
2	22.2	3.1	1298.402	1298.626	0.224	0.219	-0.776	0.107	-0.742	0.235	0.141
1	16.6	2.8	1286.262	1286.379	0.117	0.114	-1.204	0.117	-1.330	0.094	0.094
	Remaining Wt		1301.500	1356.946	55.446						
	Soln Blank		1280.015	1280.005	-0.010						
	Blank		1289.490	1289.490	0.000						

Average Downstream

Chan	Aero HiD, µm	LnHi	Mean Probits	StDev Probits	Fit Probits
Total	156.5	5.1			
8	126.1	4.8	2.031	0.266	2.599
7	94.2	4.5	1.711	0.594	2.024
6	70.5	4.3	1.581	0.318	1.452
5	52.8	4.0	0.907	0.193	0.883
4	39.6	3.7	0.316	0.161	0.314
3	29.6	3.4	-0.155	0.239	-0.256
2	22.2	3.1	-0.894	0.539	-0.825
1	16.6	2.8	-1.667	0.930	-1.395

	Mean, mg	StDev, mg
Remaining Wt	55.460	4.87
Soln Blank	-0.013	0.00
Blank	-0.017	0.01

Test #6: Base + Orientation

Duct Conditions:

Duct Diameter	6 in	Start Date	7/15/03
	0.152 m	End Date	7/17/03
Bend Surface	Smooth	**Collection Details:**	
Curvature Ratio, Ro	5	# Grids / Sample	6
Bend Angle	90 deg	Sample Time / Grid	50 sec
Flow Setpoint, DP	0.52 in H20		
Duct Velocity	3942 fpm		
	20.0 m/s		
Flow Rate	774.0 cfm		
	0.365 m3/s		
Reynolds Number	203,055		
Dean Number	90,809		

Deposition vs. size

Sed Pip Chan	Geo Mid Dp, µm	Aero Mid Dp, µm	Mid Stk	η-1, %	η-2, %	η-3, %	Mean η, %	StDev η, %
Total	89.8	140.5	15.9	96.3	97.4	95.4	96.4	1.0
8	69.6	109.0	9.6	92.8	94.8	93.4	93.7	1.1
7	52.0	81.5	5.4	86.7	90.0	90.4	89.0	2.0
6	39.0	61.0	3.0	78.7	82.5	86.4	82.5	3.9
5	29.2	45.7	1.7	70.1	72.3	81.0	74.4	5.8
4	21.9	34.2	0.95	63.2	60.5	73.9	65.9	7.1
3	16.4	25.7	0.53	60.4	49.2	64.9	58.2	8.1
2	12.3	19.2	0.30	62.7	40.9	53.7	52.4	11.0
1	7.3	11.4	0.11	78.3	42.2	28.4	49.6	25.7

Summary statistics for particles sampled upstream and downstream of the bend

Sample ID	MMAD, µm	GSD	Cm, mg/m3	R2		
Up-1	29.9	2.25	5.68	0.99		
Up-2	35.4	2.00	4.90	0.98		
Up-3	33.4	1.88	5.26	1.00		
Up-Mean	**32.9**	**2.04**	**5.28**	**0.99**	Overall h-1, %	72.4
Up-StDev	**2.8**	**0.19**	**0.39**	**0.01**	Overall h-2, %	63.7
					Overall h-3, %	68.3
Down-1	27.4	1.75	1.57	0.92	Overall h-mean, %	**68.1**
Down-2	25.3	1.73	1.78	0.96	Overall h-stdev, %	**4.4**
Down-3	22.6	1.83	1.67	0.96		
Down-Mean	**25.1**	**1.77**	**1.67**	**0.95**		
Down-StDev	**2.4**	**0.05**	**0.11**	**0.02**		

Test #6: Base + Orientation

Sample ID: Up-1

Chan	Aero HiD, µm	LnHi Dp	PreWt, mg	PostWt, mg	Cum Mass, ΔWt, mg	Frac < HiD	Mass Probits	dM, mg	Fit Mass Probits	Fit Cum Mass, mg	Fit dM, mg
Total	156.5	5.1	277.675	280.076	2.401				2.044	2.352	0.042
8	126.1	4.8	282.426	284.712	2.286	0.952	1.666	0.076	1.777	2.310	0.097
7	94.2	4.5	280.702	282.912	2.210	0.920	1.408	0.087	1.417	2.213	0.160
6	70.5	4.3	286.050	288.173	2.123	0.884	1.196	0.245	1.059	2.053	0.231
5	52.8	4.0	282.944	284.822	1.878	0.782	0.780	0.386	0.703	1.822	0.296
4	39.6	3.7	285.937	287.429	1.492	0.621	0.309	0.367	0.347	1.526	0.335
3	29.6	3.4	294.459	295.584	1.125	0.469	-0.079	0.313	-0.010	1.191	0.333
2	22.2	3.1	279.418	280.230	0.812	0.338	-0.417	0.200	-0.366	0.857	0.293
1	16.6	2.8	286.612	287.224	0.612	0.255	-0.659	0.612	-0.723	0.564	0.564
	Remaining Wt		1337.819	1450.594	112.775						
	Soln Blank		272.151	272.151	0.000						
	Blank		272.432	272.436	0.004						

Sample ID: Up-2

Chan	Aero HiD, µm	LnHi Dp	PreWt, mg	PostWt, mg	Cum Mass, ΔWt, mg	Frac < HiD	Mass Probits	dM, mg	Fit Mass Probits	Fit Cum Mass, mg	Fit dM, mg
Total	156.5	5.1	301.791	303.895	2.104				2.138	2.070	0.037
8	126.1	4.8	289.497	291.571	2.074	0.986	2.190	0.178	1.827	2.033	0.097
7	94.2	4.5	280.754	282.650	1.896	0.901	1.288	0.140	1.407	1.936	0.171
6	70.5	4.3	285.385	287.141	1.756	0.835	0.973	0.140	0.990	1.765	0.256
5	52.8	4.0	291.256	292.872	1.616	0.768	0.732	0.416	0.574	1.509	0.324
4	39.6	3.7	296.090	297.290	1.200	0.570	0.177	0.384	0.159	1.185	0.346
3	29.6	3.4	292.536	293.352	0.816	0.388	-0.285	0.254	-0.257	0.838	0.311
2	22.2	3.1	299.858	300.420	0.562	0.267	-0.622	0.300	-0.673	0.527	0.236
1	16.6	2.8	299.176	299.438	0.262	0.125	-1.153	0.262	-1.088	0.291	0.291
	Remaining Wt		1340.596	1438.446	97.850						
	Soln Blank		246.141	246.126	-0.015						
	Blank		274.043	274.047	0.004						

Sample ID: Up-3

Chan	Aero HiD, µm	LnHi Dp	PreWt, mg	PostWt, mg	Cum Mass, ΔWt, mg	Frac < HiD	Mass Probits	dM, mg	Fit Mass Probits	Fit Cum Mass, mg	Fit dM, mg
Total	156.5	5.1	279.861	282.079	2.218				2.452	2.202	0.023
8	126.1	4.8	282.977	285.149	2.172	0.979	2.039	0.058	2.109	2.179	0.072
7	94.2	4.5	300.894	303.008	2.114	0.953	1.676	0.169	1.645	2.107	0.151
6	70.5	4.3	291.429	293.374	1.945	0.877	1.160	0.187	1.185	1.956	0.257
5	52.8	4.0	290.269	292.027	1.758	0.793	0.815	0.399	0.726	1.699	0.356
4	39.6	3.7	295.644	297.003	1.359	0.613	0.286	0.387	0.268	1.343	0.402
3	29.6	3.4	301.630	302.602	0.972	0.438	-0.155	0.473	-0.191	0.941	0.369
2	22.2	3.1	286.888	287.387	0.499	0.225	-0.755	0.188	-0.649	0.572	0.275
1	16.6	2.8	277.090	277.401	0.311	0.140	-1.079	0.311	-1.108	0.297	0.297
	Remaining Wt		1321.490	1426.351	104.861						
	Soln Blank		283.499	283.546	0.047						
	Blank		297.743	297.750	0.007						

Average Upstream

Chan	Aero HiD, µm	LnHi	Mean Probits	StDev Probits	Fit Probits
Total	156.5	5.1			
8	126.1	4.8	1.965	0.270	1.904
7	94.2	4.5	1.457	0.198	1.490
6	70.5	4.3	1.110	0.120	1.078
5	52.8	4.0	0.776	0.042	0.668
4	39.6	3.7	0.258	0.071	0.258
3	29.6	3.4	-0.173	0.104	-0.153
2	22.2	3.1	-0.598	0.170	-0.563
1	16.6	2.8	-0.964	0.266	-0.973

	Mean, mg	StDev, mg
Remaining Wt	105.162	7.47
Soln Blank	0.011	0.03
Blank	0.005	0.00

Test #6: Base + Orientation

Sample ID: Down-1

Chan	Aero HiD, µm	LnHi Dp	PreWt, mg	PostWt, mg	Cum Mass, ΔWt, mg	Frac < HiD	Mass Probits	dM, mg	Fit Mass Probits	Fit Cum Mass, mg	Fit dM, mg
Total	156.5	5.1	292.181	292.837	0.656				3.101	0.655	0.002
8	126.1	4.8	282.392	283.096	0.704	0.990	2.326	0.072	2.716	0.654	0.007
7	94.2	4.5	289.471	290.103	0.632	0.963	1.792	0.016	2.196	0.647	0.021
6	70.5	4.3	296.650	297.266	0.616	0.939	1.547	0.033	1.680	0.626	0.049
5	52.8	4.0	293.909	294.492	0.583	0.889	1.220	0.109	1.167	0.576	0.089
4	39.6	3.7	296.894	297.368	0.474	0.723	0.590	0.132	0.653	0.488	0.123
3	29.6	3.4	289.395	289.737	0.342	0.521	0.054	0.170	0.139	0.364	0.132
2	22.2	3.1	287.293	287.465	0.172	0.262	-0.637	0.000	-0.375	0.232	0.109
1	16.6	2.8	294.647	294.842	0.195	0.297	-0.532	0.195	-0.889	0.123	0.123
	Remaining Wt		1345.908	1376.725	30.817						
	Soln Blank		264.238	264.256	0.018						
	Blank		266.670	266.669	-0.001						

Sample ID: Down-2

Chan	Aero HiD, µm	LnHi Dp	PreWt, mg	PostWt, mg	Cum Mass, ΔWt, mg	Frac < HiD	Mass Probits	dM, mg	Fit Mass Probits	Fit Cum Mass, mg	Fit dM, mg
Total	156.5	5.1	283.597	284.358	0.761				3.327	0.761	0.001
8	126.1	4.8	294.304	294.992	0.688	0.904	1.305	0.000	2.932	0.760	0.005
7	94.2	4.5	299.290	300.045	0.755	0.992	2.414	0.017	2.399	0.755	0.017
6	70.5	4.3	307.553	308.291	0.738	0.970	1.878	0.056	1.869	0.738	0.045
5	52.8	4.0	293.963	294.645	0.682	0.896	1.260	0.119	1.341	0.693	0.090
4	39.6	3.7	300.532	301.095	0.563	0.740	0.643	0.029	0.814	0.603	0.137
3	29.6	3.4	285.103	285.637	0.534	0.702	0.529	0.190	0.286	0.466	0.158
2	22.2	3.1	291.236	291.580	0.344	0.452	-0.121	0.200	-0.241	0.308	0.140
1	16.6	2.8	291.884	292.028	0.144	0.189	-0.881	0.144	-0.769	0.168	0.168
	Remaining Wt		1329.523	1364.275	34.752						
	Soln Blank		271.410	271.419	0.009						
	Blank		273.423	273.427	0.004						

Sample ID: Down-3

Chan	Aero HiD, µm	LnHi Dp	PreWt, mg	PostWt, mg	Cum Mass, ΔWt, mg	Frac < HiD	Mass Probits	dM, mg	Fit Mass Probits	Fit Cum Mass, mg	Fit dM, mg
Total	156.5	5.1	283.990	284.688	0.698				3.211	0.698	0.001
8	126.1	4.8	299.756	300.358	0.602	0.862	1.091	0.000	2.852	0.696	0.005
7	94.2	4.5	296.328	297.000	0.672	0.963	1.784	0.025	2.368	0.692	0.014
6	70.5	4.3	295.262	295.909	0.647	0.927	1.453	0.004	1.886	0.677	0.035
5	52.8	4.0	279.764	280.407	0.643	0.921	1.413	0.090	1.407	0.642	0.068
4	39.6	3.7	301.740	302.293	0.553	0.792	0.814	0.045	0.928	0.575	0.105
3	29.6	3.4	277.445	277.953	0.508	0.728	0.606	0.215	0.448	0.470	0.129
2	22.2	3.1	295.853	296.146	0.293	0.420	-0.202	0.050	-0.031	0.340	0.128
1	16.6	2.8	295.663	295.906	0.243	0.348	-0.390	0.243	-0.511	0.213	0.213
	Remaining Wt		1345.339	1378.007	32.668						
	Soln Blank		289.505	289.521	0.016						
	Blank		267.908	267.915	0.007						

Average Downstream

Chan	Aero HiD, µm	LnHi	Mean Probits	StDev Probits	Fit Probits
Total	156.5	5.1			
8	126.1	4.8	1.574	0.660	2.833
7	94.2	4.5	1.997	0.362	2.321
6	70.5	4.3	1.626	0.223	1.812
5	52.8	4.0	1.298	0.102	1.305
4	39.6	3.7	0.683	0.117	0.798
3	29.6	3.4	0.396	0.299	0.291
2	22.2	3.1	-0.320	0.277	-0.216
1	16.6	2.8	-0.601	0.252	-0.723

	Mean, mg	StDev, mg
Remaining Wt	32.746	1.97
Soln Blank	0.014	0.00
Blank	0.003	0.00

Test #7: High Re, Small R0

Duct Conditions:

Duct Diameter	8 in	Start Date	2/27/03
	0.203 m	End Date	3/5/03
Bend Surface	Seamed	**Collection Details:**	
Curvature Ratio, Ro	3	# Grids / Sample	3
Bend Angle	90 deg	Sample Time / Grid	100 sec
Flow Setpoint, DP	3.25 in H20		
Duct Velocity	5342 fpm		
	27.1 m/s		
Flow Rate	1864.7 cfm		
	0.880 m3/s		
Reynolds Number	366,915		
Dean Number	211,838		

Deposition vs. size

Sed Pip Chan	Geo Mid Dp, µm	Aero Mid Dp, µm	Mid Stk	η-1, %	η-2, %	η-3, %	Mean η, %	StDev η, %
Total	89.8	140.5	16.2	85.4	95.8	97.8	93.0	6.7
8	69.6	109.0	9.7	85.0	92.6	95.5	91.0	5.4
7	52.0	81.5	5.4	83.9	87.4	91.2	87.5	3.7
6	39.0	61.0	3.1	81.8	80.4	84.4	82.2	2.0
5	29.2	45.7	1.7	78.5	72.4	75.3	75.4	3.0
4	21.9	34.2	0.96	73.3	64.5	64.5	67.5	5.1
3	16.4	25.7	0.54	65.3	58.4	54.2	59.3	5.6
2	12.3	19.2	0.30	52.9	55.5	46.7	51.7	4.5
1	7.3	11.4	0.11	5.1	59.8	46.3	37.1	28.5

Summary statistics for particles sampled upstream and downstream of the bend

Sample ID	MMAD, µm	GSD	Cm, mg/m3	R2		
Up-1	34.8	1.84	2.54	0.99		
Up-2	35.6	1.82	2.56	0.98		
Up-3	38.2	1.81	2.46	0.96		
Up-Mean	**36.2**	**1.83**	**2.52**	**0.98**	Overall η-1, %	64.8
Up-StDev	**1.8**	**0.01**	**0.06**	**0.02**	Overall η-2, %	65.4
					Overall η-3, %	66.7
Down-1	23.4	2.00	0.90	0.95	Overall η-mean, %	**65.7**
Down-2	29.2	1.66	0.89	0.99	Overall η-stdev, %	**1.0**
Down-3	28.3	1.64	0.82	0.96		
Down-Mean	**27.0**	**1.76**	**0.87**	**0.96**		
Down-StDev	**3.1**	**0.20**	**0.04**	**0.02**		

Test #7: High Re, Small R0

Sample ID: Up-1

Chan	Aero HiD, µm	LnHi Dp	PreWt, mg	PostWt, mg	Cum Mass, ΔWt, mg	Frac < HiD	Mass Probits	dM, mg	Fit Mass Probits	Fit Cum Mass, mg	Fit dM, mg
Total	156.5	5.1	1337.864	1340.200	2.336				2.459	2.320	0.025
8	126.1	4.8	1345.269	1347.551	2.282	0.977	1.993	0.054	2.108	2.295	0.080
7	94.2	4.5	1340.468	1342.696	2.228	0.954	1.683	0.180	1.628	2.215	0.169
6	70.5	4.3	1356.530	1358.578	2.048	0.877	1.159	0.174	1.154	2.046	0.288
5	52.8	4.0	1329.049	1330.923	1.874	0.802	0.850	0.559	0.682	1.758	0.395
4	39.6	3.7	1328.533	1329.848	1.315	0.563	0.158	0.443	0.210	1.363	0.436
3	29.6	3.4	1338.984	1339.856	0.872	0.373	-0.323	0.391	-0.262	0.927	0.386
2	22.2	3.1	1321.187	1321.668	0.481	0.206	-0.821	0.174	-0.734	0.541	0.275
1	16.6	2.8	1326.151	1326.458	0.307	0.131	-1.120	0.307	-1.206	0.266	0.266
	Remaining Wt		1331.470	1455.699	124.229						
	Soln Blank		1336.331	1336.325	-0.006						
	Blank		1345.407	1345.420	0.013						

Sample ID: Up-2

Chan	Aero HiD, µm	LnHi Dp	PreWt, mg	PostWt, mg	Cum Mass, ΔWt, mg	Frac < HiD	Mass Probits	dM, mg	Fit Mass Probits	Fit Cum Mass, mg	Fit dM, mg
Total	156.5	5.1	1332.243	1334.653	2.410				2.466	2.394	0.026
8	126.1	4.8	1351.589	1353.899	2.310	0.959	1.734	0.060	2.106	2.368	0.084
7	94.2	4.5	1330.859	1333.109	2.250	0.934	1.503	0.115	1.620	2.283	0.161
6	70.5	4.3	1323.391	1325.526	2.135	0.886	1.205	0.249	1.137	2.102	0.308
5	52.8	4.0	1325.498	1327.384	1.886	0.783	0.781	0.591	0.657	1.794	0.420
4	39.6	3.7	1320.789	1322.084	1.295	0.537	0.094	0.430	0.177	1.374	0.457
3	29.6	3.4	1316.130	1316.995	0.865	0.359	-0.361	0.263	-0.304	0.917	0.396
2	22.2	3.1	1331.516	1332.118	0.602	0.250	-0.675	0.373	-0.785	0.521	0.273
1	16.6	2.8	1326.591	1326.820	0.229	0.095	-1.310	0.229	-1.266	0.248	0.248
	Remaining Wt		1323.682	1448.619	124.937						
	Soln Blank		1336.422	1336.440	0.018						
	Blank		1320.096	1320.118	0.022						

Sample ID: Up-3

Chan	Aero HiD, µm	LnHi Dp	PreWt, mg	PostWt, mg	Cum Mass, ΔWt, mg	Frac < HiD	Mass Probits	dM, mg	Fit Mass Probits	Fit Cum Mass, mg	Fit dM, mg
Total	156.5	5.1	1292.954	1295.132	2.178				2.365	2.158	0.030
8	126.1	4.8	1303.073	1305.122	2.049	0.941	1.561	0.028	2.002	2.129	0.093
7	94.2	4.5	1306.359	1308.380	2.021	0.928	1.460	0.072	1.512	2.036	0.190
6	70.5	4.3	1335.356	1337.305	1.949	0.895	1.253	0.222	1.026	1.846	0.308
5	52.8	4.0	1286.219	1287.946	1.727	0.793	0.817	0.503	0.542	1.538	0.399
4	39.6	3.7	1306.991	1308.215	1.224	0.562	0.156	0.386	0.058	1.139	0.410
3	29.6	3.4	1314.051	1314.889	0.838	0.385	-0.293	0.555	-0.427	0.729	0.334
2	22.2	3.1	1314.090	1314.373	0.283	0.130	-1.127	0.114	-0.911	0.394	0.217
1	16.6	2.8	1355.798	1355.967	0.169	0.078	-1.421	0.169	-1.396	0.177	0.177
	Remaining Wt		1350.253	1471.248	120.995						
	Soln Blank		1331.646	1331.709	0.063						
	Blank		1326.117	1326.140	0.023						

Average Upstream

Chan	Aero HiD, µm	LnHi	Mean Probits	StDev Probits	Fit Probits
Total	156.5	5.1			
8	126.1	4.8	1.763	0.217	2.071
7	94.2	4.5	1.549	0.118	1.587
6	70.5	4.3	1.205	0.047	1.106
5	52.8	4.0	0.816	0.034	0.627
4	39.6	3.7	0.136	0.037	0.148
3	29.6	3.4	-0.326	0.034	-0.331
2	22.2	3.1	-0.874	0.230	-0.810
1	16.6	2.8	-1.284	0.163	-1.289

	Mean, mg	StDev, mg
Remaining Wt	123.387	2.10
Soln Blank	0.025	0.04
Blank	0.019	0.01

Test #7: High Re, Small R0

Sample ID: Down-1

Chan	Aero HiD, µm	LnHi Dp	PreWt, mg	PostWt, mg	Cum Mass, ΔWt, mg	Frac < HiD	Mass Probits	dM, mg	Fit Mass Probits	Fit Cum Mass, mg	Fit dM, mg
Total	156.5	5.1	1323.596	1324.411	0.815				2.747	0.813	0.004
8	126.1	4.8	1325.963	1326.777	0.814	0.999	3.029	0.035	2.435	0.809	0.012
7	94.2	4.5	1424.226	1425.005	0.779	0.956	1.704	0.002	2.012	0.797	0.027
6	70.5	4.3	1326.380	1327.157	0.777	0.953	1.678	0.100	1.593	0.770	0.052
5	52.8	4.0	1315.098	1315.775	0.677	0.831	0.957	0.013	1.175	0.717	0.085
4	39.6	3.7	1318.183	1318.847	0.664	0.815	0.895	0.129	0.757	0.632	0.116
3	29.6	3.4	1326.917	1327.452	0.535	0.656	0.403	0.117	0.339	0.516	0.134
2	22.2	3.1	1451.122	1451.540	0.418	0.513	0.032	0.192	-0.079	0.382	0.130
1	16.6	2.8	1417.610	1417.836	0.226	0.277	-0.591	0.226	-0.496	0.252	0.252
	Remaining Wt		1322.551	1365.403	42.852						
	Soln Blank		1318.523	1318.530	0.007						
	Blank		1411.133	1411.123	-0.010						

Sample ID: Down-2

Chan	Aero HiD, µm	LnHi Dp	PreWt, mg	PostWt, mg	Cum Mass, ΔWt, mg	Frac < HiD	Mass Probits	dM, mg	Fit Mass Probits	Fit Cum Mass, mg	Fit dM, mg
Total	156.5	5.1	1341.826	1342.581	0.755				3.329	0.755	0.001
8	126.1	4.8	1333.806	1334.557	0.751	0.995	2.556	0.019	2.900	0.754	0.006
7	94.2	4.5	1322.772	1323.504	0.732	0.970	1.874	0.076	2.321	0.747	0.023
6	70.5	4.3	1313.789	1314.445	0.656	0.869	1.121	0.000	1.746	0.724	0.060
5	52.8	4.0	1313.852	1314.532	0.680	0.901	1.285	0.168	1.174	0.664	0.116
4	39.6	3.7	1318.752	1319.264	0.512	0.678	0.463	0.135	0.601	0.548	0.162
3	29.6	3.4	1345.238	1345.615	0.377	0.499	-0.002	0.170	0.028	0.386	0.165
2	22.2	3.1	1330.846	1331.053	0.207	0.274	-0.600	0.088	-0.544	0.221	0.122
1	16.6	2.8	1301.392	1301.511	0.119	0.158	-1.004	0.119	-1.117	0.100	0.100
	Remaining Wt		1321.688	1365.030	43.342						
	Soln Blank		1306.677	1306.736	0.059						
	Blank		1343.813	1343.818	0.005						

Sample ID: Down-3

Chan	Aero HiD, µm	LnHi Dp	PreWt, mg	PostWt, mg	Cum Mass, ΔWt, mg	Frac < HiD	Mass Probits	dM, mg	Fit Mass Probits	Fit Cum Mass, mg	Fit dM, mg
Total	156.5	5.1	1298.362	1299.040	0.678				3.471	0.678	0.001
8	126.1	4.8	1346.711	1347.376	0.665	0.981	2.071	0.000	3.032	0.677	0.004
7	94.2	4.5	1294.943	1295.624	0.681	0.990	2.326	0.022	2.440	0.673	0.017
6	70.5	4.3	1336.032	1336.691	0.659	0.972	1.911	0.031	1.852	0.656	0.048
5	52.8	4.0	1299.533	1300.161	0.628	0.926	1.448	0.180	1.266	0.608	0.099
4	39.6	3.7	1330.871	1331.319	0.448	0.661	0.415	0.113	0.680	0.510	0.145
3	29.6	3.4	1300.414	1300.749	0.335	0.494	-0.015	0.113	0.094	0.364	0.153
2	22.2	3.1	1309.975	1310.197	0.222	0.327	-0.447	0.103	-0.492	0.211	0.116
1	16.6	2.8	1365.443	1365.562	0.119	0.176	-0.933	0.119	-1.078	0.095	0.095
	Remaining Wt		1309.458	1349.443	39.985						
	Soln Blank		1306.500	1306.526	0.026						
	Blank		1338.624	1338.640	0.016						

Average Downstream

Chan	Aero HiD, µm	LnHi	Mean Probits	StDev Probits	Fit Probits
Total	156.5	5.1			
8	126.1	4.8	2.552	0.479	2.789
7	94.2	4.5	1.968	0.322	2.258
6	70.5	4.3	1.570	0.406	1.730
5	52.8	4.0	1.230	0.250	1.205
4	39.6	3.7	0.591	0.265	0.680
3	29.6	3.4	0.129	0.237	0.154
2	22.2	3.1	-0.338	0.330	-0.372
1	16.6	2.8	-0.843	0.221	-0.897

	Mean, mg	StDev, mg
Remaining Wt	42.060	1.81
Soln Blank	0.031	0.03
Blank	0.004	0.01

Test #8: High Re, Large R0

Duct Conditions:

Duct Diameter	8 in	Start Date	7/16/03
	0.203 m	End Date	7/21/03
Bend Surface	Smooth	**Collection Details:**	
Curvature Ratio, Ro	12	# Grids / Sample	3
Bend Angle	90 deg	Sample Time / Grid	120 sec
Flow Setpoint, DP	3.25 in H20		
Duct Velocity	5342 fpm		
	27.1 m/s		
Flow Rate	1864.7 cfm		
	0.880 m3/s		
Reynolds Number	366,915		
Dean Number	105,919		

Deposition vs. size

Sed Pip Chan	Geo Mid Dp, µm	Aero Mid Dp, µm	Mid Stk	η-1, %	η-2, %	η-3, %	Mean η, %	StDev η, %
Total	89.8	140.5	16.2	91.4	82.3	83.9	85.9	4.9
8	69.6	109.0	9.7	88.9	82.4	86.5	85.9	3.3
7	52.0	81.5	5.4	85.4	81.9	87.6	84.9	2.9
6	39.0	61.0	3.1	81.0	80.5	87.2	82.9	3.7
5	29.2	45.7	1.7	75.5	78.0	85.1	79.5	5.0
4	21.9	34.2	0.96	68.7	74.0	80.8	74.5	6.1
3	16.4	25.7	0.54	60.3	68.0	72.2	66.8	6.0
2	12.3	19.2	0.30	50.1	58.8	54.9	54.6	4.4
1	7.3	11.4	0.11	24.7	26.8	-47.6	1.3	42.3

Summary statistics for particles sampled upstream and downstream of the bend

Sample ID	MMAD, µm	GSD	Cm, mg/m3	R2		
Up-1	35.1	2.03	1.84	0.96		
Up-2	34.5	1.83	2.09	0.98		
Up-3	34.7	1.72	1.96	0.94		
Up-Mean	**34.7**	**1.86**	**1.96**	**0.96**	Overall η-1, %	63.6
Up-StDev	**0.3**	**0.15**	**0.13**	**0.02**	Overall η-2, %	67.8
					Overall η-3, %	70.0
Down-1	23.4	1.99	0.67	1.00	Overall η-mean, %	**67.2**
Down-2	25.5	1.97	0.67	0.98	Overall η-stdev, %	**3.2**
Down-3	20.1	2.03	0.59	0.91		
Down-Mean	**23.0**	**2.00**	**0.64**	**0.96**		
Down-StDev	**2.7**	**0.03**	**0.05**	**0.05**		

Test #8: High Re, Large R0

Sample ID: Up-1

Chan	Aero HiD, µm	LnHi Dp	PreWt, mg	PostWt, mg	Cum Mass, ΔWt, mg	Frac < HiD	Mass Probits	dM, mg	Fit Mass Probits	Fit Cum Mass, mg	Fit dM, mg
Total	156.5	5.1	290.728	293.077	2.349				2.119	2.309	0.042
8	126.1	4.8	289.623	291.788	2.165	0.922	1.416	0.000	1.813	2.267	0.108
7	94.2	4.5	283.665	285.891	2.226	0.948	1.622	0.179	1.400	2.159	0.189
6	70.5	4.3	292.995	295.042	2.047	0.871	1.133	0.277	0.989	1.970	0.281
5	52.8	4.0	288.863	290.633	1.770	0.754	0.686	0.462	0.580	1.689	0.355
4	39.6	3.7	289.818	291.126	1.308	0.557	0.143	0.459	0.171	1.334	0.381
3	29.6	3.4	290.956	291.805	0.849	0.361	-0.355	0.253	-0.238	0.954	0.345
2	22.2	3.1	290.441	291.037	0.596	0.254	-0.663	0.206	-0.647	0.608	0.266
1	16.6	2.8	281.728	282.118	0.390	0.166	-0.970	0.390	-1.056	0.342	0.342
	Remaining Wt		1442.847	1548.336	105.489						
	Soln Blank		274.229	274.236	0.007						
	Blank		271.443	271.440	-0.003						

Sample ID: Up-2

Chan	Aero HiD, µm	LnHi Dp	PreWt, mg	PostWt, mg	Cum Mass, ΔWt, mg	Frac < HiD	Mass Probits	dM, mg	Fit Mass Probits	Fit Cum Mass, mg	Fit dM, mg
Total	156.5	5.1	281.544	284.086	2.542				2.500	2.526	0.025
8	126.1	4.8	286.050	288.502	2.452	0.965	1.807	0.003	2.143	2.501	0.082
7	94.2	4.5	288.809	291.258	2.449	0.963	1.792	0.271	1.661	2.419	0.179
6	70.5	4.3	285.224	287.402	2.178	0.857	1.066	0.227	1.182	2.240	0.310
5	52.8	4.0	291.365	293.316	1.951	0.768	0.731	0.530	0.705	1.931	0.430
4	39.6	3.7	289.820	291.241	1.421	0.559	0.148	0.523	0.228	1.500	0.480
3	29.6	3.4	283.423	284.321	0.898	0.353	-0.377	0.379	-0.249	1.021	0.426
2	22.2	3.1	292.276	292.795	0.519	0.204	-0.827	0.075	-0.726	0.595	0.304
1	16.6	2.8	295.337	295.781	0.444	0.175	-0.936	0.444	-1.203	0.291	0.291
	Remaining Wt		1426.378	1547.271	120.893						
	Soln Blank		283.494	283.482	-0.012						
	Blank		285.713	285.710	-0.003						

Sample ID: Up-3

Chan	Aero HiD, µm	LnHi Dp	PreWt, mg	PostWt, mg	Cum Mass, ΔWt, mg	Frac < HiD	Mass Probits	dM, mg	Fit Mass Probits	Fit Cum Mass, mg	Fit dM, mg
Total	156.5	5.1	302.335	304.521	2.186				2.777	2.180	0.013
8	126.1	4.8	293.663	295.859	2.196	0.990	2.326	0.209	2.379	2.167	0.053
7	94.2	4.5	296.586	298.573	1.987	0.909	1.334	0.000	1.841	2.114	0.137
6	70.5	4.3	283.613	285.726	2.113	0.967	1.833	0.372	1.307	1.977	0.270
5	52.8	4.0	281.350	283.091	1.741	0.796	0.829	0.546	0.775	1.707	0.404
4	39.6	3.7	301.299	302.494	1.195	0.547	0.117	0.455	0.243	1.303	0.459
3	29.6	3.4	294.503	295.243	0.740	0.339	-0.417	0.341	-0.290	0.844	0.394
2	22.2	3.1	294.823	295.222	0.399	0.183	-0.906	0.072	-0.821	0.450	0.257
1	16.6	2.8	288.242	288.569	0.327	0.150	-1.038	0.327	-1.353	0.192	0.192
	Remaining Wt		1440.609	1555.314	114.705						
	Soln Blank		290.381	290.372	-0.009						
	Blank		249.410	249.409	-0.001						

Average Upstream

Chan	Aero HiD, µm	LnHi	Mean Probits	StDev Probits	Fit Probits
Total	156.5	5.1			
8	126.1	4.8	1.850	0.457	2.112
7	94.2	4.5	1.583	0.231	1.634
6	70.5	4.3	1.344	0.425	1.159
5	52.8	4.0	0.748	0.073	0.687
4	39.6	3.7	0.136	0.017	0.214
3	29.6	3.4	-0.383	0.031	-0.259
2	22.2	3.1	-0.798	0.124	-0.731
1	16.6	2.8	-0.981	0.052	-1.204

	Mean, mg	StDev, mg
Remaining Wt	113.696	7.75
Soln Blank	-0.005	0.01
Blank	-0.002	0.00

Test #8: High Re, Large R0

Sample ID: Down-1

Chan	Aero HiD, µm	LnHi Dp	PreWt, mg	PostWt, mg	Cum Mass, ΔWt, mg	Frac < HiD	Mass Probits	dM, mg	Fit Mass Probits	Fit Cum Mass, mg	Fit dM, mg
Total	156.5	5.1	289.096	289.931	0.833				2.760	0.831	0.004
8	126.1	4.8	283.474	284.291	0.817	0.981	2.070	0.004	2.446	0.827	0.012
7	94.2	4.5	278.630	279.443	0.813	0.976	1.977	0.000	2.022	0.815	0.028
6	70.5	4.3	281.244	282.064	0.820	0.984	2.154	0.089	1.600	0.787	0.053
5	52.8	4.0	282.482	283.213	0.731	0.878	1.163	0.079	1.180	0.734	0.087
4	39.6	3.7	279.800	280.452	0.652	0.783	0.781	0.125	0.761	0.647	0.119
3	29.6	3.4	294.006	294.533	0.527	0.633	0.339	0.133	0.341	0.528	0.137
2	22.2	3.1	293.688	294.082	0.394	0.473	-0.068	0.140	-0.079	0.390	0.133
1	16.6	2.8	288.683	288.937	0.254	0.305	-0.510	0.254	-0.499	0.257	0.257
	Remaining Wt		1422.069	1459.582	37.513						
	Soln Blank		262.413	262.412	-0.001						
	Blank		291.284	291.279	-0.005						

Sample ID: Down-2

Chan	Aero HiD, µm	LnHi Dp	PreWt, mg	PostWt, mg	Cum Mass, ΔWt, mg	Frac < HiD	Mass Probits	dM, mg	Fit Mass Probits	Fit Cum Mass, mg	Fit dM, mg
Total	156.5	5.1	288.184	288.993	0.809				2.676	0.806	0.004
8	126.1	4.8	291.073	291.865	0.792	0.979	2.033	0.000	2.357	0.802	0.014
7	94.2	4.5	284.193	285.005	0.812	0.990	2.326	0.034	1.926	0.787	0.032
6	70.5	4.3	284.602	285.380	0.778	0.962	1.771	0.079	1.498	0.755	0.061
5	52.8	4.0	288.151	288.850	0.699	0.864	1.099	0.109	1.072	0.694	0.095
4	39.6	3.7	281.470	282.060	0.590	0.729	0.611	0.120	0.646	0.599	0.125
3	29.6	3.4	282.454	282.924	0.470	0.581	0.204	0.124	0.220	0.475	0.136
2	22.2	3.1	280.853	281.199	0.346	0.428	-0.182	0.053	-0.206	0.338	0.125
1	16.6	2.8	285.674	285.967	0.293	0.362	-0.353	0.293	-0.633	0.213	0.213
	Remaining Wt		1426.861	1465.012	38.151						
	Soln Blank		284.405	284.438	0.033						
	Blank		278.389	278.388	-0.001						

Sample ID: Down-3

Chan	Aero HiD, µm	LnHi Dp	PreWt, mg	PostWt, mg	Cum Mass, ΔWt, mg	Frac < HiD	Mass Probits	dM, mg	Fit Mass Probits	Fit Cum Mass, mg	Fit dM, mg
Total	156.5	5.1	290.562	291.282	0.720				2.896	0.719	0.002
8	126.1	4.8	302.094	302.793	0.699	0.971	1.893	0.025	2.591	0.717	0.007
7	94.2	4.5	283.656	284.330	0.674	0.936	1.523	0.000	2.179	0.709	0.017
6	70.5	4.3	285.386	286.064	0.678	0.942	1.569	0.059	1.769	0.692	0.035
5	52.8	4.0	295.629	296.248	0.619	0.860	1.079	0.000	1.362	0.658	0.060
4	39.6	3.7	290.718	291.348	0.630	0.875	1.150	0.088	0.954	0.598	0.088
3	29.6	3.4	289.440	289.982	0.542	0.753	0.683	0.168	0.546	0.509	0.110
2	22.2	3.1	290.846	291.220	0.374	0.519	0.049	0.079	0.139	0.400	0.116
1	16.6	2.8	291.308	291.603	0.295	0.410	-0.228	0.295	-0.269	0.284	0.284
	Remaining Wt		1430.030	1462.967	32.937						
	Soln Blank		287.877	287.935	0.058						
	Blank		262.091	262.083	-0.008						

Average Downstream

Chan	Aero HiD, µm	LnHi	Mean Probits	StDev Probits	Fit Probits
Total	156.5	5.1			
8	126.1	4.8	1.999	0.093	2.464
7	94.2	4.5	1.942	0.403	2.042
6	70.5	4.3	1.831	0.297	1.623
5	52.8	4.0	1.114	0.044	1.205
4	39.6	3.7	0.847	0.276	0.787
3	29.6	3.4	0.409	0.247	0.369
2	22.2	3.1	-0.067	0.116	-0.049
1	16.6	2.8	-0.364	0.141	-0.467

	Mean, mg	StDev, mg
Remaining Wt	36.200	2.84
Soln Blank	0.030	0.03
Blank	-0.005	0.00

APPENDIX D: MODULE TO CALCULATE PARTICLE VELOCITY

The following Microsoft Visual Basic module (ModDrag2.bas) performs iterative calculations needed to determine particle velocity for motion outside of Stokes regime. This module can be inserted within a Microsoft Excel spreadsheet as a macro. Then, the individual functions can be called upon to calculate either terminal radial velocity or terminal settling velocity. This module was used in Chapter III and Chapter IV to calculate particle radial velocity.

```
'This Visual Basic module performs iterative calculations
'when calculating particle motion outside of Stokes regime.
'This module can be used within excel as a macro. Tom Peters December, 2003

'Definition of terms - units follow the underline character
'Dp_um - particle diameter
'Rho_p_kg_m3 - particle density
'Rho_g_kg_m3 - gas density
'Mu_g_kg_m_s - gas viscosity
'CD - drag coefficient
'Re_p - particle Reynolds number
'Vts - terminal settling velocity
'Vr - particle radial velocity

Option Explicit

Function CalcVr!(Dp_um!, InVelocity_m_s!, r_m!, _
    Optional Rho_p_kg_m3! = 1000, Optional Rho_g_kg_m3! = 1.2, _
    Optional Mu_g_kg_m_s! = 0.000018)

  Dim CDRe2!, Re_p!, Vr_m_s!

  'Calculate Radial Velocity Assuming Stokes Conditions Hold
  '******************Vr=Tau*Uo^2/r  r-can be any radius
  Vr_m_s = (Rho_p_kg_m3 * (Dp_um * 0.000001) ^ 2 / _
          (18 * Mu_g_kg_m_s)) * InVelocity_m_s ^ 2 / r_m

  Re_p = CalcRe_p(Dp_um, Vr_m_s, Rho_g_kg_m3, Mu_g_kg_m_s)

  If Re_p < 0.1 Then
    CalcVr = Vr_m_s  ' within Stokes regime
  Else
    ' outside Stokes regime
    CDRe2 = (8 * (Dp_um * 0.000001) ^ 3 * Rho_p_kg_m3 * _
          InVelocity_m_s ^ 2 * Rho_g_kg_m3) / (6 * r_m * Mu_g_kg_m_s ^ 2)
    Re_p = CalcReGivenCDRe2(CDRe2)
    CalcVr = Re_p * Mu_g_kg_m_s / Rho_g_kg_m3 / (Dp_um * 0.000001)
  End If
End Function
```

```
Function CalcParticleSettlingVelocity!(Dp_um!, _
    Optional Rho_p_kg_m3! = 1000, Optional Rho_g_kg_m3! = 1.2, _
    Optional Mu_g_kg_m_s! = 0.000018)

  Dim CDRe2!, Re_p!, Vts!

  Vts = Rho_p_kg_m3 * (Dp_um * 0.000001) ^ 2 * 9.81 / (18 * Mu_g_kg_m_s)
  Re_p = CalcRe_p(Dp_um, Vts, Rho_g_kg_m3, Mu_g_kg_m_s)

  If Re_p < 0.1 Then
    CalcParticleSettlingVelocity = Vts
  Else
    CDRe2 = (4 * Rho_g_kg_m3 * Rho_p_kg_m3 * (Dp_um * 0.000001) ^ 3 * 9.81) _
            / (3 * Mu_g_kg_m_s ^ 2)
    Re_p = CalcReGivenCDRe2(CDRe2)
    CalcParticleSettlingVelocity = Re_p * Mu_g_kg_m_s / Rho_g_kg_m3 / _
                                   (Dp_um * 0.000001)
  End If
End Function

Function CalcReGivenCDRe2!(CDRe2!)
  Dim Re!, CD!, NewCDRe2!, delRe!, oldRe!

  'If Cdre2 < some number then stokes holds get out of loop
  'Initial guess
  Re = CDRe2 / 24
  delRe = Re
  CD = CalcC_D(Re)
  NewCDRe2 = CD * Re ^ 2

  Do Until NewCDRe2 / CDRe2 < 1.002 And NewCDRe2 / CDRe2 > 0.998
    oldRe = Re
    If NewCDRe2 > CDRe2 Then ' new Re is too high, adjust Re downward
      Re = Re - delRe / 2
    Else
      Re = Re + delRe / 2
    End If
    delRe = Abs(Re - oldRe)
    CD = CalcC_D(Re)
    NewCDRe2 = CD * Re ^ 2
  Loop

  CalcReGivenCDRe2 = Re
End Function

Function CalcRe_p!(Dp_um!, Velocity_m_s!, _
    Optional Rho_g_kg_m3! = 1.2, Optional Mu_g_kg_m_s! = 0.000018)

  CalcRe_p = Dp_um * 0.000001 * Velocity_m_s * Rho_g_kg_m3 / Mu_g_kg_m_s

End Function

Function CalcC_D!(Re_p!)
  CalcC_D = 24 / Re_p * (1 + 0.15 * Re_p ^ 0.687)
End Function
```

REFERENCES

ACGIH (1998) *Industrial ventilation: a manual of recommended practice*. American Conference of Governmental Industrial Hygienists, Inc., Cincinnati, OH.

Agricola, G. (1556) *De Re Metallica*. Trans. H.C. Hoover & L.H. Hoover. Dover Publications, Inc., New York, NY.

Alden, J. L. & Kane, J. M. (1982) *Design of industrial ventilation systems*. Industrial Press Inc., New York, NY.

Alexander, L. G. & Coldren, C. L. (1951) Droplet transfer from suspending air to duct walls. *Ind. Eng. Chem., 43*, 1325.

Anwer, M., So, R. M. C., & Lai, Y. G. (1989) Perturbation by and recovery from bend curvature of a fully developed turbulent pipe flow. *Phys. Fluids, 1*, 1387-1397.

ASHRAE (1998) *American society of heating, refrigerating and air-conditioning engineers, fundamentals handbook*. American Society of Heating, Refrigerating Engineers, Inc., Atlanta, GA.

Azzola, J., Humphrey, J. A. C., Iocovides, H., & Launder, B. E. (1986) Developing turbulent flow in a u-bend of circular cross-section: measurement and computation. *Trans. ASME, 108*, 214-221.

Baliff, J., Greenburg, L., & Stern, A. C. (1948) Transport velocities for industrial dusts. *Amer. Ind. Hyg. Q., 9*, 85-88.

Berger, S. A. & Talbot, L. (1983) Flow in curved pipes. *Ann. Rev. Fluid Mech., 15*, 461-512.

Boersma, B. J. & Nieuwstadt, F. T. M. (1996) Large-eddy simulation of turbulent flow in a curved pipe. *Trans. ASME, 118*, 248-254.

Brockmann, J. E. (1993) Sampling and transport of aerosol. In K. Willeke & P.A. Baron, eds. *Aerosol measurement: principles, techniques, and applications* Van Nostrand Reinhold, New York.

Brockmann, J. E. (2001) Sampling and transport of aerosol. In P.A. Baron & K. Willeke, eds. *Aerosol measurement: principles, techniques, and applications*, Second ed. Van Nostrand Reinhold, New York.

Burgess, W. A., Ellenbecker, M. J., & Treitman, R. D. (1989) *Ventilation for the control of the work environment*. John Wiley & Sons, New York.

Cheng, Y.-S. & Wang, C.-S. (1975) Inertial deposition of particles in a bend. *J. Aerosol Sci., 6*, 139-145.

Cheng, Y.-S. & Wang, C.-S. (1981) Motion of particles in bends of circular pipes. *Atmospheric Environment, 15*, 301-306.

Cooper, D. W. (1982) On the products of lognormal and cumulative lognormal particle distributions. *J. Aerosol Sci., 13*, 111-120.

Crane, R. I. & Evans, R. L. (1977) Inertial deposition of particles in a bent pipe. *J. Aerosol Sci., 8*, 161-170.

Crowe, C., Sommerfeld, M., & Tsuji, Y. (1998) *Multiphase flows with droplets and particles*. CRC Press, New York, NY.

Cullen, L. (2002) *A job to die for*. Common Courage Press, Monroe, ME.

Curd, E. F., Railio, J., Gustavsson, J., Hogeling, J., Assad, M. E. H., Emilsen, J., Mazzacane, S., & Wiksten, R. (2001) Air-handling processes. In H. Goodfellow & E. Tahti, eds. *Industrial Ventilation: Design Guidebook* Academic Press, New York.

DallaValle, J. M. (1932) Determining minimum air velocities for exhaust systems. *Heating, Piping and Air Conditioning J., Sept.*, 639-641.

El-Shobokshy, M. S. (1983) Experimental measurements of aerosol deposition to smooth and rough surfaces. *Atmospheric Environment, 17*, 639-644.

Enayet, M. M., Gibson, M. M., Taylor, A. M. K. P., & Yianneskis, M. (1982) Laser-doppler measurements of laminar and turbulent flow in a pipe bend. *Int. J. Heat & Fluid Flow, Dec*, 213-219.

Fan, B. J., Wong, F. S., McFarland, A. R., & Anand, N. K. (1992) Aerosol deposition in sampling probes. *Aerosol Sci. and Technol., 17*, 326-332.

Friedlander, S. K. & Johnstone, H. T. (1957) Deposition of suspended particles from turbulent gas streams. *Ind. Eng. Chem., 49*, 1151-1156.

Gerstler, W. D. (2002) New rules for kitchen exhaust. *ASHRAE J., Nov.*, 26-33.

Gong, H., Anand, N. K., & McFarland, A. R. (1993) Numerical predictions of the performance of a shrouded probe sampling in turbulent flow. *Aerosol Sci. and Technol., 19*, 294-304.

Gregory, W. S., Martin, R. A., White, B. W., Nichols, B. D., Smith, P. R., Leslie, I. H., Fenton, D. L., Gunaji, M. V., & Blythe, J. P. (1991) Fires in large scale ventilation systems. *Nuclear Engineering and Design, 125*, 337-345.

Hacker, P. T., Brun, R. J., & Boyd, B. (1953) Impingement of droplets in 90 degree elbows. NACA Technical Note No. 2999. Lewis Flight Propulsion Laboratory, Cleveland, OH.

Hatch, T. (1940) Economy in the design of exhaust systems. *Ind. Medicine, October*, 54-59.

Hinds, W. C. (1999) Aerosol technology: properties, behavior, and measurement of ariborne particles John Wiley & Sons, Inc., New York.

Ito, H. (1987) Flow in curved pipes. *JSME Int. J., 30*, 543-552.

Landahl, H. D. & Herrmann, R. G. (1949) Sampling of liquid aerosols by wires, cylinders, and slides, and the efficiency of impaction of droplets. *J. Colloid Interface Sci., 4*, 103-136.

Leigh, J. P., Markowitz, S. B., Fahs, M. C., & Landrigan, P. J. (2000) *Cost of occupational injury and illness*. University of Michigan Press, Ann Arbor, MI.

Leith, D., Raynor, P. C., Boundy, M. G., & Cooper, S. J. (1996) Performance of industrial equipment to collect coolant mist. *AIHA Journal, 57*, 1142-1148.

Liu, B. Y. H. & Agarwal, J. K. (1974) Experimental observation of aerosol deposition in turbulent flow. *Aerosol Sci. and Technol., 5*, 145-155.

Marple, V. A. & Rubow, K. L. (1986) Chapter 4: therory and design guidelines. In J.P. Lodge & T.L. Chan, eds. *Cascade Impactor: Sampling and Data Analysis* American Industrial Hygiene Association, Akron, OH.

May, D. C. & Berard, D. L. (1987) Fires and explosions associated with aluminum dust from finishing operations. *Journal of Hazardous Materials, 17*, 81-88.

McFarland, A. R., Gong, H., Muyshondt, A., Wente, W. B., & Anand, N. K. (1997) Aerosol deposition in bends with turbulent flow. *Environ. Sci. Technol., 31*, 3371-3377.

McFarland, A. R., Wong, F. S., Anand, N. K., & Ortiz, C. A. (1991) Aerosol penetration through a model transport system: comparison of theory and experiment. *Environ. Sci. Technol., 25*, 1573-1577.

Montgomery, T. L. & Corn, M. (1970) Aerosol deposition in a pipe with turbulent airflow. *J. Aerosol Sci., 1*, 185-213.

Muhic, S. & Butala, V. (2004) The influence of indoor environment in office buildings on their occupants: expected-unexpected. *Building and Environment, 39*, 289-296.

Muyshondt, A., Anand, N. K., & McFarland, A. R. (1996) Turbulent deposition of aerosol particles in large transport tubes. *Aerosol Sci. and Technol., 24*, 107-116.

NIOSH (2002) Worker health chartbook, 2000: fatal illness. DHHS (NIOSH) 2002-118. NIOSH, Cincinnatti, OH.

NIOSH (2003) Work-related lung disease surveillance report 2002. DHHS(NIOSH) Number 2003-111. National Institute for Occupational Safety and Health, Cincinnati, OH.

Pak, S. S., Liu, B. Y. H., & Rubow, K. L. (1992) Effect of coating thickness on particle bounce in inertial impactors. *Aerosol Sci. and Technol., 16*, 141-150.

Papavergos, T. G. & Hedley, A. B. (1984) Particle deposition behavior from turbulent flows. *Chem. Eng. Res. Des., 62*, 275-295.

Peters, T. M. & Leith, D. (accepted) Particle deposition in industrial duct bends. *Ann. Occup. Hygiene*.

Peters, T. M. & Leith, D. (in press) Measurement of particle deposition in industrial ducts. *J. Aerosol Sci.,*, in press.

Plinke, M. A. E., Leith, D., Boundy, M. G., & Loffler, F. (1995) Dust generation from handling powders in industry. *Am. Ind. Hyg. Assoc. J., 56*, 251-257.

Pui, D. Y. H., Romay-Novas, F., & Liu, B. Y. H. (1987) Experimental study of particle deposition in bends of circular cross section. *Aerosol Sci. and Technol., 7*, 301-315.

Rajahns, G. S. & Thompkins, R. W. (1967) Critical velocities of mineral dusts. *Candian Mining J., October*, 85-88.

Rowe, M. (1970) Measurements and computations of flow in pipe bends. *J. Fluid Mech., 43*, 771-783.

Rütten, F., Meinke, M., & Schröder, W. (2001) Large-eddy simulations of 90° pipe bend flows. *Journal of Turbulence, 2*, 1-14.

Silverman, L., Billings, C. E., & First, M. W. (1971) *Particle size analysis in industrial hygiene*. Academic Press, New York.

Sippola, M. R. & Nazaroff, W. W. (2003) Modeling particle loss in ventilation ducts. *Atmospheric Environment, 37*, 5597-5609.

Tennekes, H. & Lumley, J. L. (1972) *A first course in turbulence*. The MIT Press, Cambridge, MA.

Torobin, L. B. & Gauvin, W. H. (1961) The drag coefficients of single spheres moving in a steady and accelerated motion in a turbulent fluid. *AIChE J, 7*, 615.

Tsai, C.-J., Pui, D. Y. H., & Liu, B. Y. H. (1990) Capture and rebound of small particles upon impact with solid surfaces. *Aerosol Sci. and Technol., 12*, 497-507.

Tunstall, M. J. & Harvey, J. K. (1968) On the effect of a sharp bend in a fully developed turbulent pipe-flow. *J. Fluid Mech., 34*, 595-608.

Turner, J. R. & Hering, S. V. (1987) Greased and oiled substrates as bounce-free impaction surfaces. *J. Aerosol Sci., 18*, 215-224.

Wallin, O. (1994) Computer simulation of particle deposition in ventilating duct systems. Bulletin no 31. Building Services Engineering, Royal Institute of Technology, Stockholm, Sweden.

Wallin, O. & Malmstrom, T. G. (1995) Particle deposition models for ventilation air ducts. *Int. J. HVAC&R Res., 1*, 194-218.

Yamano, N. & Brockmann, J. E. (1989) Aerosol sampling and transport efficiency calculation (ASTEC) and application to Surtsey/DCH aerosol sampling system. NUREG/CR-525, SAND88-1447. Sandia National Laboratories, Albuquerque, NM.